

Current sheets, plasmoids and flux ropes in the heliosphere

Part II: Theoretical aspects.

O. Pezzi · F. Pecora · J. le Roux · N. E. Engelbrecht · A. Greco · S. Servidio · H. V. Malova · O. V. Khabarova · O. Malandraki · R. Bruno · W. H. Matthaeus · G. Li · L. M. Zelenyi · R. A. Kislov · V. N. Obridko · V. D. Kuznetsov

Received: date / Accepted: date

O. Pezzi

Gran Sasso Science Institute (GSSI), Viale F. Crispi 7, 67100 L'Aquila, Italy
INFN, Laboratori Nazionali del Gran Sasso (LNGS), I-67100 Assergi, L'Aquila, Italy
Istituto per la Scienza e Tecnologia dei Plasmi, CNR, Via Amendola 122/D, I-70126 Bari, Italy
E-mail: oreste.pezzi@gssi.it

A. Greco, F. Pecora, S. Servidio
Dipartimento di Fisica, Università della Calabria, I-87036 Rende (CS), Italy

J. le Roux, G. Li
Center for Space Plasma and Aeronomic Research (CSPAR) and Department of Space Science, University of Alabama in Huntsville, Huntsville, AL 35805, USA

N. E. Engelbrecht
Centre for Space Research, North-West University, Potchefstroom, 2522, South Africa

R. Bruno
Istituto di Astrofisica e Planetologia Spaziali, Istituto Nazionale di Astrofisica (IAPS-INAF), Roma, Italy

V. D. Kuznetsov, V. N. Obridko
Pushkov Institute of Terrestrial Magnetism, Ionosphere and Radio Wave Propagation of the Russian Academy of Sciences (IZMIRAN), Moscow, 108840 Russia

O. V. Khabarova, R. A. Kislov
Pushkov Institute of Terrestrial Magnetism, Ionosphere and Radio Wave Propagation of the Russian Academy of Sciences (IZMIRAN), Moscow, 108840 Russia
Space Research Institute (IKI) RAS, Moscow, 117997 Russia

H. V. Malova
Space Research Institute (IKI) RAS, Moscow, 117997 Russia
Scobeltsyn Nuclear Physics Institute of Lomonosov Moscow State University, Moscow, 119991 Russia

O. Malandraki
IAASARS, National Observatory of Athens, Penteli, Greece

W. H. Matthaeus

Abstract Our understanding of processes occurring in the heliosphere historically began with reduced dimensionality - one-dimensional (1D) and two-dimensional (2D) sketches and models, which aimed to illustrate views on large-scale structures in the solar wind. However, any reduced dimensionality vision of the heliosphere limits the possible interpretations of *in-situ* observations. Accounting for non-planar structures, e.g. current sheets, magnetic islands, flux ropes as well as plasma bubbles, is decisive to shed the light on a variety of phenomena, such as particle acceleration and energy dissipation. In part I of this review, we have described in detail the ubiquitous and multi-scale observations of these magnetic structures in the solar wind and their significance for the acceleration of charged particles. Here, in part II, we elucidate existing theoretical paradigms of the structure of the solar wind and the interplanetary magnetic field, with particular attention to the fine structure and stability of current sheets. Differences in 2D and 3D views of processes associated with current sheets, magnetic islands and flux ropes are discussed. We finally review the results of numerical simulations and *in-situ* observations, pointing out the complex nature of magnetic reconnection and particle acceleration in a strongly turbulent environment.

Keywords Plasma turbulence · Magnetic Reconnection · Particle acceleration · Solar wind
particle acceleration

1 Introduction

The heliosphere is a highly structured medium, characterized by the presence of a variety of plasma structures observed over a wide range of scales, from the energy-containing, large scales, to kinetic (Malandraki et al., 2019). As described in Part I of this review, understanding physical processes related to the variety of large-scale plasma structures observed in the solar wind and the magnetosphere implies analyzing their fine structure. The latter, in turn, requires a comprehensive analysis of properties of current sheets (CSs), flux ropes (FRs), and plasmoids. The dipolar nature of the main solar magnetic field and, consequently, of the interplanetary magnetic field (IMF) leads to the formation of the heliospheric current sheet (HCS), which is the largest CS in the heliosphere. Its configuration has historically been modelled as a waved “ballerina skirt” that follows the solar magnetic equator and the Parker IMF spiral shape (Wilcox et al., 1980; Hoeksema et al., 1983). Similarly strong but less long-lived CSs are formed in the solar wind at different helio-latitudes owing to the presence of higher harmonics of the solar magnetic field (see Part I, Section 2.1.2). Coronal Mass Ejections (CMEs), often associated with

Department of Physics and Astronomy, University of Delaware, Newark, DE 19716, USA

L. M. Zelenyi

Space Research Institute (IKI) RAS, Moscow, 117997 Russia

explosive phenomena triggered by magnetic reconnection, as well as their interplanetary counterpart, ICMEs, significantly perturb the heliosphere and its magnetic field, producing shock waves, dubbed interplanetary shocks (ISs) at which strong CSs may occur. ISs can also be produced by long-lived Corotating Interaction Regions (CIRs) or less stable Stream Interaction Regions (SIRs) formed when a fast flow from a coronal hole overtakes the surrounding slow solar wind (Heber et al., 1999). Notably, large-scale structures, such as SIRs, ICMEs and the HCS, coexist with structures of much smaller scales. For example, reconnecting CSs and FRs or plasmoids – whose two-dimensional (2D) counterparts are magnetic islands (MIs) – are often observed not only at the edges but also within complex ICMEs and SIRs/CIRs (see Xu et al. (2011); Khabarova et al. (2016); Khabarova and Zank (2017) and Part I, Section 2.1.2). Furthermore, the HCS is often rippled and surrounded by the much wider heliospheric plasma sheet (HPS) in which numerous secondary reconnection regions produce a sea of thin CSs (TCSs), FRs as well as plasma bubbles/blobs/plasmoids (see Adhikari et al. (2019) and Part I, Section 2.1). FRs or plasmoids have been also found in the inner heliosphere (Zhao et al., 2020), in the Earth’s magnetosheath at kinetic scales (Yao et al., 2020), and in laboratory plasmas (Gekelman et al., 2019). This ensemble of structures have a significant impact on the topology of the surrounding IMF, which -in turn- regulates the propagation of charged particles of both heliospheric and galactic origin (see Dalla et al. (2013); Battarbee et al. (2017, 2018); Engelbrecht et al. (2019) and Part I, Section 3).

Another keystone of *in-situ* measurements regards the pervasive significance of both plasma turbulence and magnetic reconnection in governing small-scale processes that occur in space plasmas (e.g. Matthaeus and Velli (2011); Zank et al. (2014); Matthaeus et al. (2015); Servidio et al. (2015); le Roux et al. (2015)). In Part I, we discussed the fact that magnetic reconnection and turbulence are always linked. An analogous argument holds for CSs, the occurrence of which always suggests the formation of FRs/plasmoids/magnetic islands and vice versa. The solar wind, which embeds these magnetic and plasma structures, is a strongly turbulent and intermittent medium, characterized by a complex interplay of different phenomena (Servidio et al., 2009; Matthaeus et al., 2015; Bruno and Carbone, 2016). The energy of the magnetic field and bulk speed fluctuations injected at large scales is cross-scale transferred towards smaller scales, at which Hall and kinetic effects can be significant (Servidio et al., 2007, 2015). Spectral steepening (Leamon et al., 1998; Alexandrova et al., 2008; Sahraoui et al., 2009) and dispersive wave effects are routinely observed in the solar wind. These latter are compatible with either strongly turbulent fluctuations not described in terms of linear modes (Alexandrova et al., 2008) or kinetic Alfvén waves (KAWs) (Howes et al., 2008b; Sahraoui et al., 2009; Salem et al., 2012) and whistler waves (Beinroth and Neubauer, 1981; Gary et al., 2010; Vasko et al., 2020), although whistler modes possess a smaller power content with respect to the KAW branch (Chen et al., 2013).

Signatures of kinetic effects are often found in the particle velocity distribution function (VDFs) that exhibit non-Maxwellian properties, e.g. temperature anisotropy, heat fluxes, beams and rings (Marsch, 2006; Maruca et al., 2011; Servidio et al., 2012, 2015; Valentini et al., 2016; Perri et al., 2020). These non-equilibrium features may drive the onset of microinstabilities (Hellinger et al., 2006; Matteini et al., 2013; Bandyopadhyay et al., 2020b), although understanding the significance of linear instabilities within a turbulent environment is still under debate (Qudsi et al., 2020). The dissipation of turbulent energy is thought to locally occur at small scales (Osman et al., 2011, 2012b,a; Matthaeus et al., 2015; Vaivads et al., 2016), thus ultimately heating the plasma. Fine velocity-space structures have also been recently observed in the magnetosheath (Servidio et al., 2017) and obtained in kinetic simulations performed within solar-wind-like conditions (Pezzi et al., 2018; Cerri et al., 2018) by means of the Hermite decomposition of the plasma VDF (Grad, 1949; Tatsuno et al., 2009; Schekochihin et al., 2016). This supports the idea that non-equilibrium features in particle VDF readjust in a very complex way, resembling the development of an enstrophy velocity-space turbulent spectrum (Servidio et al., 2017). The presence of fine velocity-space structures may also enhance the dynamical role of inter-particle collisions (Pezzi et al., 2016; Pezzi, 2017; Pezzi et al., 2019a).

Magnetic reconnection, during which a local breaking of the frozen-in law causes a rapid release of magnetic energy in both flow energy and heating, goes hand in hand with plasma turbulence (Lazarian and Vishniac, 1999; Kowal et al., 2011; Lazarian et al., 2015). Indeed, CSs that separate vortices and magnetic islands in plasma turbulence often represent reconnection sites (Retinò et al., 2007; Servidio et al., 2009; Servidio et al., 2010; Haggerty et al., 2017; Phan et al., 2018). Furthermore, reconnection exhausts and jets generated by magnetic reconnection can be turbulent themselves (Franci et al., 2017; Pucci et al., 2017, 2018) and can also host secondary reconnection regions driven by nonlinear waves and/or instabilities (Lapenta et al., 2015; Lapenta et al., 2018; Wang et al., 2020). Very recent observations conducted at an unprecedented high-resolution by the Magnetospheric Multi-Scale (MMS) mission (Burch et al., 2016b; Fuselier et al., 2016) allowed, for the first time, to investigate the electron-scale magnetic reconnection by explicitly showing the electron diffusion region and by addressing the relevant question about the physical mechanism that breaks the frozen-in law in a collisionless plasma (Burch et al., 2016a; Le Contel et al., 2016; Torbert et al., 2016, 2018; Breuillard et al., 2018; Chasapis et al., 2018).

Magnetic reconnection is also a decisive phenomenon in astrophysical plasmas owing to its role in particle acceleration (Lyutikov, 2003; Uzdensky, 2011). In the planetary magnetospheres and the solar wind, signatures of particle acceleration are observed in the particle energy distribution, that often shows non-Maxwellian higher energy tails described in terms of kappa (Vasyliunas, 1968; Sarris et al., 1976; Christon et al., 1989; Collier, 1999) or power-law distributions. Although acceleration mechanisms in the solar wind and magnetospheres have common features, they also present distinctive traits due to

the different physical conditions. For example, the maximum particle energies that can be obtained in the Earth's magnetosphere do not exceed a few MeV (Zelenyi et al., 2007) since accelerated particles with gyroradii approximately equal to the magnetospheric scales leak out to the solar wind. In smaller-scale magnetospheres, the maximum acceleration energies are much smaller. For example, in Mercury's magnetosphere, due to repeating substorms and magnetotail dipolarization events, particle energies are estimated to be about 100keV. In the corona and the solar wind, even single mechanisms act on scales many orders larger, and the mechanisms in combination can contribute to the particle energy gain up to GeV. At the same time, one should note that magnetic reconnection, wave propagation and turbulent processes widely present in the solar wind are limited by MeV energies (see Part I, Section 3).

Historically, seminal works by Fermi (1949, 1954) proposed two general acceleration mechanisms based either on the stochastic interaction of particles with randomly moving magnetic clouds/inhomogeneities (second-order Fermi acceleration) or on the systematic acceleration of particles in the case of converging magnetic traps (first-order Fermi acceleration). Several acceleration mechanisms in space have been proposed and are found to be in accordance with *in-situ* observations. For example, the large-scale dawn-dusk electric field can accelerate quasi-adiabatic ions during the so-called Speiser acceleration (Speiser, 1965; Lyons and Speiser, 1982; Cowley and Shull, 1983; Ashour-Abdalla et al., 1993; Zelenyi et al., 2007). Plasma particles can also be energized by Alfvén and cyclotron waves in the proximity of the magnetopause (Drake et al., 1994; Johnson and Cheng, 2001; Panov et al., 2008) and heated by ultralow frequency (ULF) waves (Glassmeier et al., 2003; Baumjohann et al., 2006). In presence of a shock (e.g. magnetospheric bow shocks or ICME/CIR/SIR – driven interplanetary shocks) (Thampi et al., 2019; Slavin et al., 2008), nonadiabatic heating, diffusive shock acceleration (DSA), shock drift acceleration (SDA) and also stochastic shock drift acceleration (SSDA) (see Katou and Amano (2019) for a review on SDA) can occur. At variance with SDA, both DSA and SSDA assume the presence of fluctuations (e.g. pre-existing turbulence) on which particles diffuse in order to be accelerated. DSA, first introduced to address cosmic-ray acceleration at supernova remnants (Bell, 1978a,b; Blandford and Ostriker, 1978), has also been invoked to explain acceleration in solar wind (Zank et al., 2000). However, it is not easy to interpret some *in-situ* observations through the original steady-state DSA model (see Malandraki et al. (2019) for a further discussion). At the same time, SDA and SSDA are efficient in the energization of electrons at planetary bow shocks (Leroy and Mangeney, 1984; Burgess, 1987; Giacalone, 1992; Katou and Amano, 2019; Amano et al., 2020).

Other mechanisms of acceleration are directly related to magnetic reconnection. Both reconnection events of solar origin (Higginson and Lynch, 2018) and local magnetic reconnection (Khabarova et al., 2015, 2016, 2020b; Adhikari et al., 2019; Malandraki et al., 2019) can lead to particle acceleration. Near the current-sheet X-line, the electric field produced by reconnection can accelerate charged particles (Matthaeus and Lamkin, 1986; Ambrosiano et al.,

1988). Moreover, Hoshino (2005) found that electrons, trapped by the polarization (Hall) electric field produced by reconnection, are efficiently accelerated owing to a surfing acceleration mechanism. Current sheets are often unstable due to tearing instability (Zelenyi et al., 1984; Malara et al., 1992; Malara and Velli, 1996; Tenerani et al., 2015a; Primavera et al., 2019). Electric fields induced by i) the tearing instability, ii) the CS destruction (Lutsenko et al., 2005), iii) dipolarization processes in the terrestrial magnetosphere (Zelenyi et al., 1990; Delcourt and Sauvaud, 1994; Delcourt, 2002; Slavin, 2004; Delcourt et al., 2005; Apatenkov et al., 2007; Zhou et al., 2010; Ukhorskiy et al., 2017; Parkhomenko et al., 2019), or iv) other fluctuations occurring in the turbulent environment with the presence of magnetic reconnection (Malara et al., 2019) are also able to accelerate charged particles. For example, in the magnetosphere, a power-law tailed energy distribution of energetic particles has been obtained by considering the model of the CS with electromagnetic fluctuations excited by electromagnetic wave ensembles. The occurrence of electromagnetic fluctuations close to the reconnecting CSs also allows explaining additional particle acceleration (additional to the acceleration due to the large-scale electrostatic E_y) often observed in velocity distributions at open field lines (Grigorenko et al., 2013). Temperature and density inhomogeneities across the reconnecting CS may also speed up the formation of secondary plasmoids, as has recently been shown using test-particle (Catapano et al., 2015, 2016, 2017) and PIC simulations (Karimabadi et al., 2013; Lu et al., 2019) as well as spacecraft observations (Lu et al., 2019).

Furthermore, numerical simulations show that particles can be efficiently energized due to the contraction of magnetic islands (MIs) (Drake et al., 2006) and their merging (Drake et al., 2013). The combined role of these different mechanisms and their relative importance has been described by Zank et al. (2014) via analytical solutions, finding that MIs contraction and merging are the dominant acceleration mechanisms. Further models discussing the effect of multiple FRs and the combined role of magnetic reconnection-related acceleration mechanisms and DSA have been developed by le Roux et al. (2015) and Zank et al. (2015a); le Roux et al. (2016), respectively. le Roux et al. (2018) self-consistently coupled energetic particles, for which the transport equation is solved, and MHD turbulence that controls the FRs dynamics. The role of small-scale FRs has been recently considered by le Roux et al. (2019); Mingalev et al. (2019). Magnetic reconnection is thus an efficient mechanism able to accelerate particles locally, at least at levels comparable with DSA (Garrel et al., 2018). An analysis of spacecraft observations also supports these findings. Local particle acceleration at the HCS has been reported, e.g., by Zharkova and Khabarova (2012, 2015). Khabarova et al. (2015, 2016, 2020b); Khabarova and Zank (2017); Adhikari et al. (2019); Malandraki et al. (2019) found observational evidence for local particle acceleration associated with the occurrence of reconnecting CSs and MIs. Recurrent (stochastic or turbulent) magnetic reconnection occurring at the HCS, MIs inside the rippled HCS and smaller CSs within the HPS presumably energizes charged particles via the mechanisms proposed by (Zank et al., 2014, 2015b; le Roux et al., 2015, 2016, 2019).

Atypical energetic particle events (AEPEs), not easily explained in terms of the DSA mechanism, are instead well described by local particle acceleration in regions filled with small-scale MIs of width $< \sim 0.01$ AU (Khabarova et al., 2016; Khabarova and Zank, 2017). Prior findings regarding locally accelerated ions have recently been systematized by Adhikari et al. (2019); Chen et al. (2019c). A local origin of some suprathermal electrons observed in the solar wind, as reflected in the specific features of pitch-angle electron distributions, has also been suggested by Khabarova et al. (2020b). Explosive particle acceleration (Pecora et al., 2018; Pecora et al., 2019b) that combines several types of acceleration mechanisms mentioned above can finally take place, e.g. in the solar corona.

It is important to note that different mechanisms can co-act simultaneously in space plasmas. This can be clearly seen in observations (e.g., Khabarova et al. (2016); Adhikari et al. (2019) and Part I, Section 3.1, 3.2). However, this effect may considerably complicate the interpretation of the observed picture (Malandraki et al., 2019). Note that, in presence of turbulent fluctuations, stochastic acceleration of charged particles (of both Fermi types) (Milovanov and Zelenyi, 2001; Trotta et al., 2020; Sioulas et al., 2020) and, in general, various acceleration mechanisms mentioned above can operate (Artemyev et al., 2009b; Kobak and Ostrowski, 2000; Parkhomenko et al., 2019; Ergun et al., 2020b,a). We also remark here that Milovanov and Zelenyi (2001) generalized second order Fermi acceleration for systems with long-range correlations of spatial turbulence structures (Comisso and Sironi, 2018, 2019). This process can be considered as a transport process in the velocity space. In this perspective, the “random movement” term is usually described by the Gaussian variance $\langle V^2(t) \rangle \sim t$ for velocities of scattered particles $V(t)$. Meanwhile, the Gaussian variance in principle ignores long-range dynamical correlations occurring in turbulent self-organized systems. The effect of correlations appears in multi-scale nonrandom acceleration events that do not comply with standard velocity diffusion. A fractional-dynamic approach solves the issue of describing stochastic acceleration in the presence of the long-range correlations (Milovanov and Zelenyi, 1994; Metzler and Klafter, 2000, 2004; Zimbardo et al., 2017). Fractional generalization of Einstein’s Brownian motion and the subsequent fractional kinetic equations are believed to provide a powerful framework that can be applied to many physical systems (Perri and Zimbardo, 2007, 2012; Zimbardo and Perri, 2013; Zimbardo et al., 2015; Zimbardo and Perri, 2017). The fractional equation allows incorporating spatial and temporal effects of long-range correlations and is capable of describing both particle super-diffusion (i.e., persistent random walks), and sub-diffusion (anti-persistent random walks) (Zimbardo et al., 2006), while the well-known Fermi acceleration dynamics scales as $V(t) \sim t^{1/3}$ in the true random classical case.

These observations ultimately confirm the idea that heliospheric structures, such as CSs, FRs and plasmoids, have a complex topology and, in general, are far from being planar or spherically-symmetric. Due to both non-stationarity and non-uniformity of the solar wind, acceleration processes can take place

everywhere where the electric field is present and the scales of magnetic inhomogeneities are of the order of the proton or electron gyroradii. Plasma turbulence complexly links stream propagation, magnetic reconnection and particle energization in a puzzling multi-scale and multi-process scenario. Owing to strong nonlinearities, numerical simulations are important to properly interpret *in-situ* observations.

Obviously, fully three-dimensional (3D) models retain the complete physical picture of the described phenomena. Indeed, small-scale phenomena (e.g., secondary magnetic reconnection, waves/instabilities and ripples of the HCS) are hardly described within a 2D approach. However, 2D or quasi-2D models have been adopted owing to their capability to properly paint the picture of several physical phenomena, at least at a qualitative level. For example, the basic physics of magnetic reconnection is well depicted employing 2D models (Matthaeus and Lamkin, 1986; Ambrosiano et al., 1988). On the other hand, Kowal et al. (2011) stressed the importance of considering the fully 3D space and the presence of a guide field. Moreover, Kowal et al. (2012) pointed out that turbulent fluctuations superimposed to the reconnecting CSs can enhance the acceleration rate since magnetic reconnection becomes fast and a thick volume filled with several multiple reconnecting regions is formed, thus leading to a first-order acceleration mechanism. Other advanced studies have been focused on kinetic simulations, in which it is possible to describe the non-ideal mechanism leading to magnetic reconnection. Several studies, often focusing on the relativistic regime, confirmed that the first-order Fermi mechanism related to reconnection can accelerate particles to energies described by a power-law distribution (Guo et al., 2015, 2016b; Li et al., 2019; Xia and Zharkova, 2018, 2020). The fully 3D space guarantees the interplay of several wave modes and instabilities, leading to turbulence (Huang et al., 2017; Lapenta et al., 2015; Lapenta et al., 2018). The contribution of several drifts has also been analyzed by Li et al. (2017), finding that the major energization is due to the particle curvature drift along the induced electric field. The particle energization created by FR merging has recently been investigated by Du et al. (2018).

It is important to emphasize that even while 3D models include distinctive effects not included in 2D, some very important effects occur in both geometries even if details may differ. For example, multiple secondary island formation occurs even in 2D incompressible MHD (Matthaeus and Lamkin, 1986; Wan et al., 2013). Turbulence also elevates reconnection rates in 2D and 2.5D MHD and Hall MHD (Matthaeus and Lamkin, 1985, 1986; Smith et al., 2004) as well as in the more realistic 3D geometry as discussed above. While it is almost always preferable to have a 3D picture of natural phenomena, often the 2D models are preferred because they can achieve larger systems sizes and higher Reynolds numbers, these also being important and even crucial parameters in describing observations of natural processes.

We finally remark that the description of solar-wind turbulence has faced similar debates about 2D vs 3D models. The strong wavevector anisotropy of MHD turbulence with respect to the guide field (Shebalin et al., 1983),

also supported by spacecraft observations revealing the “Maltese Cross” pattern in the two-dimensional correlation function measurements of solar wind fluctuations (Matthaeus et al., 1990a), motivated the development of a two-component model, which is composed by fluctuations with wavevector parallel to the ambient magnetic field (slab) and by fluctuations with wavevector quasi-perpendicular to the ambient magnetic field (2D) (Bieber et al., 1996; Ghosh et al., 1998) (see (Oughton et al., 2017; Oughton and Matthaeus, 2020) for recent reviews on MHD turbulence in the solar wind). Moreover, numerical simulations performed in the kinetic regime showed that a 2.5D approach describes well solar-wind dynamics in the inertial range and at sub-proton scales (Servidio et al., 2014, 2015; Wan et al., 2015; Li et al., 2016; Franci et al., 2018), although it has been claimed that a fully 3D approach should be retained to properly model nonlinear couplings at large-scale in the incompressible limit (Howes, 2015). A contrasting, and even puzzling, result in the realm of kinetic PIC simulations is that averages of the electromagnetic work conditioned on local values of the current density (a rough equivalent of an Ohm’s law) behaves very similarly in 2.5D and in 3D, and, perhaps surprisingly, both behave very much like collisional MHD (Wan et al., 2016).

This part of the review follows Part I (Khabarova et al., 2020a), which, mainly focuses on providing the general information about the objects of this review and observations of non-planar magnetic structures and their association with particle acceleration. The structure of this part of the review is the following. In Sect. 2 we provide details on some models adopted in order to describe the dynamics of CSs and MIs, with particular emphasis on the formation of their fine structure. We also discuss their stability properties and overview theoretical and numerical models aimed at analyzing the impact of CSs, FRs and MIs on the transport of energetic particles, in particular on galactic cosmic rays in the heliosphere (HCS). Then, in Sect. 3 we speculate about the theoretical approaches usually employed to describe particle acceleration within contracting/merging FRs. Sect. 4 is dedicated to the description of recent advances in numerical studies of the evolution of plasma turbulence and, in particular, the appearance of numerous discontinuities representing potential reconnection and heating sites. The discussion of the results covers both high-resolution fluid (MHD and Hall MHD) and kinetic simulations. Particle acceleration in such complex environments is described in Sect.5. Finally, we summarize the discussed results and make conclusions about the past and future development of studies of CRs, FRs/plasmoids and MIs in Sect. 6.

2 Current sheets: their fine structure, stability and the ability to accelerate particles

As introduced above, FRs, blobs/plasmoids/bubbles, CSs and MIs are ubiquitous features in the dynamics of astrophysical plasmas. In this Section, we revisit the basic dynamics of current sheets by highlighting, in particular, the formation of their fine structure and their stability properties.

One can roughly classify planar and conic current sheets as either “thick” or “thin” structures based on the ratio of their transverse scale to the proton gyroradius. In the thick CSs, electric currents are supported by plasma drift currents in circular magnetic field gradients, repeating the shapes of large-scale structures themselves. For CSs of this type, the presence of a neutral magnetic surface is not necessary and they are quite stable relative to the tearing mode. Meanwhile, crossings of thin CSs (TCSs) are characterized by the occurrence of the neutral line altogether with a strong jump of the magnetic field in their vicinity. These CSs seem to be a reservoir of free energy. Therefore, it is quite possible that these very common structures in space plasmas are responsible for the energy storage and release, magnetic reconnection, plasma acceleration and other important processes in planetary magnetospheres (Retinò et al., 2007; Ergun et al., 2020b), in the solar wind (Zelenyi et al., 2010, 2011, 2019), and the solar corona (Syrovatskiĭ, 1971).

As discussed in Part I of this review, current sheets also exhibit a fine structure. They are multi-layered, containing several TCSs embedded into the main CS of much wider thickness (Malova et al., 2017). Cascading or production of similar current sheets around the main one is a well-known process observed over a wide range of scales. In general, a conglomerate of current sheets formed around the mother current sheet and resembling the multi-scaled heliospheric plasma sheet (HPS) (see Part I) is observed. Below we describe the main physical mechanisms responsible for the formation of the fine structure of current sheets. By developing a quasi-adiabatic model, Zelenyi et al. (2004) demonstrated that CSs are multi-scaled and meta-stable structures that can be quite stable for a long time but then can spontaneously be destroyed by tearing instability. TCSs are also sensitive to the impact of a wide spectrum of kink and oblique waves, which leads to their instability in variable conditions. This process is followed by the explosive CS destruction and the release of the energy excess in a form of plasma acceleration and wave activity. Note that excited waves of different types can generally coexist also after the CS destruction. Electromagnetic turbulence can hence develop in the TCS-filled plasmas. As a result, plasma particles can be accelerated by plasma turbulence, and this mechanism is common for the magnetospheric and the solar wind plasmas.

2.1 Quasi-adiabatic model of thin current sheets in space plasmas

It should be noted that the first analytical and mathematically-simple model of a thin one-dimensional (1D) current sheet was proposed by Harris (1962). In this model, only the tangential component of the magnetic field was taken into account. Further analysis of proton dynamics in the neutral plane with the reversed magnetic field that also considered a finite but small normal magnetic field was done by Speiser (1965), who showed that in such CSs protons are demagnetized near the neutral plane and their quasi-adiabatic integral of

transverse (along z coordinate) oscillations

$$I_z = \frac{1}{2\pi} \oint p_z dz \quad (1)$$

is approximately conserved.

A semi-analytical 1D model of the TCS in the collisionless space plasma was proposed by (Zelenyi et al., 2000, 2004) based on the quasi-adiabatic description of ions with the plasma anisotropic pressure tensor and magnetized electrons in the fluid approximation. In this model, the general self-consistent system of Vlasov-Maxwell equations has the following simple form:

$$\frac{dB_x}{dz} = \frac{4\pi}{c} (j_{i,y}(z) + j_{e,y}(z)) \quad (2)$$

$$j_{i,y} = e \int v_y f_i(z, v) dv \quad (3)$$

being f_i the ion distribution function and $j_{i,y}$ the ion current density in the y -direction. The ion distribution function can be obtained at any location inside the current sheet by mapping the source distribution from the edges of the TCS to the neutral plane using Liouville's theorem; thus it can be re-written as a function of a quasi-adiabatic integral I_z . Electron current density $j_{e,y}$ can be calculated in the guiding center approach. The detailed description of the basic model and its modifications can be found in Zelenyi et al. (2011) and references therein.

Later, numerical models of TCS were adopted to verify the semi-analytical model (Zelenyi et al., 2004). Comparison of model results with experimental observations from the Cluster satellites in the Earth's magnetotail demonstrated a good agreement between them (Artemyev et al., 2009a). The application of the model to the case of the heliospheric current sheet (HCS) and similarly strong current sheets (SCSs) in the solar wind was made by Malova et al. (2017). The general configuration of the model is shown in Fig. 1 (a). Particles move from current sheet edges toward the neutral plane. Within the CS plane, particles are demagnetized and move along serpentine-like orbits; afterwards, they go outward and carry the electric current across the current sheet. Since electrons are magnetized, their curvature electric current dominates in the plane of the neutral sheet. As a result, the electron-determined current flows within a thin current sheet is embedded in a thicker current sheet created by protons, as it is shown schematically in Fig. 1 (b). This is in good accordance with observations showing that TCSs are located within much thicker Harris-like background current sheets which can be called plasma sheets analogous to the HPS (see Malova et al. (2018) and Figure 1 of Part I).

Figure 1(c) displays self-consistent solutions for the module of the tangential component of the magnetic field as a function of the z coordinate. Here the parameter n_r is the relative concentration of quasi-adiabatic particles; it varies from 1 to 0. The black curve corresponds to the case when all particles are quasi-adiabatic ($n_r = 1$ or 100%) and the green curve corresponds to the opposite case of a pure Harris-like current sheet with the isotropic pressure

distribution ($n_r = 0$ or there is 0% of quasi-adiabatic particles). From panels (b) and (d) of Fig. 1, one can easily figure out that the background current sheet has a very smooth and wide profile. The corresponding green curve has a width of about 10^2 proton gyro-radii, and the ordered thinner proton current peak is manifested in the central part of CS. The electron current is the narrowest, and at some parameters, it is seen in the region of the neutral plane [Fig. 1(b)]. Panel (b) of Fig. 1 also shows that a very narrow $|\mathbf{B}|$ peak of the proton current becomes noticeable for $n_r \geq 0.3$ (see the case with $n_r = 0.3$, shown by the dark blue curve).

One may conclude that in TCSs electrons may carry only a part of the azimuthal electric current due to curvature drifts, whereas the main part of the cross-sheet current is carried by demagnetized quasi-adiabatic protons (Zelenyi et al., 2011; Malova et al., 2017, 2018). As seen from Figs. 1 (b-c), the central part of the multi-scale current sheet is a very narrow structure with a thickness of several proton Larmor radii ρ_L , while the wider background part of the SCS with negligible current density has a thickness $L = 100\rho_L$. Therefore Fig. 1 (b-c) demonstrate the multiscale character of a thin current configuration embedded in a much thicker plasma sheet in which the plasma density tends to have an almost uniform distribution, while the current density vanishes in the same region.

2.2 Current sheet dynamics and formation of multiple current sheets in the solar wind

The current sheet filamentation *via* tearing instability was proposed as a key factor of sub-storm activity in the Earth's magneto-tail since the early papers (e.g., Coppi et al. (1966)), in which the 1D Harris sheet equilibrium solution has been used for the analysis of current sheets stability. It further was shown that the existence of a finite but small normal component B_z in the current sheet can lead to a strong stabilizing effect due to the electron compressibility (see, e.g. Schindler (1979) and references therein). Many other possible mechanisms of sub-storm triggering were proposed to solve this problem (see details in the review by Zelenyi et al. (2010)). In particular, the stochastic particles motion (Buechner and Zelenyi, 1989; Kuznetsova and Zelenyi, 1991), pitch angle scattering (Coroniti, 1980), transient electrons (Sitnov et al., 1997, 2002), and current-driven instabilities (Lui, 1996, and references therein) were considered and analyzed in detail.

Meanwhile, it was later shown that all these mechanisms cannot destroy the strong stabilization effect of electrons, at least in the Harris-like current-sheet case (Pellat et al., 1991). Over time this paradoxical result had lead to the loss of interest of scientists in the tearing mode as a trigger of substorm onset (Zelenyi et al., 2011). In two decades, experimental observations of the Earth's magnetotail performed during the Cluster mission time made clear that magnetotail TCSs are principally different from well-known Harris-like

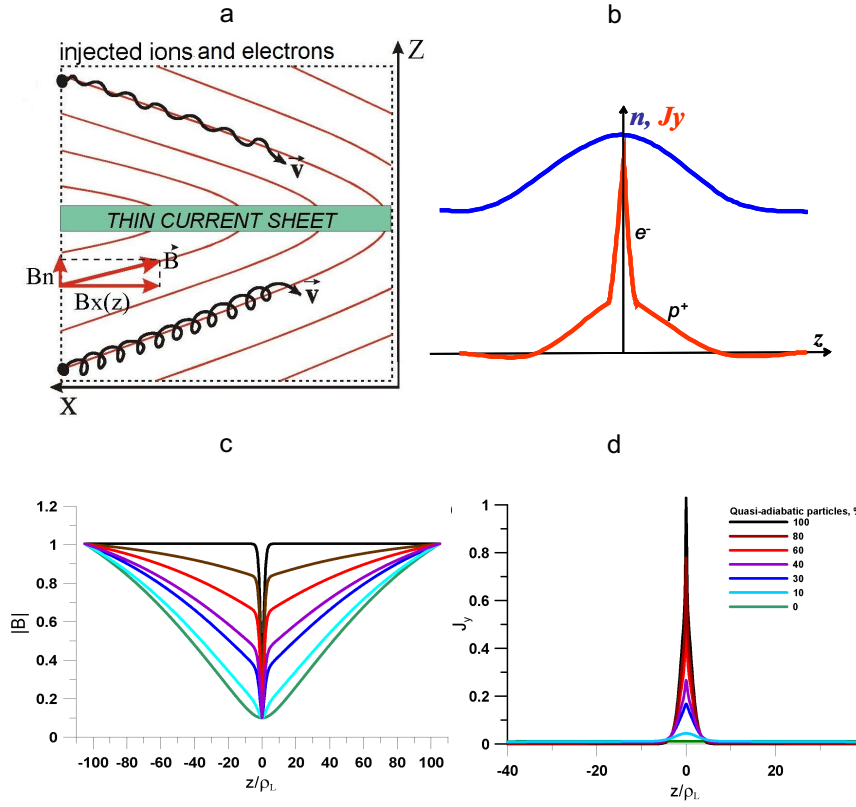


Fig. 1: (Color online) Multi-scaled structure of SCSs/HCS: (a) General scheme of the model (adapted from Zelenyi et al. (2006)); (b) Schematic view of the embedding of current sheets (adapted from Zelenyi et al. (2006)). Multiscale CSs are embedded in the thicker plasma sheet in which the plasma density tends to constant at the edges, i.e. $n(L) \rightarrow n_0$. Regions of differently-dominated plasma populations can be seen; (c) Self-consistent profiles $|\mathbf{B}(z/\rho_L)|$ (adapted from Malova et al. (2017)); (d) Current density profile $J_y = j_y/enV_{D1}$ within the current sheet (adapted from Malova et al. (2017)). Colored curves correspond to different densities of quasi-adiabatic particles (as a percentage of the total number of particles). Transverse coordinate z showed in the abscissa is normalized to the proton gyroradius ρ_L , $|\mathbf{B}|$ and n are normalized to their values at $100z/\rho_L$.

configurations, therefore some additional factors may control the TCS stability (Runov et al., 2005, 2006; Zelenyi et al., 2003).

These results enabled a solution to the old problem, finally forming the paradigm that associates the substorm activity with the onset of tearing-type instability. The idea that magnetotail current sheets can be unstable only at some narrow regions in the parameter space was for the first time formulated

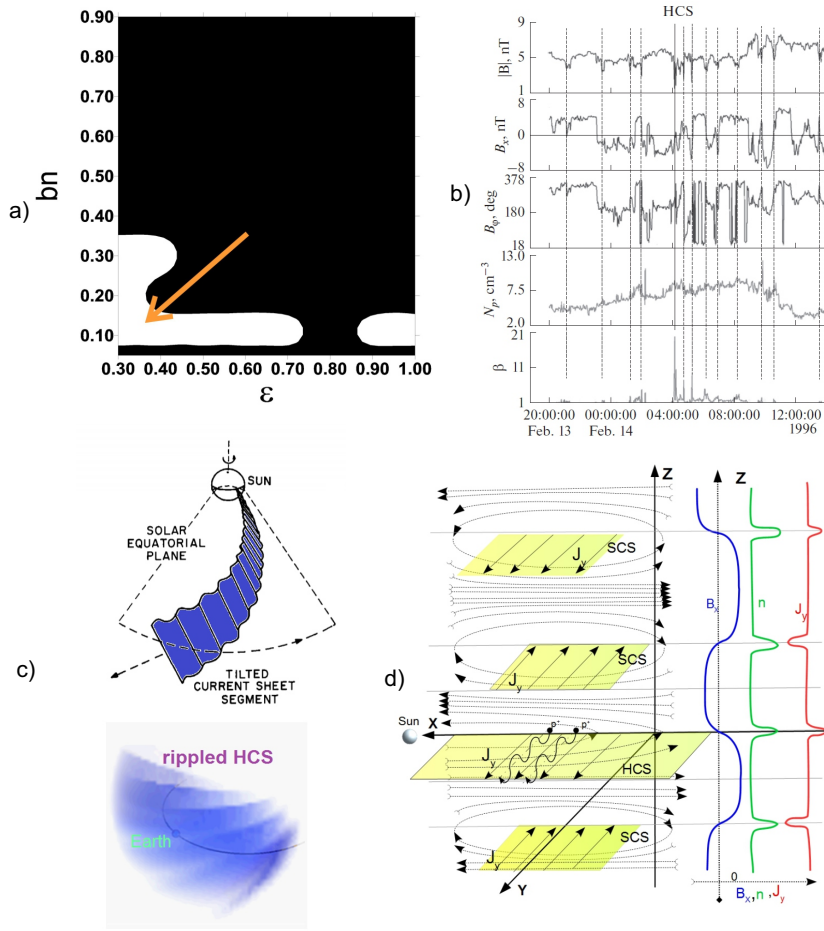


Fig. 2: Current sheet dynamics and multi-sheet current configurations in the solar wind: observations and theoretical interpretations. a) Stable (black) and unstable (white) regions of a thin current sheet under the tearing mode, according to the model by Zelenyi et al. (2008) (adapted from Zelenyi et al. (2008)). Red arrow indicates a possible direction of the switch of the current sheet state from the stable to unstable. b) Example of observations of the prolonged HPS/HCS crossing at the Earth's orbit (reproduced from Malova et al. (2018)). From top to bottom: the magnitude of the IMF, the radial component of the IMF in the GSE coordinate system, the azimuthal angle of the IMF, the solar wind density, and the plasma beta. Multiple strong current sheets (indicated by vertical lines) are observed within the HPS. c) HCS ripples as predicted by Behannon et al. (1981) (upper panel) and observed in the solar wind via interplanetary scintillations (lower panel) (adapted from Khabarova et al. (2015)). d) Configuration of the magnetic field lines in the vicinity of the HCS (central yellow plane) surrounded by magnetic islands/blobs (left sketch), and corresponding reconstructed profiles of the magnetic field B_x , the electric current j_y and the plasma density n .

by Galeev and Zelenyi (1976). Further, Zelenyi et al. (2008) investigated this effect in details in the frame of a quasi-adiabatic model of TCS supported by satellite observations. It was concluded that the thinning of the magnetotail current sheet is followed by an increase of the anisotropy in the ion and electron distribution functions. Hence, finally, the magnetotail becomes a new metastable equilibrium with a TCS in the equatorial plane that can spontaneously be destroyed, being accompanied by the processes of fast magnetic reconnection.

Both observational and theoretical studies allow suggesting that tearing instability and magnetic reconnection of thin current sheets can play a substantial role in the formation of a system of multiple current sheets in the solar wind (see, e.g., Wang et al. (1998); Réville et al. (2020) and references therein). More recently, the stability of tearing mode and the onset of fast magnetic reconnection have received a detailed attention (Tenerani et al., 2015a,b; Pucci et al., 2017, 2018).

As discussed in Part I, Section 2.3.1, crossings of sector boundaries are often associated with prolonged observations of multiple thin current sheets generally following the heliospheric plasma sheet (HPS) shape (see also Liu et al. (2014)). These current sheets with a thickness of several proton gyroradii (Behannon et al., 1981; Khabarova et al., 2015; Xu et al., 2015) are often called strong current sheets (mentioned above in paragraph 2.1) (see Malova et al. (2017)). A possible theoretical interpretation of such events and a typical HPS/HCS crossing observed by a 1 AU spacecraft were discussed by Malova et al. (2018). The corresponding figures are reproduced here as Fig. 2 (a) and (b), respectively.

Fig. 2 (a) shows stable and unstable regions in the parameter space, where b_n is the transverse magnetic component normalized to the total magnetic field at current sheet edges, and ε is the ratio of the thermal velocity to the drift flow plasma velocity. Stability properties of TCSs can be changed during their formation and possible evolution under changing external conditions. An example of this process is shown in Figure 2 (a) with the red arrow that indicates the direction of a possible switch of a TCS from the stable to the unstable state under evolving external conditions, following the decrease in the magnetic transverse component b_n and the relative increase in the plasma flow velocity with respect to the thermal speed (i.e. the decreasing parameter ε , see, e.g., Zelenyi et al. (2009b); Zelenyi et al. (2011)).

Figure 2 (b) depicts numerous current sheets observed within the HPS at 1 AU. The beginning of the HPS crossing is characterized by a sharp change in the azimuthal IMF angle direction that was generally stable before. It further becomes very unstable and varies many times for hours along with the corresponding signatures of current sheet crossings in the IMF components and the plasma beta until the IMF direction changes to the opposite. It was acknowledged tens of years ago that studying the nature of multiple SCSs in the solar wind is very important for the understanding of current sheet dynamics in the heliosphere. Crooker et al. (1993, 2004) proposed a mechanism of the formation of multiple current sheets due to the large-scale radial fold-

ing/bending of the HCS and magnetic tubes with a subsequent formation of giant loops, which, however, was not confirmed. Modern views on this point suggest that both the loops and HCS folding/rippling exist but at far smaller scales, produced by local dynamical processes (see Part I, Section 2.3.1).

Generally, two main hypotheses on the formation of a set of multiple current sheets in the solar wind near the HCS have been developed:

- exogenous: the solar corona is the source of current sheets in the solar wind.
- endogenous: wave and reconnection processes locally trigger multiple CSs in the HCS/HPS vicinity.

Note that, the exogenous factor may lead, e.g., to the distortion and the consequent destruction of neutral surfaces originated from the top of coronal streamers (see, e.g., Sanchez-Diaz et al. (2019), and references therein). On the other hand, the two following mechanisms can be attributed to the endogenous factors:

1. The development of wave processes as a result of the impact of non-stationary flows/streams, owing to which the HCS can possess a folded or highly rippled form with ripples crossed for tens of minutes at 1 AU (Behannon et al., 1981; Khabarova et al., 2015). The rippled HCS is shown in Figure 2(c). The upper panel is adapted from Behannon et al. (1981). They gave a correct explanation of the fine structure of the HCS/HPS, suggesting the existence of the plissé-like shape of the HCS, crossing of which may be reflected in observations of numerous current sheets. The direction of ripples was suggested to be perpendicular to the radial (sunward) direction, which indeed can be the case either at far heliocentric distances where the Parker spiral twist angle is near 90° or in front of/behind fast streams pushing the HCS (see Figure 22 and Figure 30 in Part I of the review). The lower panel in Figure 2(c) shows observational evidence for the formation of HCS ripples. It is easy to see that the crossing of a ripple can be interpreted as an intersection of pairs of current sheets with the opposite direction of the flowing electric current (Mingalev et al., 2019).
2. The development of current sheet-associated instabilities (mainly, tearing instability) in the solar wind, accompanied by magnetic reconnection and the formation of plasmoids/magnetic islands (see Gosling (2007); Ruffenach et al. (2012); Khabarova et al. (2015); Tenerani et al. (2015b,a); Pucci et al. (2017); Khabarova and Zank (2017); Adhikari et al. (2019) and Section 2.1.4. of Part I). The electric currents can flow at both internal and external surfaces of such closed structures.

It is important to note that the origin of magnetic islands and plasmoids, as well as blobs and bubbles surrounding the HCS, may be of the combined exogenous-endogenous origin (see Part I and Janvier et al. (2014)). The largest of these magnetic structures can be formed due to the splitting of streamer current sheets and subsequent magnetic reconnection during the extension and evolution of streamers in the solar wind (Somov, 2013). It is shown that multi-sheet magneto-plasma configurations are unstable in principle (Dahlburg and

Karpen, 1995), i.e. magnetic fields tend to reconnect, which leads to the formation of magnetic islands contributing to changes of the magnetic surface topology and stratification of the current system within the HCS (Zelenyi and Milovanov, 2004; Sanchez-Diaz et al., 2019). An idea about magnetic reconnection of coronal streamers above loops appeared in 1990th (see McComas et al. (1991); Antiochos and DeVore (1999); Wang et al. (2000); Somov (2013)). Later, it was suggested that coronal streamers can eject a series of sequentially arranged magnetic blobs adjacent with magnetic flux ropes into the solar wind. In the plane perpendicular to the neutral surface at the cusp of a streamer, these structures represent a chain of blobs or 2D magnetic islands that can be observed not only in-situ but also in white light (e.g., Wang et al. (2000); Song et al. (2009); Wang and Hess (2018)). This process has been modelled as well (e.g., Higginson and Lynch (2018)). Owing to the impact of the dynamical processes occurring in the surrounding plasma and the development of tearing and other instabilities, magnetic bubbles/blobs originated from the corona can be distorted, split or merged. As a result, all those structures create an HCS turbulent/intermittent environment consisting of multiple current sheets occurring within the system of numerous magnetic islands. In this perspective, it is clear that a fully 3D approach is quite important in order to properly understand the dynamics of these structures.

Figure 2(d) schematically shows a possible configuration of the HCS surrounded by several magnetic islands. On the right of the sketch, the corresponding profiles of the magnetic field, the plasma and electric current density are shown as a function of the transversal z -coordinate. Such current structures are relatively thin and can be comparable by width with the proton gyroradii. In such current configurations, electrons can be magnetized while protons move along quasi-adiabatic (serpentine-like) orbits (Zelenyi et al., 2004, 2011; Malova et al., 2017). Two protons on quasi-adiabatic trajectories are shown in Fig. 2(d) in the HCS plane.

Therefore, multiple current sheets embedded in the HPS are self-consistent structures with characteristic peaks of the plasma density, the plasma beta and the alternating direction of the electric current in the adjacent current sheets. Owing to their small thicknesses and large spatial scales, such magnetic configurations can be described in the frame of an almost one-dimensional quasi-adiabatic model (see (Zelenyi et al., 2004)) in which spatial characteristics in the direction transverse to the current sheet midplane are most important.

2.3 Oblique low-frequency electromagnetic modes and TCS stability

As described above, TCSs can become unstable when they are influenced by the electromagnetic modes propagating along the magnetic field. Meanwhile, modes with the wave vector $\mathbf{k} = k\mathbf{e}_x$ in the GSM system of coordinates represents a limiting case of a more general situation when modes propagate in the arbitrary direction with respect to the magnetic field (e.g., for $\mathbf{k} = k\mathbf{e}_y$, these are well-known kink and sausage modes (Lapenta and Brackbill, 1997;

Daughton, 1999; Büchner and Kuska, 1999)). These fluctuations could be either symmetric or asymmetric with respect to $z = 0$ plane. A lot of research were devoted to the analysis of all possible instabilities both analytical (Lapenta and Brackbill, 1997; Daughton, 1999; Yoon and Lui, 2001) and numerical (Pritchett et al., 1996; Zhu and Winglee, 1996; Büchner and Kuska, 1999; Karimabadi et al., 2003).

All these studies were limited to the case of 1D Harris equilibrium with $B_z \neq 0$. Meanwhile, it is known that real TCSs cannot be described by this model (see above). Some alternative approaches were suggested by Sitnov et al. (2004), who studied lower-hybrid drift perturbation in the y-direction, although considering electrons as a cold neutralizing background. Silin et al. (2002) studied electromagnetic perturbations in current sheets, in the limit of an infinitely thin 1D current sheet (so-called Syrovatsky's sheet). Moreover, Zelenyi et al. (2009a) showed that different values of the growth rate are possible in TCSs as a function of angle θ with respect to the direction of magnetic field lines. This implies that different types of wave modes can exist at the neutral plane of the magnetotail simultaneously to form a complex turbulent structure (Milovanov et al., 2001).

Zelenyi et al. (1998) suggested analyzing the problem from another perspective. In particular, they studied the state of the magnetotail after that all linear CS modes grew up and nonlinearly interacted with each other (see Zelenyi et al. (1998) for details about such interaction). It is important to point out that the resulting CS state keeps an intrinsic variability, i.e. modes may grow and decay, but on average, the system remains steady. Such a system is, hence, in the so-called non-Equilibrium Steady State (NESS). In the NESS state, particles (e.g., ions as suggested in Zelenyi et al. (1998)) supporting the cross-tail current in the current sheet drift through current sheet-associated magnetic turbulence and are scattered by magnetic fluctuations. The fluctuating part of the electric current is determined by this scattering and controls the parameters of magnetic fluctuations via Maxwell equations. Magnetic fluctuations, in turn, govern peculiarities of ion scattering. Therefore, the fluctuating part of the electric current and magnetic fluctuations are coupled self consistently, while the average current should have an exact value supporting the current sheet magnetic field reversal considered as a boundary condition.

Technically, methods of fractal geometry appear to be very effective to describe particle scattering in the ensemble of multi-scale magnetic fluctuations with certain fractal properties. This analysis uniquely defines the fractal measures of turbulence necessary for the self-consistency of a system. The final task is to convert these measures to the observable standard characteristics of turbulence, such as Fourier spectra. Zelenyi et al. (1998) adopted a simple assumption, namely, the Taylor hypothesis that magnetic structures are frozen into the bulk of moving plasma and their characteristics are determined by the Doppler effect in the frame of an observer/spacecraft. Bringing all these considerations together, Zelenyi et al. (1998) obtained the so-called universal shape of the spectra of magnetic fluctuations: $\delta B/B \sim k^{-7/3}$, where k is the wavenumber. Certainly, such spectral indexes are expected to exist as

“universal” only within the frequency (wavelength) domain in which the Taylor hypothesis operates. A theoretical analysis predicted that there should be well-defined spectral breaks at large- and small k boundaries of the universal interval. An analysis of numerous satellite observations brought together by Zelenyi et al. (1998) confirmed that the spectral index of $7/3$ is indeed quite common for magnetospheric processes in numerous cases.

2.4 Effects of the occurrence of current sheets, flux ropes and magnetic islands for the transport of energetic particles in the heliosphere

Beyond the importance to accelerate particles, that will be the content of next section, drift along HCS as well as drift due to gradients in and the curvature of the heliospheric magnetic field (HMF) play an integral role in the modulation of galactic cosmic rays, as evinced by more than half a century of neutron monitor (e.g. Caballero-Lopez et al., 2019, and references therein) and spacecraft observations (e.g. Gieseler et al., 2017), of cosmic-ray intensities. The characteristic 22-year cycle of alternating peaks and plateaux corresponding respectively to negative and positive heliospheric magnetic field polarities seen from neutron monitor observations can in principle be explained by invoking the drift patterns of charged particles in the heliosphere, where, in the former case positively charged cosmic rays drift Earthwards along with the heliospheric current sheet, and in the latter from the polar regions (see, e.g., Jokipii et al., 1977; Jokipii and Thomas, 1981; Burger et al., 1985; Potgieter, 2013). This has led to implementing these effects, especially CSs drift, in cosmic ray transport codes since earlier works by Jokipii and Kopriva (1979) and Kota and Jokipii (1983) as well as in subsequent studies. Implementing drift effects due to the HCS in such a code is, however, not a straightforward endeavour, and several approaches to this problem have been implemented in the past. For example, the approach of Kota and Jokipii (1983) numerically calculated the required drift velocities, while studies like those of Strauss et al. (2012) and Pei et al. (2012) numerically calculate perpendicular particle distances from a modelled HCS, using this distance as an input for an approximate expression for the current sheet drift speed which is calculated assuming a locally flat sheet (see also Burger et al. (1985)). The approach of Burger (2012) calculates drift velocities directly by assuming a transition function over the HCS and has also been successfully implemented in CR modulation studies (e.g. Engelbrecht and Burger, 2015). All of these approaches, however, treat the HCS as a differentially thin surface, doubtlessly motivated by the fact that high energy galactic cosmic rays have large Larmor radii, this being the characteristic length scale associated with drift processes in a scatter-free environment Forman et al. (1974), which are assumed to be much greater than the thickness of the current sheet. This quantity is observed to be approximately 10^4 km at 1 au, and to increase with heliocentric radial distance (see, e.g., Smith et al., 2001). Turbulence in the HMF does, however, act so as to reduce the drift scale, and hence drift effects, as has been shown theoretically (e.g.

Bieber and Matthaeus, 1997), from numerical CR modulation studies (e.g. Ferreira et al., 2003; Burger et al., 2008) and from numerical test-particle simulations of diffusion and drift coefficients (e.g. Minnie et al., 2007; Tautz and Shalchi, 2012). Various approaches have been taken to model this effect (for a review, see Burger and Visser, 2010), which imply that the assumption that drift processes would be unaffected by physical processes taking place within the finite thickness of the HCS may not always be correct. To investigate this, the turbulence-reduced drift length scale proposed by Engelbrecht et al. (2017) is used in what is to follow, as it yields results for the turbulence-reduced drift coefficient in reasonable agreement with numerical simulations of that quantity in various turbulence scenarios, and has been used successfully in *ab initio* CR modulation studies (e.g. Moloto et al., 2018). This length scale is given by

$$\lambda_A = R_L \left[1 + \frac{\lambda_{\perp}^2}{R_L^2} \frac{\delta B_T^2}{B_0^2} \right]^{-1}, \quad (4)$$

where R_L denotes the maximal Larmor radius to which this drift scale reduces to for low levels of turbulence, δB_T^2 the total transverse magnetic variance, B_0 the HMF magnitude, and λ_{\perp} the perpendicular mean free path. The inherent three-dimensionality of heliospheric magnetic turbulence has long been taken into account in the various scattering theories used to describe the diffusion of charged particles. An example of this is the study of Bieber et al. (1994), who invoke the observed composite slab/2D nature of turbulence at Earth (see, e.g., Matthaeus et al., 1990b; Bieber et al., 1996) to resolve the then long-standing issue of parallel mean free paths derived from the quasilinear theory of Jokipii (1966) for magnetostatic turbulence being considerably smaller than expected from simulations (Palmer, 1982). Since then, more advanced theories of particle scattering take this geometry into account, and require also as key inputs information as to the behaviour of turbulence power spectra (see, e.g., Matthaeus et al., 2003b; Shalchi, 2009; Ruffolo et al., 2012), being sensitive in particular to the behaviour of the 2D turbulence spectrum at low wavenumbers (Shalchi et al., 2010; Engelbrecht and Burger, 2015) (See Dundovic et al. (2020) for a recent review of theoretical models and test-particle simulations). For demonstration, as input for Eq. 4 an expression of the perpendicular mean free path derived by Engelbrecht and Burger (2015) from a scattering theory proposed by Shalchi (2010) will be employed, given by

$$\lambda_{\perp} \approx a^2 C_{-1} \lambda_{\parallel} \frac{\delta B_{2D}^2}{B_0^2} \log \left[\frac{3\lambda_{out} + 2\sqrt{\lambda_{\parallel}\lambda_{\perp}}}{3\lambda_{2D} + 2\sqrt{\lambda_{\parallel}\lambda_{\perp}}} \right], \quad (5)$$

with C_{-1} a normalisation constant for the 2D turbulence power spectrum employed in that study, $a^2 = 1/3$ a constant chosen based on the results of numerical test particle simulations of the perpendicular diffusion coefficient by Matthaeus et al. (2003b), while the parallel mean free path λ_{\parallel} is modelled using the quasilinear theory result employed by Burger et al. (2008). The quantity λ_{2D} denotes the length scale at which the break between the energy-containing and inertial ranges occurs on the 2D turbulence power spectrum, and λ_{out} the

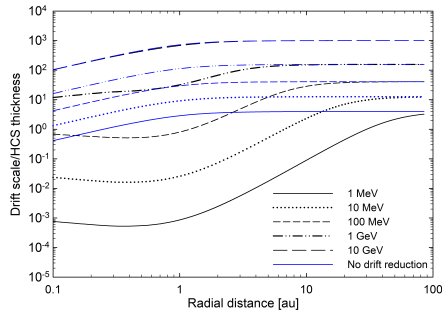


Fig. 3: Ratio of proton turbulence-reduced drift scale (black lines) and Larmor radius (blue lines) at various energies to the HCS thickness, as a function of heliocentric radial distance in the solar ecliptic plane.

length scale at which the energy range begins. The spectrum employed by Engelbrecht and Burger (2015) to derive Eq. 5 is assumed to decrease with decreasing wavenumber at scales larger than λ_{out} , following physical considerations as discussed by Matthaeus et al. (2007). Observationally, it is unclear how to model this latter quantity, given uncertainties as to observations of turbulence quantities (see, e.g., Goldstein and Roberts, 1999), and various estimates for this quantity, which can have a considerable effect on perpendicular mean free paths, have been proposed. Adhikari et al. (2017) argue that the largest turbulent injection scale should correspond with the solar rotation rate, while Engelbrecht and Burger (2013) found that scaling of this quantity being proportional to the 2D correlation scale, as modelled using the Oughton et al. (2011) turbulence transport model, would lead to the differential galactic CR proton intensities computed with their ab initio modulation code to be in reasonable agreement with observations. The quantity λ_{out} can, however, be indirectly calculated if it is assumed that magnetic island sizes can give one a measure of the 2D ultrascale Matthaeus et al. (2007). Engelbrecht (2019b) does this by making use of observed magnetic island sizes reported by Khabarova et al. (2015) and calculating corresponding values for λ_{out} from an expression for the 2D ultrascale derived from an observationally-motivated form for the 2D turbulence power spectrum (the same as that used to derive Eq. 5). The results are quite close to the scaling used by Engelbrecht and Burger (2013) for this quantity, and are used as inputs for Equations 5 and 4.

To roughly ascertain the validity of the assumption of a negligibly thin HCS, the ratio of the proton drift scale to the HCS thickness is plotted in Figure 3 as a function of heliocentric radial distance, for the purposes of simplicity in the solar ecliptic plane, and assuming a Parker HMF. For the purposes of comparison, the current sheet thickness is assumed to scale as $\sim r$, with a value of 10^4 km at Earth (Smith et al., 2001). Turbulence quantities are modelled using the simple power-law scalings employed by Engelbrecht (2019a) (based

on the turbulence transport model results of Chhiber et al. (2019)). The ratios are also only evaluated to 85 au, as these assumptions are no longer valid in the heliosheath. Fig. 3 shows ratios of the drift scale to HCS thickness for both the weak scattering (blue lines) and turbulence-reduced (black lines) cases at various energies. A ratio considerably larger than one would imply that physical processes occurring within the current sheet could safely be neglected when the transport of particles is modelled. For the weak-scattering drift length scale, this ratio is greater than unity for all proton energies considered, barring for a small distance in the very inner heliosphere at 1 MeV. When the effects of turbulence on the drift scale are taken into account, the picture changes considerably. At the highest energies, corresponding to galactic CR protons above 100 MeV, and beyond $\sim 1 - 10$ au, the ratio is very large. Below this energy, and in the very inner heliosphere, it quickly drops below unity, and considerably so at the lowest energies shown. The implication is that the finite thickness of the current sheet, as well as the detailed physics thereof, need to be taken into account when the transport of such particles is being studied. This is especially relevant given the recent interest in the effects of drift on solar energetic particles (see, e.g., Dalla et al., 2013; Marsh et al., 2013), and has to some degree been taken into account (e.g. Battarbee et al., 2018; Engelbrecht et al., 2019). It is nevertheless also surprising that relatively low-energy (≤ 100 MeV) galactic protons may also be influenced by these effects, and that the detailed physics of the HCS might also need to be incorporated in CR transport models.

3 Kinetic Transport Theory of Energetic Particle Acceleration by Small-Scale Flux Ropes

Irrespective of whether small-scale magnetic flux ropes (SMFRs) originate in a turbulent plasma through magnetic reconnection at large-scale (primary) current sheets or because of the presence of a significant guide/background magnetic field in the turbulent plasma, they form a dynamic turbulence component that generates electric fields through processes like contraction and merging (reconnection) of neighbouring SMFRs that can accelerate particles. Evidence from simulations suggest an efficient acceleration of charged particles traversing regions filled with dynamic SMFRs that can result in power-law spectra for energetic particles as first pointed out by Matthaeus et al. (1984) and Ambrosiano et al. (1988) and confirmed later by many others such as Gray and Matthaeus (1992); Dmitruk et al. (2004a); Drake et al. (2006, 2010, 2013); Li et al. (2015, 2017, 2018).

Theoretical explanation of the main SMFR acceleration mechanisms in the simulations often rely on kinetic transport theories constructed based on the first and second adiabatic invariants combined with magnetic flux conservation (e.g., Drake et al. (2006, 2013); Zank et al. (2014)), guiding center kinetic transport theory (e.g., Dahlin et al. (2016, 2017)), and the closely related focused transport theory (le Roux et al., 2015, 2018; Li et al., 2018). These

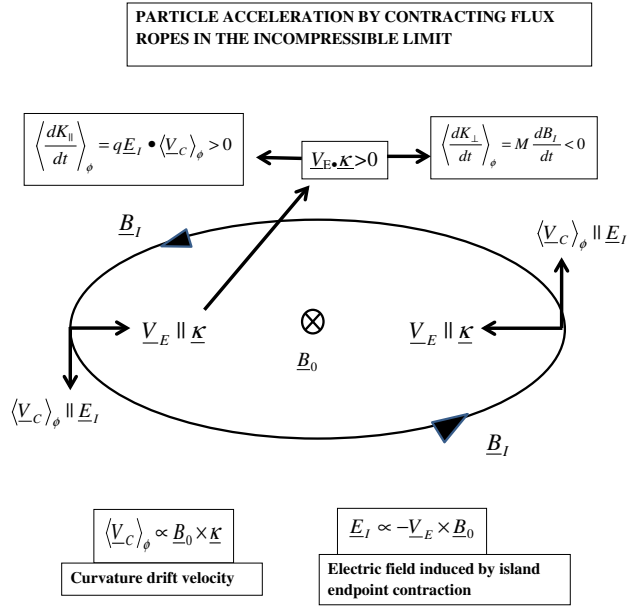


Fig. 4: A schematic diagram of energetic ion acceleration by a contracting quasi-2D SMFR in the incompressible limit (reproduced from le Roux et al. (2018)). Shown is the island (twist) magnetic field component \mathbf{B}_I of the SMFR structure in the 2D plane perpendicular to the locally uniform guide field (axial) component \mathbf{B}_0 of the SMFR pointing into the page. \mathbf{V}_E is the contraction velocity (plasma drift velocity) at the endpoints of the island, and $\boldsymbol{\kappa} = (\mathbf{b} \cdot \nabla) \mathbf{b}$ is the magnetic curvature vector which points in the same direction as the contraction velocity. Thus, for a contracting island $\mathbf{V}_E \cdot \boldsymbol{\kappa} > 0$. This ensures parallel kinetic energy gain from curvature drift acceleration by the in-plane electric field $\mathbf{E}_I \approx -\mathbf{V}_E \times \mathbf{B}_0$ induced by contraction because $q\mathbf{E}_I \cdot \langle \mathbf{V}_C \rangle_{\phi} \propto \mathbf{V}_E \cdot \boldsymbol{\kappa} > 0$, where $\langle \mathbf{V}_C \rangle_{\phi}$ is the curvature drift velocity, but perpendicular kinetic energy loss from Lagrangian betatron acceleration (combination of betatron and grad-B drift acceleration) because $M dB/dt \propto -\mathbf{V}_E \cdot \boldsymbol{\kappa} < 0$, where M is the magnetic moment (see Eq. (6) and its discussion).

theoretical approaches, besides providing familiar non-resonant acceleration concepts for SMFRs, also show promise in reproducing simulation results of acceleration on macro scales (scales larger than the magnetic island size) where the limitation of nearly gyrotropic particle phase angle distributions inherent in these approaches is less problematic (e.g., Li et al. (2018)). This opened up the possibility that such kinetic transport theories can be used to model particle acceleration by SMFRs on large scales in the solar wind, which is computationally beyond the capability of full kinetic particle simulations of acceleration especially.

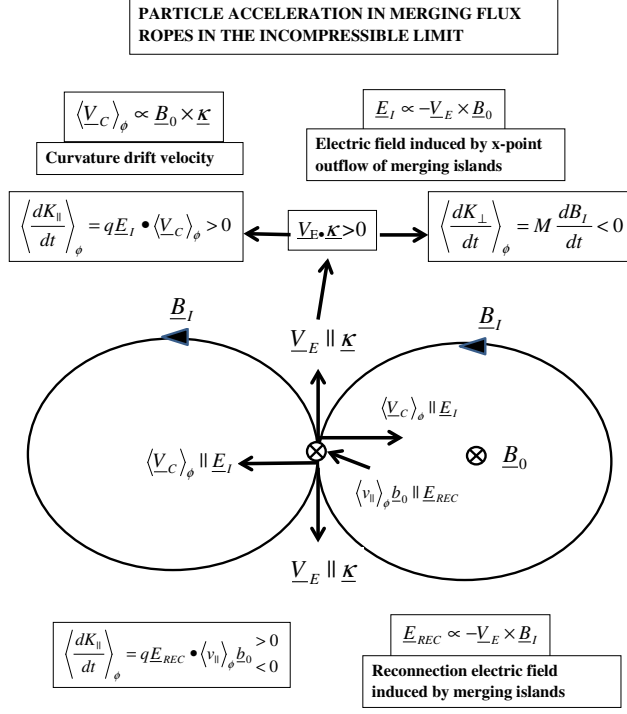


Fig. 5: A schematic diagram of ion acceleration by two merging (reconnecting), quasi-2D flux ropes in the incompressible limit (reproduced from le Roux et al. (2018)). Shown is the island magnetic field \mathbf{B}_I in the 2D plane perpendicular to a uniform guide field component \mathbf{B}_0 pointing into the page. \mathbf{V}_E is the x-point plasma outflow drift velocity in the merging area at the center of the merging magnetic islands pointing in the same direction as the magnetic curvature vector $\boldsymbol{\kappa} = (\mathbf{b} \cdot \nabla)\mathbf{b}$. Thus, in the merging region (reconnecting area) $\mathbf{V}_E \cdot \boldsymbol{\kappa} > 0$, resulting in parallel kinetic energy gain from curvature drift acceleration and perpendicular kinetic energy loss from Lagrangian betatron acceleration (see Eq. (6) and the caption of Figure 4). In the center of the merging area, the reconnection electric field $\mathbf{E}_{REC} = -\mathbf{V}_E \times \mathbf{B}_I$ points into the page. Energetic particle guiding center motion along/against \mathbf{B}_0 results in parallel kinetic energy gain/loss from the reconnection electric field.

This promise prompted Zank et al. (2014) and le Roux et al. (2015, 2018) to develop kinetic focused transport theories that unify the main non-resonant SMFR acceleration mechanisms identified in simulations. Expressed in terms of guiding center kinetic theory, the main acceleration mechanisms are: (i) parallel guiding center motion acceleration by the parallel reconnection electric field generated when neighboring SMFRs form secondary (small-scale) reconnecting current sheets between them to merge (e.g., Oka et al. (2010)), (ii) curvature drift acceleration by the motional electric field generated when

SMFRs contract or merge (e.g., Drake et al. (2006, 2013); Li et al. (2017, 2018)), (iii) Lagrangian betatron acceleration which involves magnetic moment conservation when the magnetic field strength in the plasma drift flow frame slowly varies in time and space. This mechanism includes grad-B drift acceleration by the motional electric field generated in contracting and merging SMFRs (e.g., Dahlin et al. (2016, 2017)). In focused transport theory the same acceleration mechanisms manifest in terms of non-uniform plasma flow effects in SMFRs. In this context the main SMFR acceleration mechanisms identified in kinetic particle simulations are SMFR compression acceleration, SMFR incompressible parallel shear flow acceleration referring to the SMFR shear flow tensor in the limit of a SMFR flow with a zero divergence, while acceleration by the parallel reconnection electric field is the same as in guiding center kinetic theory (Zank et al., 2014; le Roux et al., 2015, 2018). Having studied how the SMFR acceleration mechanisms in focused transport theory and guiding center kinetic transport theory are connected, le Roux et al. (2018) concluded that: (i) SMFR compression acceleration can be viewed as combining curvature drift momentum gain from the motional electric field induced by magnetic island compression with Lagrangian betatron momentum gain (momentum gain from unified betatron and grad-B drift acceleration) due to the increasing magnetic field strength resulting from magnetic island compression (magnetic-island-containing area shrinks as a result). This mechanism is illustrated diagrammatically in Figure 6. (ii) SMFR incompressible parallel shear flow acceleration can be interpreted as combining curvature drift momentum gain in the motional electric field generated by magnetic island contraction or merging with competing Lagrangian betatron momentum loss from the decreasing magnetic field strength resulting from magnetic island contraction or merging (magnetic-island-containing area is conserved). For illustration of shear-flow acceleration in contracting magnetic islands, see Figure 4, and in merging magnetic islands, see Figure 5. Figure 5 also illustrates parallel guiding center motion acceleration by the parallel reconnection electric field generated in the merging process. (iii) Focused transport theory also includes an acceleration mechanism connected to parallel guiding center motion momentum gain or loss from the non-inertial force associated with the parallel component of the acceleration of the plasma flow in SMFRs (le Roux et al., 2018). This mechanism can be traced back as being part of the term in guiding center kinetic theory describing the effect of the electric field on drift inertia that also is the source of the curvature drift acceleration mechanism. From the SMFR focused transport equations, diffusive Parker type transport equations were derived assuming that on large spatial scales in the solar wind pitch-angle scattering will inevitably result in near-isotropic accelerated energetic particle distributions (the diffusive approximation). Accordingly, the distributions were expanded out to the second anisotropic moment in pitch-angle space using Legendre polynomials (Zank et al., 2014; le Roux et al., 2015). By inspecting the SMFR focused transport equation it is clear that SMFR compression acceleration, first advocated by Zank et al. (2014) and later also by le Roux et al. (2015, 2018); Li et al. (2018); Du et al. (2018), can be considered as the only true

1st order Fermi SMFR acceleration mechanism because it involves energy gain without competing energy losses. In the Parker transport equation limit, however, SMFR compression acceleration appears to be a 1st order Fermi acceleration only in terms of the dominating isotropic part of the distribution function because SMFR compression acceleration also contributes to 2nd order Fermi acceleration through second anisotropic moment of the particle distribution (le Roux et al., 2018). Because the second moment of the distribution function is small compared to the dominating isotropic part of the distribution function, the net compression acceleration for the total distribution function still yields 1st Fermi acceleration mechanism consistent with the focused transport equation. In contrast, SMFR incompressible parallel shear flow acceleration in the Parker transport equation is intrinsically a second order Fermi acceleration mechanism during significant pitch-angle scattering with net acceleration originating from the second anisotropic moment in the particle distribution expansion. In the focused transport equation this mechanism acts like a 1st order Fermi acceleration mechanism when pitch angle scattering is weak because shear-flow acceleration tends to beam particles along the magnetic field so that energy losses become negligible. This is consistent with discussions by Drake et al. (2010) of incompressible magnetic island contraction leading to 1st order Fermi acceleration because the betatron energy losses are negligible compared to curvature drift acceleration when pitch-angle scattering is weak. SMFR parallel guiding center motion acceleration by both the parallel reconnection electric field force and by the parallel component of the non-inertial force associated with the acceleration of the plasma flow also yield 2nd order Fermi acceleration in the Parker transport equation limit of focused transport theory, but with the difference that net acceleration comes from the 1st anisotropic moment of the particle distribution expansion. Thus, for a purely isotropic particle distribution only first Fermi SMFR acceleration will be operative (see also, Drake et al. (2010)), while the other mechanisms need a distribution with a pitch-angle anisotropy to yield a net acceleration effect.

3.1 The Small-scale Flux Rope Acceleration Mechanisms

3.1.1 A Guiding center kinetic theory perspective

SMFRs detected near Earth have cross sections of $L_I \sim 0.01 - 0.001 AU$ (M. L. Cartwright, 2010; Khabarova et al., 2015) where energetic protons, e.g., have gyro-radii $r_g \ll L_I$ for a wide range of energies that easily includes energies in the MeV range. Thus, standard guiding center kinetic theory, which is restricted to gyro-radii much less than scale of the electromagnetic field in the plasma, is well suited for modeling energetic particle acceleration in SMFR regions up to several MeV as observed (e.g., Khabarova and Zank (2017)). In guiding center kinetic theory, the gyro-phase-averaged rate of change in kinetic energy for energetic charged particles interacting with dynamic SMFRs can be expressed in different ways:

$$\begin{aligned}
\left\langle \frac{dK}{dt} \right\rangle_{\phi} &\approx \left[q\mathbf{E} \cdot \left(v_{\parallel}\mathbf{B} + mv_{\parallel}\mathbf{b} \times \frac{d\mathbf{b}}{dt} + \frac{mv_{\parallel}^2}{qB}\mathbf{b} \times \boldsymbol{\kappa} \right) \right]_{\parallel} \\
&+ \left[M \frac{\partial B}{\partial t} + q\mathbf{E} \cdot \left(\frac{M}{q} \frac{\mathbf{B} \times \nabla \mathbf{B}}{B^2} + \frac{M}{q} (\nabla \times \mathbf{b})_{\parallel} \mathbf{b} \right) \right]_{\perp} \approx \\
&\left[qE_{\parallel}v\mu + mv\mu \left(\mathbf{V}_E \cdot \frac{d\mathbf{b}}{dt} \right) + mv^2\mu^2 (\mathbf{V}_E \cdot \boldsymbol{\kappa}) \right]_{\parallel} \\
&+ \left[(1 - \mu^2) M' \left(\frac{\partial B}{\partial t} + (\mathbf{V}_E \cdot \nabla) B \right) + (1 - \mu^2) B \frac{dM'}{dt} \right]_{\perp} \approx \\
&\left[qE_{\parallel}v\mu - mv\mu \left(\frac{d\mathbf{V}_E}{dt} \cdot \mathbf{b} \right) + mv^2\mu^2 (\mathbf{V}_E \cdot \boldsymbol{\kappa}) \right]_{\parallel} \\
&+ \left[-mv^2 \frac{1}{2} (1 - \mu^2) [(\mathbf{V}_E \cdot \boldsymbol{\kappa}) + (\nabla \cdot \mathbf{V}_E)] \right]_{\perp}
\end{aligned} \tag{6}$$

where q is the net particle charge, v_{\parallel} is the parallel guiding velocity component, \mathbf{b} is the unit vector along the SMFR magnetic field, $\boldsymbol{\kappa} = (\mathbf{b} \cdot \nabla)\mathbf{b}$ is its magnetic curvature, M is the magnetic moment of a gyrating particle, $\mathbf{E} \cdot \mathbf{b} = E_{\parallel}$ is the parallel reconnection electric field component associated with merging SMFR pairs, μ is the cosine of the particle pitch angle, \mathbf{V}_E is the electric field drift (plasma drift) velocity (velocity at which the SMFR magnetic field is contracting or merging), and M' is the maximum magnetic moment (magnetic moment when $\mu = 0$).

In Eq. (6), first and second line, the basic SMFR acceleration mechanisms are grouped in terms of parallel kinetic energy changes (terms in first square bracket) and perpendicular kinetic energy changes (terms in second square bracket). The mechanisms are: (1) Parallel guiding center motion acceleration by the parallel reconnection electric field component E_{\parallel} generated in reconnection regions between merging neighbouring SMFRs (first term in first square bracket), (2) the effect of the electric field force on the drift inertia term minus curvature drift acceleration (second term in first square bracket in which $d/dt = \partial/\partial t + (\mathbf{V}_E \cdot \nabla)$), (3) curvature drift acceleration by the motional electric field induced by contracting or merging SMFRs (third term in the first square bracket), (4) betatron acceleration due to time variations in the SMFR magnetic field strength (first term in the second square bracket), (5) grad-B drift acceleration by the motional electric field induced by contraction and merging of SMFRs (second term in the second square bracket) and, (6) parallel drift acceleration by $E_{REC\parallel}$ (the last term in second square bracket). Direct comparison of the terms in the first two lines of Eq. (6) with the corresponding terms in the third and fourth lines reveals that one can express the curvature drift acceleration term in terms of $\mathbf{V}_E \cdot \boldsymbol{\kappa}$ (advection of curved SMFR magnetic field at plasma drift velocity), and the grad-B drift acceleration term in terms of $(\mathbf{V}_E \cdot \nabla)B$ (advection of the perpendicular gradient in SMFR magnetic field strength at the plasma drift velocity). This

version of the grad-B drift acceleration term can be combined with the betatron acceleration term into a Lagrangian betatron acceleration expression $M'dB/dt = M'(\partial B/\partial t + (\mathbf{V}_E \cdot \nabla)B)$ that tracks the time and spatial variations in the SFMR magnetic field strength B following the SMFR flow due to contraction or merging processes (first two terms in second square bracket, in line three of Eq. (6)) (e.g., Dahlin et al. (2016, 2017)). Comparison of the last terms in line two and line four indicates that approximate conservation of the magnetic moment M requires a small E_{\parallel} value. Furthermore, comparing the terms in the fourth line with those in the sixth line of Eq. (6) reveals that the Lagrangian betatron acceleration expression can be related to a combination of the $\mathbf{V}_E \cdot \boldsymbol{\kappa}$ and the $\nabla \cdot \mathbf{V}_E$ terms, assuming approximate magnetic moment conservation (i.e. a small E_{\parallel} -value). Thus, Lagrangian betatron acceleration is a competition between incompressible SMFR contraction or merging ($\mathbf{V}_E \cdot \boldsymbol{\kappa} > 0$) resulting in energy loss because $dB/dt < 0$ and compressible contraction or merging ($\nabla \cdot \mathbf{V}_E < 0$) resulting in energy gain because $dB/dt > 0$. Inspection of the middle term in the first square bracket and the corresponding middle terms in lines 3 and 5 of Eq. (6) reveals how the drift inertia term in line one was converted into a term modelling parallel guiding center motion acceleration by the parallel component of the non-inertial force associated with the acceleration of the plasma drift velocity $d\mathbf{V}_E/dt$.

Combining the first two terms of the fifth line and separately the last term in the fifth line with the first term in the sixth line of Eq. (6), results in the expression

$$\left\langle \frac{dK}{dt} \right\rangle_{\phi} \approx v\mu \left(q\mathbf{E}_{REC} - m \frac{d\mathbf{V}_E}{dt} \right) \cdot \mathbf{b} + mv^2 \frac{1}{2} (3\mu^2 - 1) (\mathbf{V}_E \cdot \boldsymbol{\kappa}) - mv^2 \frac{1}{2} (1 - \mu^2) (\nabla \cdot \mathbf{V}_E) \quad (7)$$

The combined term containing $\mathbf{V}_E \cdot \boldsymbol{\kappa}$ in Eq. (7) unifies curvature drift acceleration with Lagrangian betatron and parallel drift acceleration, but it seems that the last term associated with $\nabla \cdot \mathbf{V}_E$ combines Lagrangian betatron acceleration with parallel drift acceleration only without a contribution from curvature drift acceleration. The latter raises a question because this contradicts the standard Parker cosmic-ray transport equation in which the $\nabla \cdot \mathbf{V}_E$ -term has been shown to combine curvature drift acceleration with Lagrangian betatron and parallel drift acceleration (Kota, 1977; G. M. Webb, 1981). By introducing the shear flow tensor into the bottom line of equation Eq. (6) using the relationship

$$\mathbf{V}_E \cdot \boldsymbol{\kappa} = -\mathbf{b} \cdot (\mathbf{b} \cdot \nabla) \mathbf{V}_E = - \left[b_i b_j \sigma_{ij} + \frac{1}{3} (\nabla \cdot \mathbf{V}_E) \delta_{ij} \right] \quad (8)$$

where we relate the magnetic curvature advection term, $\mathbf{V}_E \cdot \boldsymbol{\kappa}$, to the parallel shear-flow term, $\mathbf{b} \cdot (\mathbf{b} \cdot \nabla) \mathbf{V}_E$, which in turn is expressed in terms of the shear-flow tensor σ_{ij}

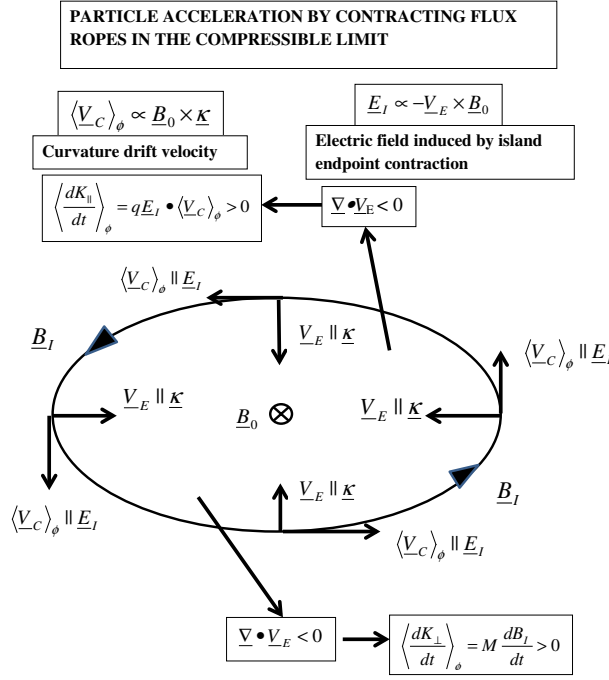


Fig. 6: A schematic diagram of ion acceleration in a compressible contracting quasi-2D SMFR (reproduced from le Roux et al. (2018)). Shown is the island magnetic field (twist component) B_I in the 2D plane perpendicular to a uniform guide field component B_0 pointing into the page. In the compressible limit the divergence of the contraction velocity $\nabla \cdot \mathbf{V}_E < 0$ results in perpendicular kinetic energy gain of energetic particles from the Lagrangian betron acceleration term $M dB/dt \propto -\nabla \cdot \mathbf{V}_E > 0$ (see Eq. (6) and its discussion) because the island magnetic field strength increases with time (Eq. (6)). Since $\mathbf{V}_E \cdot \boldsymbol{\kappa} > 0$ for compressible contraction, there is also parallel kinetic energy gain from curvature drift acceleration, but because $|\nabla \cdot \mathbf{V}_E| \gg \mathbf{V}_E \cdot \boldsymbol{\kappa} > 0$ in the compressible limit, perpendicular kinetic energy gain from Lagrangian betatron acceleration is expected to be dominant.

$$\sigma_{ij} = \frac{1}{2} \left[\frac{\partial V_{Ei}}{\partial x_j} + \frac{\partial V_{Ej}}{\partial x_i} - \frac{2}{3} (\nabla \cdot \mathbf{V}_E) \delta_{ij} \right] \quad (9)$$

one finds that

$$\begin{aligned} \left\langle \frac{dK}{dt} \right\rangle_\phi &\approx v\mu \left(q \mathbf{e}_{REC} - m \frac{d\mathbf{V}_E}{dt} \right) \cdot \mathbf{b} - mv^2 (3\mu^2 - 1) \mathbf{b} \cdot (\mathbf{b} \cdot \nabla) \mathbf{V}_E \\ &\quad - \frac{1}{3} mv^2 (\nabla \cdot \mathbf{V}_E) + \frac{1}{3} mv^2 \frac{1}{2} (3\mu^2 - 1) (\nabla \cdot \mathbf{V}_E) \end{aligned} \quad (10)$$

In Eq. (10) the $\mathbf{b} \cdot (\mathbf{b} \cdot \nabla) \mathbf{V}_E$ -term can be viewed as a combination of curvature drift acceleration with Lagrangian betatron and parallel drift acceleration acting collectively as plasma drift parallel shear flow acceleration in SMFRs. The first $\nabla \cdot \mathbf{V}_E$ -term in Eq. (9) is exactly the $\nabla \cdot \mathbf{V}_E$ -term appearing in the standard Parker cosmic-ray transport equation that has been shown before to combine curvature drift acceleration with Lagrangian betatron and parallel drift acceleration. The last $\nabla \cdot \mathbf{V}_E$ -term in Eq. (10) depends on the factor $(3\mu^2 - 1)$ just like the $\mathbf{b} \cdot (\mathbf{b} \cdot \nabla) \mathbf{V}_E$ -term, providing evidence that it too unifies curvature drift acceleration with Lagrangian betatron and parallel drift acceleration. The difference between the two $\nabla \cdot \mathbf{V}_E$ -terms is that the first term accelerates the isotropic part of the distribution function while the second term affects the energy of particles belonging to the anisotropic part of the particle distribution as discussed above (for more details, see le Roux et al. (2018)).

3.1.2 The Connection Between Guiding Center Kinetic and Focused Transport Theory

By doing the substitution $\mathbf{V}_E = \mathbf{U}_\perp$ (which follows from specifying the macroscale electric field in contracting and merging SMFRs as the induced motional electric field $\mathbf{E} = -\mathbf{U} \times \mathbf{B}$ where \mathbf{U} is the plasma flow velocity in SMFRs) in Eq. (10), we get the expression

$$\begin{aligned} \left\langle \frac{dK}{dt} \right\rangle_\phi &= v\mu \left(q\mathbf{E} - m \frac{d\mathbf{U}_\perp}{dt} \right) \cdot \mathbf{b} - \frac{1}{2} (1 - \mu^2) (\nabla \cdot \mathbf{U}_\perp) \\ &\quad - \frac{1}{2} (3\mu^2 - 1) \mathbf{b} \cdot (\mathbf{b} \cdot \nabla) \mathbf{U}_\perp \end{aligned} \quad (11)$$

This expression reveals the close connection between standard guiding-center kinetic theory and focused transport kinetic theory that we use to model particle acceleration by dynamic small-scale flux ropes because, according to focused transport theory, the relative momentum rate of change is given by

$$\begin{aligned} \frac{1}{p} \left\langle \frac{dp}{dt} \right\rangle_\phi &= \mu \left(\frac{q\mathbf{E}}{p} - \frac{1}{v} \frac{d\mathbf{U}}{dt} \right) \cdot \mathbf{b} - \frac{1}{2} (1 - \mu^2) (\nabla \cdot \mathbf{U}) \\ &\quad - \frac{1}{2} (3\mu^2 - 1) \mathbf{b} \cdot (\mathbf{b} \cdot \nabla) \mathbf{U} \end{aligned} \quad (12)$$

The main difference is that guiding-center kinetic theory describes particle acceleration in terms of the non-uniform plasma drift velocity $\mathbf{V}_E = \mathbf{U}_\perp$, whereas focused transport theory does it in terms of the total non-uniform plasma flow velocity in SMFRs. Thus, from the perspective of focused transport theory, we have four SFMR acceleration mechanisms. From left to right in Eq. (12) they are acceleration by the parallel reconnection electric field force, the parallel non-inertial force due to the acceleration of the SMFR flow,

compression of the SMFR flow, and parallel SMFR shear flow. These mechanisms form the basis of our focused and Parker transport theories for energetic particle acceleration by and propagation through a field of dynamic SMFRs.

3.2 Focused and Parker Transport Equations for Particle Acceleration by SMFRs

By applying standard perturbation analysis to the focused transport equation containing Eq. (12) we derived a modified focused transport equation that models how energetic particles respond in a statistical average sense on large spatial scales to both the non-uniform solar wind flow and interplanetary magnetic field, and to a collection of dynamic SMFRs advected with the solar wind flow (le Roux et al., 2015, 2018). The derivation was done assuming that SMFR dynamics occur mainly in a 2D plane perpendicular to the guide field (axial) component B_0 of the SMFR assuming a strong guide field (J. Birn, 1989; Dmitruk et al., 2004a). The 2D plane contains the magnetic island (twist) component B_I of the SMFR and the SMFR flow U_I determining contraction or merging of the magnetic island. In the inner heliosphere, it appears that assuming a strong guide field so that $B_I/B_0 \ll 1$ is reasonable (Smith et al., 2006). For simplicity, no distinction is made in the derivation between the guide field and the background magnetic field. This approach has some support from observational evidence that the SMFR guide field is aligned with the solar wind spiral magnetic field (Zheng and Hu, 2018). The modified focused transport equation is presented compactly as

$$\begin{aligned}
\left(\frac{df}{dt}\right)_{SW} = & -\nabla \cdot \left[\left\langle \frac{d\mathbf{x}}{dt} \right\rangle^I (\varepsilon_I) f \right] - \frac{1}{p^2} \frac{\partial}{\partial p} \left[p^2 \left\langle \frac{dp}{dt} \right\rangle^I (\varepsilon_I) f \right] \\
& - \frac{\partial}{\partial \mu} \left[\left\langle \frac{d\mu}{dt} \right\rangle^I (\varepsilon_I) f \right] \\
& + \frac{\partial}{\partial \mu} \left[D_{\mu\mu}^I (\varepsilon_I) \frac{\partial f}{\partial \mu} + D_{\mu p}^I (\varepsilon_I) \frac{\partial f}{\partial p} \right] \\
& + \frac{1}{p^2} \frac{\partial}{\partial p} \left[p^2 \left(D_{p\mu}^I (\varepsilon_I) \frac{\partial f}{\partial \mu} + D_{pp}^I (\varepsilon_I) \frac{\partial f}{\partial p} \right) \right]
\end{aligned} \tag{13}$$

where $f(x, p, \mu, t)$ is the energetic charged particle distribution. On the left-hand side of this equation, $(df/dt)_{SW}$ represents the standard focused transport equation for energetic particle transport in the non-uniform solar wind flow and interplanetary magnetic field (e.g., Isenberg (1997)). On the right-hand side, there are additional terms to model the interaction of energetic particles with dynamic SMFRs. In the top line $\langle dp/dt \rangle^I$ models the average energetic particle momentum rate of change in response to average SMFR quantities (the average SMFR compression, parallel shear flow, parallel reconnection electric field due to SMFR merging, and the parallel acceleration

of the SMFR flow). In the absence of pitch-angle scattering, the acceleration is coherent but can become stochastic if particles undergo significant pitch-angle scattering. In the bottom line, D_{pp}^I signifies the variance in the energetic particle rate of momentum change due statistical fluctuations in the SMFR quantities expressed in terms of the variance in the SMFR compression, parallel shear flow, parallel reconnection electric field, and the parallel acceleration of the SMFR flow (for more details, see le Roux et al. (2015, 2018)). Recently, a simplified telegrapher type Parker transport equation was derived from the modified focused transport equation by assuming that on large spatial scales the energetic particle distribution will inevitably become nearly isotropic due to significant levels of pitch-angle scattering (le Roux et al., 2019). This was accomplished by expanding the energetic particle distribution function $f(x, p, \mu, t)$ out to the second moment with respect to μ with aid of Legendre polynomials and deriving the zeroth, first and second moments of the modified focused transport equation (see also Zank et al. (2014); le Roux et al. (2015, 2018)). The first and second moment equations were simplified to enable a closed evolution equation for the isotropic part of the distribution function $f_0(x, p, t)$ in the form of a telegrapher type Parker transport equation. Discussion of the simplifications can be found in le Roux et al. (2019). The telegrapher type Parker transport equation we derived is given by

$$\begin{aligned}
& \frac{3\kappa_{\parallel}^I}{v^2} \frac{\partial}{\partial t} \left[\frac{\partial f_0}{\partial t} + (\mathbf{U}^{coh} \cdot \nabla) f_0 - (\nabla \cdot \mathbf{U}^{coh}) \frac{p}{3} \frac{\partial f_0}{\partial p} \right. \\
& \left. - \frac{1}{p^2} \frac{\partial}{\partial p} \left(p^2 D_{pp}^{Istoch} \frac{\partial f_0}{\partial p} \right) \right] \\
& + \frac{\partial f_0}{\partial t} + \left[\mathbf{U}^{coh} - \frac{1}{3p^2} \frac{\partial}{\partial p} (p^3 (U_{EA}^{coh} - U^{Istoch}) \mathbf{b}) \right] \cdot \nabla f_0 \\
& - \left[(\nabla \cdot \mathbf{U}^{coh}) + (\nabla \cdot (U_{EA}^{coh} + U^{Istoch}) \mathbf{b}) \right] \frac{p}{3} \frac{\partial f_0}{\partial p} \\
& = \nabla \cdot (\kappa_{\parallel}^I \mathbf{b} \mathbf{b} \cdot \nabla f_0) + \frac{1}{p^2} \frac{\partial}{\partial p} \left[p^2 (D_{pp}^{coh} + D_{pp}^{Istoch}) \frac{\partial f_0}{\partial p} \right] \\
& + \frac{2}{3} p U_{EA}^{coh} (\mathbf{b} \cdot \nabla) \frac{\partial f_0}{\partial p}
\end{aligned} \tag{14}$$

In Eq. (14) the superscript 'coh' refers to a combination of background solar wind and average SMFR quantities, whereas the superscript 'Istoch' indicates the variance of fluctuating SMFR quantities only. Accordingly, U^{coh} models the net advection effect on energetic particles stemming from the combination of the solar wind velocity with the mean plasma flow velocity in dynamic SMFRs, $U_{EA}^{coh} \mathbf{b}$ represents the net parallel advection effect on energetic particles from the average parallel component of the electric field and of the acceleration of the plasma flow in the background solar wind and in SMFRs, and $U^{Istoch} \mathbf{b}$ refers to the average, field-aligned advection effect produced by the variance of statistical fluctuations in SMFR fields. κ_{\parallel}^I denotes the parallel dif-

fusion coefficient as a consequence of particle pitch-angle scattering by random magnetic mirroring forces in SMFRs (for more information, see le Roux et al. (2015, 2016, 2018)). Furthermore, there are two categories of second-order Fermi acceleration in Eq. (14). D_{pp}^{coh} models second-order Fermi acceleration when particles undergoing pitch-angle scattering on macro scales respond to the average parallel electric field and acceleration of the plasma flow, the parallel shear flow tensor, and the flow compression for both the background solar wind and SMFRs, whereas D_{pp}^{Istoch} describes second-order Fermi acceleration when particles experience the variance effects from fluctuations in the same SMFR quantities. The more familiar diffusive Parker transport equation can be recovered by neglecting the additional transport terms in the top line of Eq. (14). Besides the well-known telegrapher term (first term in line one of Eq. (14) containing the second-order time derivative, there are also less familiar additional telegrapher terms involving second and third-order partial derivatives (rest of terms in line one and two of Eq. (14)). The telegrapher Parker transport equation addresses a deficiency in the diffusive Parker transport equation where some particles propagate to larger distances than physically possible by restoring causality. However, the causality in particle transport is only restored for leading edge particle pulses that are nearly isotropic, that is, for particles that experience significant pitch-angle scattering. This kind of telegrapher equation is less accurate when it comes to model unscattered particle escape from the acceleration site during early times, resulting in a cutoff in the particle distribution spatially that is too abrupt so that the maximum distance particles reach as a function of time is underestimated (e.g., Effenberger and Litvinenko (2014); Malkov and Sagdeev (2015)). Since we model energetic particle acceleration inside the SMFR acceleration region on macro scales, where particles are expected to be scattered by low-frequency wave turbulence and by fluctuating magnetic mirroring forces inside these structures to maintain near-isotropic distributions, the telegrapher Parker equation should be applicable.

3.3 Solutions of the Diffusive Parker Transport Equation for Acceleration by SMFRs

Various analytical steady-state solutions for spatial transport in planar geometry, but also some in spherical geometry, were found for simplified versions of the diffusive Parker transport equation, that is, Eq. (14) neglecting telegrapher terms in the top line (e.g., Zank et al. (2014, 2015b); le Roux et al. (2015, 2016); Zhao et al. (2018); le Roux et al. (2019)). The solutions either emphasized first-order Fermi due to the average SMFR compression and/or acceleration by the mean parallel reconnection electric field in the mixed-derivative transport term (see last term in Eq. (14)) generated during SMFR merging (Zank et al., 2014, 2015b; Zhao et al., 2018), or second-order Fermi acceleration involving the variance in the SMFR compression/parallel shear flow and/or 1st order Fermi acceleration (le Roux et al., 2015, 2016, 2019). Irrespective of

whether first-order or second-order Fermi SMFR acceleration in the solutions was emphasized, two key predictions were made that was verified by spacecraft data analysis: (1) the accelerated particle flux form spatial peaks in the SMFR acceleration region so that the flux amplification factor downstream of the particle injection point increases with particle energy, and (2) the accelerated particle spectra evolve through the SMFR region by becoming harder downstream of the injection location (Zank et al., 2015b; le Roux et al., 2016; Zhao et al., 2018; Adhikari et al., 2019; le Roux et al., 2019; Khabarova et al., 2016). In the new work le Roux et al. (2019) present both time-dependent and steady-state analytical solutions of Eq. (14) in planar geometry in which all the basic SMFR acceleration mechanisms present in the underlying focused transport theory (see Eq. (12)) are unified. The solutions are based on solving a simplified version of the telegrapher Parker transport equation Eq. (14) in which the solar wind flow velocity is defined in the x-direction as $\mathbf{U}_0 = U_0 \mathbf{e}_x$ and the background magnetic field is specified in the x-z-plane according to the expression $\mathbf{B}_0 = B_0 (\cos(\psi) \mathbf{e}_x + \sin(\psi) \mathbf{e}_z)$ where ψ is the spiral magnetic field angle (the angle between \mathbf{B}_0 and \mathbf{U}_0). The transport equation is

$$\begin{aligned} & \tau_{SC}^I \frac{\partial^2 f_0}{\partial t^2} + \frac{\partial f_0}{\partial t} + U_0^I \frac{\partial f_0}{\partial x} + \langle \nu_{COM}^I \rangle \frac{p}{3} \frac{\partial f_0}{\partial p} = \\ & = \kappa_{xx}^I \frac{\partial^2 f_0}{\partial x^2} + \frac{1}{p^2} \frac{\partial}{\partial p} \left(p^2 D_{pp}^I \frac{\partial f_0}{\partial p} \right) + \frac{2}{3} U_E^I \frac{\partial}{\partial x} \left(p \frac{\partial f_0}{\partial p} \right) - \frac{f_0}{\tau_{esc}} + \\ & + \frac{dN/dt}{4\pi p_0^2} \delta(x - x_0) \delta(p - p_0) \end{aligned} \quad (15)$$

where in the first term, the telegrapher term, τ_{SC} , is the time scale for particle pitch-angle scattering by random magnetic mirroring forces in SMFRs. For simplicity, the other telegrapher terms in the top line of Eq. (14) were neglected. In the third term in Eq. (15), the advection term, the effective advection velocity in the x-direction $U_0^I = U_0 - U_E^I$, where U_0 is the background solar wind flow velocity, and $U_E^I = \left(3\kappa_{\parallel}^I / v \right) \langle \nu_{REC} \rangle \cos(\psi)$ is an advective velocity along the background magnetic field \mathbf{B}_0 projected in the x-direction using the factor $\cos(\psi)$. The U_E^I advection effect is associated with particle interaction with the mean parallel reconnection electric field in numerous merging SMFRs generating an average relative momentum rate of change $\langle \nu_{REC}^I \rangle$. The fourth term in Eq. (15) contains the mean SMFR compression rate $\langle \nu_{COM}^I \rangle$ to model first-order Fermi SMFR acceleration, while the first term on the right hand side of Eq. (15) includes the diffusion coefficient in the x-direction κ_{xx}^I , which is related to the parallel diffusion coefficient κ_{\parallel}^I according to the expression $\kappa_{xx}^I = \kappa_{\parallel}^I \cos^2(\psi)$. In the second term on the right of Eq. (15) we find the total momentum diffusion coefficient for second-order Fermi acceleration by SMFRs $D_{pp}^I = p^2 D_0^I = D_{pp}^{Icoh} + D_{pp}^{Istoch}$ where D_{pp}^{Icoh} refers to second-order Fermi acceleration when particles undergo pitch-angle scattering on macro scales in response to the average parallel electric field and

acceleration of the plasma flow, the parallel shear flow tensor, and the flow compression in SMFRs, whereas D_{pp}^{Istoch} describes second-order Fermi acceleration when particles experience the variance effects from fluctuations in the same four SMFR quantities. This is followed by the third mixed derivative transport term which determines particle acceleration by the mean parallel reconnection electric field in numerous merging SMFRs. The second last term determines the rate of particle escape from the SMFR region which depends on the escape time scale τ_{esc} (see also, Zhao et al. (2018)) whereas the last term represents a particle source in which particles in a thin spherical momentum shell with radius p_0 are continuously injected at a rate dN/dt in the SMFR region at location $x = x_0$. As an example, we present the steady-state solution of Eq. (15) which is

$$f_0(x, p) = \frac{1}{2\pi} \left(\frac{dN/dt}{4\pi p_0^3} \right) \sqrt{\frac{1}{\bar{D}_0^I \kappa_0^I}} e^{\frac{1}{2} \frac{U_0^I + q U_E^I/3}{\kappa_0^I} (x-x_0)} \left(\frac{p}{p_0} \right)^{-\frac{q}{2}} K_0 \left(2\sqrt{\alpha\beta} \right) \quad (16)$$

where K_0 is the modified Bessel function of the first kind and

$$\begin{aligned} \bar{D}_0^I &= D_0^I \left[1 - \frac{1}{9} \frac{(U_E^I)^2}{\kappa_0^I D_0^I} \right] \\ q &= 3 \left[1 - \frac{1}{9} \frac{\langle \nu_{COM}^I \rangle - U_0^I U_E^I / \kappa_0^I}{D_0^I} \right] / \left[1 - \frac{1}{9} \frac{(U_E^I)^2}{\kappa_0^I D_0^I} \right] \\ \alpha &= \frac{1}{4\kappa_0^I} \left[(x-x_0)^2 + \frac{\kappa_0^I}{D_0^I} \left[\ln \left(\frac{p}{p_0} \right) - \frac{1}{3} \left(\frac{U_E^I}{\kappa_0^I} \right) (x-x_0) \right]^2 \right] \\ \beta &= \left(\frac{1}{2} \frac{U_0^I}{\kappa_0^I} \right)^2 \kappa_0^I + \left(\frac{q}{2} \right)^2 \bar{D}_0^I + \frac{1}{\tau_{esc}} \end{aligned} \quad (17)$$

The solution includes all four SMFR acceleration mechanisms listed in the underlying focused transport equation (see Eq. (12)) that appears in the Parker transport equation as first-order Fermi acceleration, second-order Fermi acceleration, and acceleration by the mixed-derivative transport term. By taking limits of the solution, the basic characteristics of observations of energetic particle acceleration and transport through a dynamic SMFR region in the solar wind, namely, energetic particle distribution spatial peak formation and spectral hardening as discussed above. If $\ln^2(p/p_0) \gg (x-x_0)^2$ in the parameter α in $K_0(2\sqrt{\alpha\beta})$, one finds that

$$f_0(x, p) \propto e^{-\frac{U_0}{2\kappa_0}(x-x_0)} \left(\frac{p}{p_0} \right)^{-\frac{1}{2} \left[q + |q| \sqrt{1 + (2/q)^2 \tau_{D_0^I} \left[1/\tau_{\kappa_0^I} + 1/\tau_{esc} \right]} \right]} \quad (18)$$

In the opposite limit $\ln^2(p/p_0) \ll (x-x_0)^2$

$$f_0(x, p) \propto e^{-\frac{1}{2} \left[\frac{U_0^I}{\kappa_0^I} (x-x_0) \sqrt{1+4\tau_{\kappa_0^I} \left[(q/2)^2 / \tau_{D_0^I} + 1 / \tau_{esc} \right]} - \frac{U_0^I}{\kappa_0^I} (x-x_0) \right]} / \kappa_0^I \left(\frac{p}{p_0} \right)^{-\frac{q}{2}} \quad (19)$$

where $\tau_{\kappa_0^I} = \kappa_0^I / U_0^I{}^2$ is the diffusion time scale and $\tau_{D_0^I} = 1 / D_0^I$ is the time scale for second-order Fermi acceleration. In Eq. (18) and Eq. (19) we let $U_E^I = 0$, thus removing the effects of average parallel reconnection electric field in the mixed-derivative transport term and in spatial advection ($U_0^I = U_0$) in Eq. (15), but not in second-order Fermi acceleration. The mixed-derivative transport term was found to counteract spatial peak formation by forming a plateau in the accelerated particle distribution contrary to observations (Zank et al., 2014). Both solution limits Eq. (18) and Eq. (19) indicate that, because energetic particle diffusive transport occurs against the solar wind flow upstream of the particle injection point at $x = x_0$ ($x < x_0$), the particle distribution decays exponentially with increasing upstream distance from the injection point (thus no spatial peak in the particle distribution). Since diffusive transport unfolds in the direction of the solar wind flow downstream of the injection point ($x > x_0$) during acceleration, the particle distribution increases exponentially with increasing distance downstream when sufficiently close to the injection point because then limit Eq. (18) applies. However, sufficiently far downstream of the injection point, the particle distribution at lower energies decays first with increasing distance because then limit Eq. (19) is applicable. The decay at higher energies occurs progressively further downstream of the particle source when Eq. (19) becomes applicable at those distances. Thus, peaks form in the accelerated downstream distribution that shifts increasingly to larger distances downstream with increasing particle energy. Consider the accelerated particle spectra. Close to the injection point the particle spectra form power laws steeper than $f_0(p) \propto (p/p_0)^{-q/2}$ at most energies above the injection energy ($p > p_0$) because Eq. (18) is valid. With increasing distance from the injection point expression in Eq. (18) holds progressively at increasingly high particle energies only while at lower energies (Eq. (19)) applies where the spectrum approaches the harder power law $f_0(p) \propto (p/p_0)^{-q/2}$ for a growing energy interval. Thus, with increasing distance downstream of the injection point the accelerated particle spectrum becomes increasingly hard on average while assuming a more exponential character as it bends over more strongly at lower energies. Inspection of Eq. (18) also reveals that more efficient particle escape results in a steeper spectrum (Zhao et al., 2018) and a larger spatial diffusion coefficient produces a harder spectrum as particles sample more SMFRs in a given time interval.

3.3.1 Second Order Fermi SMFR Acceleration

Zhao et al. (2018) and Adhikari et al. (2019) had great success in reproducing the observed features of accelerated ions in SMFR regions at 1 AU and 5

AU in the equatorial plane using an analytical steady-state solution of their Parker transport equation in which 1st order Fermi SMFR compression acceleration appears to be the dominant acceleration mechanism, but without considering second-order Fermi SMFR acceleration or connecting the acceleration and transport time scales to SMFR properties. In Figure 7 we illustrate steady-state solution (Eq. (16)) in the limit where second-order Fermi SMFR acceleration due to the variance in the SMFR compression and parallel shear flow is the dominant acceleration mechanism. The left panel in Figure 7 shows the spatial variation in the accelerated proton distribution function amplification factor for different particle energies downstream of the injection point at $x - x_0 > 0$ by choosing an amplification factor of one for all energies at the injection location. The theoretical maximum amplification factor varies between $\sim 2.8 - 5.4$ for proton energies in the range $0.144 - 3.31$ MeV, thus increasing with energy. Figure 10 of Khabarova and Zank (2017), based on a superposed epoch analysis of energetic ion flux enhancements in the vicinity of 126 thin primary reconnecting current sheet events at 1 AU, suggests that the average intensity maximum amplification factor of energetic ion flux varies between $\sim 4.5 - 7.5$ in the energy range $0.112 - 4.75$ MeV (LEMS30 detector of EPAM instrument on the ACE spacecraft), and between $\sim 3.5 - 5.5$ in the energy range $0.066 - 4.75$ MeV (LEMS120 detector of EPAM) with the largest amplification factor occurring at the highest energies. The latter range of maximum amplification factors agrees best with the analytical results. The analytical solution also predicts a systematic shift in the position of the maximum amplification factor. It varies from $\sim 0.05 - 0.1$ AU from low to high particle energies downstream of the injection point that does not appear to be present in the observations averaged over many events in Fig. 10 of Khabarova and Zank (2017). Although such a shift does not appear to be present in Fig. 10 of Khabarova and Zank (2017), it is present in energetic ion observations of SMFR acceleration behind an interplanetary shock from the Ulysses spacecraft at ~ 5 AU reported by Zhao et al. (2018), and in anomalous cosmic ray observations from the Voyager 2 spacecraft behind the solar wind termination shock (Zank et al., 2015b).

In Figure 7, right panel, we present the corresponding accelerated energetic proton spectra from our analytical solution for second-order Fermi acceleration at the particle injection point (solid black curve), and at increasing distances further downstream of the injection location: 0.05 AU (solid red curve), 0.1 AU (solid blue curve), 0.15 AU (dashed green curve), 0.2 AU (dashed cyan curve), and 0.25 AU (dashed magenta curve). The spectra are normalized so that the distribution function at the injection point has a value of one at the lowest momentum shown which is $p/p_0 = 1.5$, where p_0 is the injection momentum specified to be at a suprathermal proton kinetic energy of $T \approx 1$ keV. At the particle injection location the accelerated spectrum is close to a power law, being slightly softer than $f_0(p) \propto p^{-5}$ (in terms of differential intensity it is somewhat harder than $j_T(T) \propto T^{-1.5}$) except at the lowest momenta where the spectrum steepens somewhat. Inspection of the spectral evolution with increasing distance downstream of the injection point reveals that the

spectra become progressively harder and more exponential so that spectra at low energies are considerably harder compared to high energies. If one would fit a power law to the exponential spectrum at 0.2 AU downstream of the injection location (dashed cyan curve), the spectrum would be approximately a $f_0(p) \propto p^{-4}$ ($j_T(T) \propto T^{-1}$) above ~ 100 keV ($p/p_0 > 10$). This basic trend of spectral hardening and increasing exponential nature of accelerated proton spectra produced by SMFRs with increasing distance inside the SMFR region is consistent with SMFR acceleration events at 1 AU reported by Adhikari et al. (2019). The variation in the power-law index through the SMFR region from ~ -1.5 to ~ -1 for particle energies ~ 100 keV $< T < 1$ MeV in the second event discussed by Adhikari et al. (2019) is close to the result reported here. A similar hardening trend in the energetic particle spectra through an SMFR at ~ 5 AU was detected in Ulysses data as reported by Zhao et al. (2018).

We conclude that one can potentially reproduce the observed flux amplification of energetic ions as a function of particle energy and the evolution of the accelerated spectra through SMFR regions at 1 AU by focusing solely on second-order Fermi SMFR acceleration of energetic ions in response to statistical fluctuations (variance) in the compression and the parallel shear flow in SMFRs, and we found that this can be accomplished with reasonable SMFR parameters (for more detail, see le Roux et al. (2019)). Based on the SMFR parameters that we used we found that stochastic acceleration by the variance in the parallel reconnection electric field is the dominant second-order Fermi acceleration mechanism. Unfortunately, we were unable to model particle acceleration for this mechanism using the solution of Eq. (16) because this analytical solution only holds for $D_0^I = D_{pp}^I/p^2$ being a constant while for this mechanism D_0^I depends on particle speed. Second-order Fermi acceleration involving the variance in the SMFR parallel shear flow was the second most efficient, while second-order Fermi acceleration due to the variance in SMFR compression was the least efficient. However, due to our limited knowledge of the SMFR parameters that enter into the acceleration expressions, and because of limitations of the analytical solutions, it is difficult to draw definitive conclusions about the ranking of the different second-order Fermi acceleration mechanisms associated with the variance in SMFR fields. Further progress requires intensifying data analysis of SMFR acceleration events, while at the same time increasing the sophistication of the solutions.

3.3.2 First Order SMFR Fermi Acceleration

Consider Figure 8 where we show an analytical solution of Eq. (16) in the limit where first-order Fermi acceleration of energetic ions in response to the mean compression rate of SMFRs in an SMFR region at 1 AU is the dominant acceleration mechanism. Inspection of the results in the left panel for the spatial variation in the amplification factor in the accelerated particle distribution downstream of the particle injection point shows that they are remarkably similar to the results in Figure 7 for second-order Fermi acceleration. In other

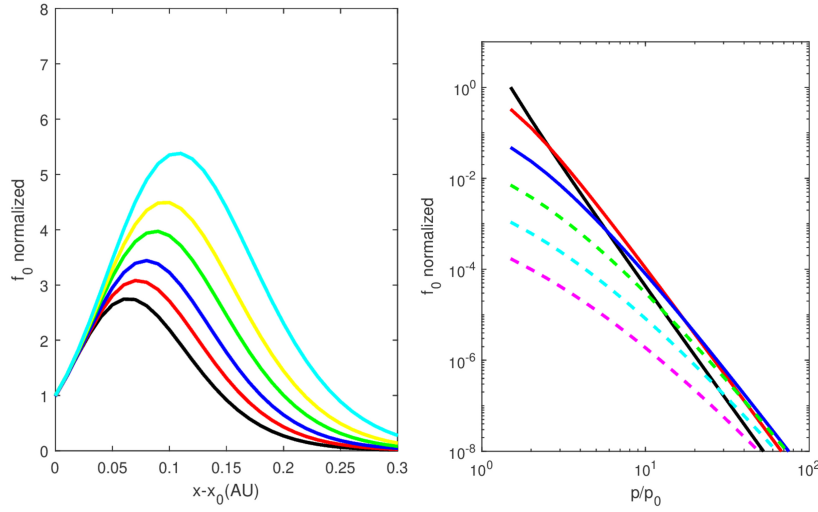


Fig. 7: The 1D steady-state analytical solution (Eq. (16)) for energetic proton 2nd order Fermi acceleration by SMFRs in a uniform SMFR region in the vicinity of 1 AU (reproduced from le Roux et al. (2019)). The solution combines second order Fermi acceleration due the variance in the SMFR compression rate and in the SMFR incompressible parallel shear flow. Left panel: The direction-averaged proton distribution function $f_0(x, p)$ as a function of distance in AU relative to the particle injection position x_0 ranging from $x - x_0 = 0 - 0.3$ AU in the downstream direction (in the direction of the solar wind flow) for the particle energies 144 keV (black), 256 keV (red), 0.44 MeV (blue), 0.81 MeV (green), 1.44 MeV (yellow), and 3.31 MeV (cyan). The energy intervals were chosen to fall inside the energy intervals in the observed energetic flux enhancements at 1 AU in Fig. 10 of Khabarova and Zank (2017). The different curves for $f_0(x)$ were normalized to a value of 1 at $x - x_0 = 0$ AU to reveal the amplification factor of f_0 from the particle injection location to the peak in $f_0(x)$ further downstream for each particle energy. Since the differential intensity as a function of kinetic energy T is $j_T(T) = p^2 f_0(p)$, the amplification factor for f_0 also serves as the amplification factor for j_T . Right panel: Normalized $f_0(x, p)$ as a function particle momentum p in the solar wind frame normalized to p_0 (the injection momentum). The spectra are displayed for the following values of $x - x_0$: 0 AU (solid black), 0.05 AU (solid red), 0.1 AU (solid blue), 0.15 AU (dashed green), 0.2 AU (dashed cyan), and 0.25 AU (dashed magenta). The curves were multiplied with the same factor so that the black curve has a value of one at the minimum momentum $p/p_0 = 1.5$. At $p/p_0 = 1$ the proton kinetic energy $T \approx 1$ keV while at the maximum momentum $p/p_0 = 100$, $T \approx 10$ MeV.

words, with both first and second-order second Fermi SMFR acceleration the observed enhanced energetic ion flux in SMFR regions at 1 AU in Fig. 10 of Khabarova and Zank (2017) were reproduced reasonably well. The SMFR parameters specified in the first-order Fermi solution closely follow those used in the second-order Fermi solution, except for the characteristic cross-section of SMFRs that was reduced by a factor of four. However, the reduced value falls within the range of possibility given the little that we know of the statistics of SMFR parameters in SMFR acceleration regions in the solar wind, thus accentuating the need for more detailed analysis of SMFR properties in SMFR acceleration regions. As can be seen in Figure 8, right panel, similar to the results for second-order Fermi acceleration, the modelled accelerated spectra for first-order Fermi acceleration are power laws at the particle injection point, exhibiting the same rollover trend qualitatively at lower particle energies downstream of the injection point (see also Zhao et al. (2018); Adhikari et al. (2019)). Quantitatively, however, the spectral rollover trend at lower particle energies and overall increasing spectral hardening downstream of the injection location is notably stronger in the case of first-order Fermi acceleration due to the cutoff in the downstream spectrum at the injection momentum. This illuminates a key difference between the first Fermi acceleration solution, where all the particles that arrive downstream of the injection point have been accelerated systematically to momenta larger than the injection momentum to form the low-energy cutoff at the injection momentum, and the second-order Fermi solution where particles arriving downstream experienced stochastic acceleration which lowers the probability for a low-energy cutoff at the injection momentum. This predicted difference in the spectral evolution for the two acceleration mechanisms downstream of the injection point might potentially help identify the dominant operating SMFR acceleration mechanism in observations. Based on the evolution of the spectral power-law index through the SMFR region in SMFR acceleration event two of Adhikari et al. (2019), the event with spectral power-law indices closest to our results, the less strong spectral hardening in the second-order Fermi acceleration case is closer to the observed hardening trend. More SMFR acceleration events need to be studied before conclusions can be drawn with confidence. The success of our SMFR acceleration results for both first-order Fermi acceleration (see also Zhao et al. (2018); Adhikari et al. (2019)) and second-order Fermi acceleration is partially due to the term for particle escape from the SMFR region which ensured steepened accelerated particle spectra with more realistic slopes. The particle escape term reflects the need for more sophisticated solutions that specify finite boundaries for the SMFR acceleration region and allow for multi-dimensional transport. It must be pointed out that the need for steeper accelerated spectra in the solution can partly be the result of modelling particle acceleration in the test particle limit. The considerable pressure in the accelerated test particle spectra indicates that the energy exchange between the particles and SMFRs should be modelled self-consistently, thus contributing also to steeper accelerated particle spectra (le Roux et al., 2016, 2018).

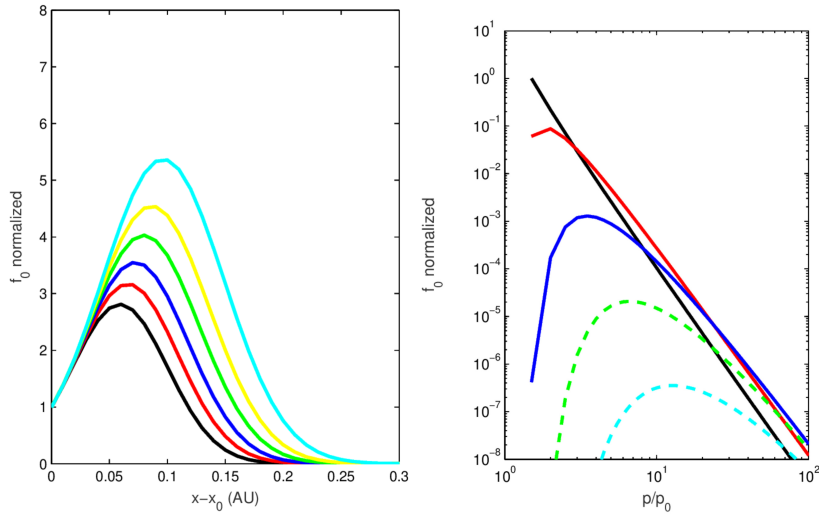


Fig. 8: The 1D steady-state solution for energetic proton first order Fermi acceleration or mean SMFR compression acceleration in a uniform SMFR region in the vicinity of 1 AU (Eq. (16)) (reproduced from le Roux et al. (2019)). Left panel: The same format as Figure 7, left panel. Right panel: Same format as Figure 7, right panel.

4 Numerical modeling of magnetic reconnection, formation of coherent structures, their dynamics and corresponding properties of turbulence.

Magnetic reconnection is a fundamental process that occurs ubiquitously in both space and laboratory plasmas. This process consists of an intense magnetic energy release that heats and accelerates particles (Drake et al., 2006; Hesse et al., 2016). One way in which reconnection may be triggered is via the tearing instability of thin current sheets. In a recent work (Pucci et al., 2018), it has been discussed the critical aspect ratios for the fastest tearing mode growth times, required to reach values comparable to ideal time-scales for current sheet equilibria that are different from the Harris current sheet.

It is now widely accepted that magnetic reconnection takes place in turbulent environments, where an energy cascade, from large to smaller spatial scales, is present (Matthaeus et al., 2015; Bruno and Carbone, 2016). The interplay of magnetic reconnection and plasma turbulence is hence decisive for assessing the role of this process in natural systems and can include the effects of turbulence on magnetic reconnection and, vice-versa, the influence of reconnection on turbulence (Matthaeus and Velli, 2011; Karimabadi et al., 2013). For example, it has been observed that turbulence can increase the reconnection rate (Matthaeus and Lamkin, 1986; Smith et al., 2004; Lapenta, 2008; Loureiro et al., 2009; Lazarian and Vishniac, 1999; Kowal et al., 2011,

2012; Lazarian et al., 2015). Analogously, plasma jets generated by reconnection can also supply energy for sustaining the turbulent cascade (Lapenta, 2008; Pucci et al., 2017; Cerri et al., 2017; Pucci et al., 2018). All the above, recent studies suggest that the intense current sheets naturally produced by turbulence, and that represent the boundaries of magnetic islands, might be the preferred sites of magnetic reconnection. For this reason, reconnection is a crucial ingredient of turbulence itself (Matthaeus and Lamkin, 1986; Servidio et al., 2010). These small-scale coherent structures are also thought to be the sites of inhomogeneous dissipation, where kinetic effects and plasma heating are concentrated (Servidio et al., 2011a; Osman et al., 2011; Servidio et al., 2012; Greco et al., 2012; Osman et al., 2012b; Wu et al., 2013; Servidio et al., 2015; Wan et al., 2015), together with local accelerations of energetic particles (Comisso and Sironi, 2018, 2019; Pecora et al., 2018).

Due to the strong nonlinearity of complex, multi-scale plasmas, the adoption of high-resolution numerical simulations is mandatory. Therefore, for practical reasons, considerable progress in the area of reconnection and turbulence has been made in the context of reduced dimensionality models that have an ignorable coordinate, or a weak dependency along the magnetic field as in the case of Reduced MHD (Rappazzo et al., 2017) (see Oughton et al. (2017) for a recent review). Much of the progress in 3D turbulent reconnection has been either experimental (Brown et al., 2006) or in a 3D numerical setup that is in effect nearly-2D (Kowal et al., 2009; Daughton et al., 2011). It is obvious that the full 3D case is substantially more complex and much less understood, both theoretically (Schindler et al., 1988; Priest and Pontin, 2009) and from the point of view of simulations (Dmitruk and Matthaeus, 2006; Borgogno et al., 2005; Lapenta et al., 2015; Lapenta et al., 2016).

Weakly 3D cases, often studied in Reduced MHD, have interesting properties (Oughton et al., 2017). For weakly 3D setups, it has been confirmed that some 2D-like effects persist (Rappazzo et al., 2007; Daughton et al., 2011). There are however some fundamentally 3D effects that occur even in Reduced MHD. An example is in the study of the geometry of current sheets and the trajectories of field lines that pass through them (Zhdankin et al., 2013; Wan et al., 2014; Rappazzo et al., 2017). In 2D rectilinear geometry the presence of a current sheet in one plane guarantees that a similar current sheet will be present at all other planes at different distances along the ignorable coordinate. Furthermore the central field line, the X-line, pass through each of these identical current sheet. This is in essence a trivial restatement of two-dimensionality. However in the weakly 3D Reduced MHD case (Wan et al., 2014) the behavior of field lines passing through current sheets do not have this property. Instead, a field line passing through an X-point central to a current sheet on one plane, will likely depart nearby current sheets on nearby planes. Consequently X-points are usually found at varying distances relative to what had been their coincident current sheet. But of course reconnection in MHD only occurs when the X-point is co-located with a strong current, so this meandering has a leading order effect on where reconnection occurs and how strong it will be (Wan et al., 2014). This inherently 3D effect is further

complicated by the fact that current sheets in reduced MHD have a finite extent along the guide field (Zhdankin et al., 2013). Further study also showed (Rappazzo et al., 2017) that reduced MHD current sheets tend to wander in the transverse directions *diffusively*, while field lines also wander randomly, but somewhat independently of the current sheets. This is clearly a much more complex scenario than the 2D case, even though Reduced MHD is only weakly 3D. This complexity will however have potentially major impact on physical phenomena such as nanoflares (Rappazzo et al., 2007; Gomez et al., 2000).

In general, it is well established that turbulence plays an essential role in accelerating the reconnection process both in 2D (Matthaeus and Lamkin, 1986) and in 3D (Lazarian and Vishniac, 1999). While the physics of reconnection revealed in the 2D can be applied in some circumstances to 3D, it is likely also that there are essential physical effects that occur in reconnection only in a strongly 3D systems, not the least of which is the very nature of reconnection itself in a full 3D representations (see, e.g., Priest and Pontin (2009)). These challenging problems have not been included in any complete way in the present review, where we concentrated, instead, on the progress in understanding reconnection in a turbulent environment which is very well magnetized and anisotropic.

First numerical attempts to model magnetic reconnection were based on an MHD approach, where the plasma is treated as a collisional magneto-fluid. Turbulence tends to dynamically generate relaxed regions –where non-linearities are depleted– separated by sheets of strong gradients (i.e. current) (Matthaeus et al., 2015), where magnetic reconnection can occur (Matthaeus and Montgomery, 1980; Carbone and Veltri, 1990; Retinò et al., 2007; Servidio et al., 2009; Rappazzo et al., 2010; Servidio et al., 2010, 2011b). Figure 9 shows the in-plane magnetic field lines with X-points and O-points identified (left), and the associated current sheets (right), for a 2D magnetohydrodynamics (MHD) simulation (Servidio et al., 2010). A sea of interacting magnetic island, with boundaries characterized by intense current sheets, is found. Current sheets are often co-located with reconnection sites.

The *in-situ* observations conducted with the Cluster mission have revealed that physical ingredients beyond the pure MHD description –namely the Hall and the kinetic terms– can have a significant role in characterizing the magnetic reconnection process (Øieroset et al., 2001; Vaivads et al., 2004; Retinò et al., 2007; Sundkvist et al., 2007). Indeed, their effects become important when characteristic dynamical scales are comparable with the ion skin depth $d_i = c/\omega_{pi}$ (ω_{pi} being the ion plasma frequency). This motivated huge numerical efforts to include these ingredients and a variety of numerical simulations, ranging from Hall-MHD to Vlasov-Maxwell, have been performed.

The Hall term, which brings the dynamics of whistler waves and dispersive effects into the system, increases the reconnection rate (Ma and Bhattacharjee, 2001; Birn et al., 2001; Smith et al., 2004; Lu et al., 2010; Papini et al., 2019), while the distribution of reconnection rates become broader than the MHD case (Donato et al., 2012). At variance with the pure MHD case, the magnetic energy is more frequently released through explosive, catastrophic

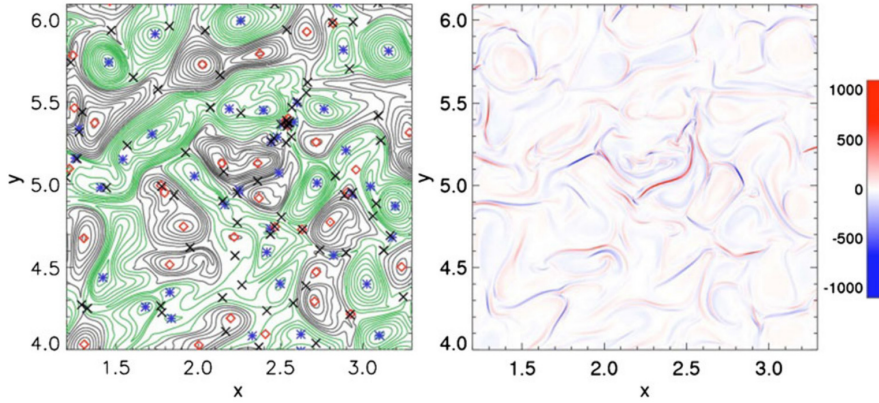


Fig. 9: (Color online). 2D MHD simulation result, showing the concurrency of current sheets and magnetic reconnection sites. Left: Contour plot of the magnetic potential a with the position of all the critical points: O-points (blue stars for the maxima and red open diamonds for the minima) and X-points (black), from a small section of a high-resolution 2D MHD simulation. Right: Shaded contour plot of the current density j in the same region. In between magnetic islands, intense current density peaks are present. Several reconnection sites are observed associated with current sheets. (reproduced from Servidio et al. (2010)).

events, that lead to fast magnetic reconnection onset (Cassak et al., 2005, 2007). The topology of the current sheets also changes and a quadrupolar structure of the out-of-plane magnetic field is observed (Fig. 10), as expected from theory (Sonnerup, 1979).

Several efforts have been performed to understand at which extent MHD and Hall-MHD models, based on a collisional closure, properly describe turbulence in almost collisionless systems where the collisional closure may not be valid (e.g., Pezzi et al. (2017b); Perrone et al. (2018); González et al. (2019); Papini et al. (2019)). In general, Hall MHD simulations retain turbulence properties (spectral features, intermittency, reconnection...) up to the sub-proton range of wavenumbers. However, together with the presence of the Hall physics, genuinely kinetic effects are also significant at scales $l \sim d_i$ (Valentini et al., 2008, 2011a,b; Howes et al., 2008a; Parashar et al., 2009; Schekochihin et al., 2009; TenBarge et al., 2013; TenBarge and Howes, 2013; Matteini et al., 2013; Franci et al., 2015; Vásconez et al., 2015; Valentini et al., 2016; Parashar and Matthaeus, 2016; Pucci et al., 2016; Cerri et al., 2017; Cerri and Califano, 2017; Pezzi et al., 2017c,b,a; Grošelj et al., 2017; Franci et al., 2018; Parashar et al., 2018; Hellinger et al., 2019; Franci et al., 2020; Califano et al., 2020). Indeed, since magnetic reconnection onsets in a weakly-collisional plasma, the plasma is free to explore the full phase-space and can exhibit non-equilibrium features, such as temperature anisotropy, rings, beams of accelerated particles along or across the local magnetic field (Osman et al., 2011, 2012b; Servidio

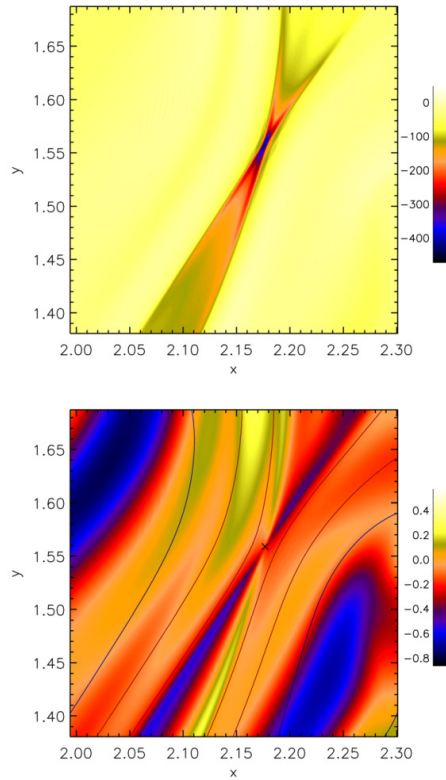


Fig. 10: (Color online). 2D Hall-MHD simulation result, indicating the typical quadrupolar structure of the reconnection site due to the Hall term. Top: Contour plot of the out-of-plane component of the current j_z in a sub-region of the simulation box. The bifurcation of the sheet and the typical structure of a reconnection region are clearly visible. Bottom: A contour plot of the out-of-plane component of the magnetic field b_z , in the same sub-region. The magnetic flux a is also represented as a line contour. A quadrupole in the magnetic field can be identified, revealing the presence of Hall activity (reproduced from Donato et al. (2012)).

et al., 2015). Both hybrid, where electrons are assumed to be fluid while protons are kinetic, and fully-kinetic models have been employed to gain insights on the magnetic reconnection onset at kinetic scales (Birn et al., 2001; Mangeney et al., 2002; Zeiler et al., 2002; Pritchett, 2008; Scudder and Daughton, 2008; Lu et al., 2010; Zenitani et al., 2011; Greco et al., 2012; Aunai et al., 2013; Wu et al., 2013; Karimabadi et al., 2013; Leonardis et al., 2013; Valentini et al., 2014; Wan et al., 2015; Lapenta et al., 2015; Lapenta et al., 2016; Shay et al., 2018; Lapenta et al., 2020). Kinetic simulations are usually employed within two different numerical approaches: Particle-In-Cell (PIC) and Eulerian Vlasov codes. Since the computational cost of PIC algorithms is in

general smaller with respect to low-noise Eulerian codes, PIC codes are able to capture the full plasma dynamics (including electron scales, although with unrealistic electron to ion mass ratio). However, at variance with noise-free Eulerian algorithms, PIC codes are affected by statistical noise and may fail in providing a clean description of small-scale fluctuations and particle distribution functions in phase space. Very recently, first Eulerian fully-kinetic codes have been implemented to describe plasma dynamics at electron scales without noise (Schmitz and Grauer, 2006a; Umeda et al., 2009, 2010; Tronci and Camporeale, 2015; Delzanno, 2015; Umeda and Wada, 2016, 2017; Ghizzo et al., 2017; Juno et al., 2018; Roytershteyn et al., 2019; Skoutnev et al., 2019; Pezzi et al., 2019).

The introduction of the kinetic physics leads to several novelties regarding magnetic reconnection (Burch et al., 2016a; Torbert et al., 2018; Shuster et al., 2019; Chen et al., 2019b; Jiang et al., 2019). In the diffusion region, collisionless and collisional plasma processes affect the change of magnetic field topology. Within a general fluid framework, non-ideal mechanisms are modelled through a resistive term, which can take into account both electron-ion collisions as well as the presence of an anomalous resistivity produced by wave-particle interactions and/or turbulence. Owing to poor collisionality, non-ideal effects are induced by collisionless processes, such as electron pressure tensor gradients and electron inertia effects. It is thus decisive to describe the system through kinetic model to evaluate the role of these terms in shaping magnetic reconnection.

Within the hybrid framework, it has been reported that kinetic effects are concentrated close to intense current sheets (Valentini et al., 2007; Servidio et al., 2012; Greco et al., 2012; Valentini et al., 2014; Servidio et al., 2015; Valentini et al., 2016; Valentini, F. et al., 2017). The role of alpha particles in characterizing kinetic scales turbulence has been analyzed in the detail showing that both protons and alpha particles are not in thermal equilibrium and manifest a preferentially perpendicular heating (Gary et al., 2003; Hellinger et al., 2005; Ofman and ViñAs, 2007; Ofman et al., 2011; Perrone et al., 2011, 2013, 2014b,a; Maneva et al., 2013, 2014, 2015; Maneva and Poedts, 2018; Valentini et al., 2016). Figure 11 displays four indicators of non-Maxwellian features in the proton distribution function in the proximity of a current sheet, identified through the Partial Variance of Increments (PVI) method (Greco et al., 2009). Recently a similar proxy of non-Maxwellianities based on the entropy density has been adopted by Liang et al. (2019, 2020); Pezzi et al. (2020). The ϵ parameter (panel (a)), which locally quantifies deviations of the proton VDF with respect to the associated Maxwellian distribution clearly shows a broad region of significant non-Maxwellianity surrounding the X-point. Out-of-equilibrium features emerge as temperature anisotropy (b) as well as higher VDF moments such as heat fluxes (c) and kurtosis (d). Note also that the heat flux is peaked in the exhaust region, this resembling the presence of outflows.

As suggested above, velocity-space is complexly structured in view of wave-particle interactions and turbulent cascade. Recently the Hermite decompo-

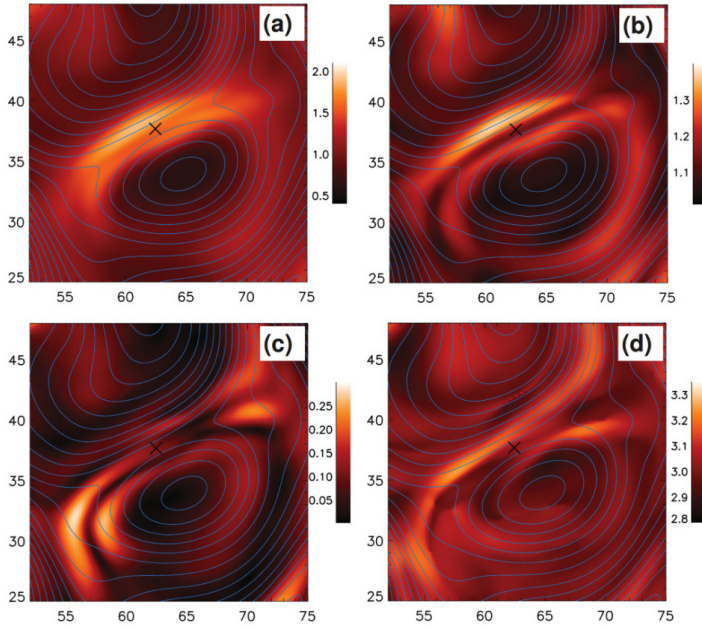


Fig. 11: (Color online) Hybrid Eulerian Vlasov simulation results, indicating the concentration of kinetic effects close to current sheets. Contour plots of several indicators of non-Maxwellian features in the proton velocity distribution function, in the vicinity of an intense current sheet, identified through the PVI method (black cross in all panels): (a) ϵ parameter, that evaluates the local deviation of the distribution function from the associated Maxwellian (in per cent); (b) Proton temperature anisotropy T_{\perp}/T_{\parallel} , being the parallel direction evaluated with respect to the local magnetic field; (c) heat flux, evaluated as the third-order moment of the proton distribution function; and (d) kurtosis (fourth-order moment) of the proton distribution function. (reproduced from Greco et al. (2012)).

sition of the proton distribution function has been adopted to highlight this complexity (Grad, 1949; Tatsuno et al., 2009; Pezzi et al., 2016; Schekochihin et al., 2016; Servidio et al., 2017). Indeed, the distribution function is decomposed in velocity-space by adopting a 3D Hermite transform, whose one-dimensional basis is:

$$\psi_m(v) = \frac{H_m\left(\frac{v-u}{v_{th}}\right)}{\sqrt{2^m m!} \sqrt{\pi} v_{th}} e^{-\frac{(v-u)^2}{2v_{th}^2}}, \quad (20)$$

where u and v_{th} are now the local proton bulk and thermal speed, respectively, and $m \geq 0$ is an integer (we simplified the notation suppressing the spatial dependence). The above projection quantifies high-order corrections to

the particle velocity DF. A highly distorted DF produces plasma enstrophy (Knorr, 1977), defined as

$$\Omega(\mathbf{x}, t) \equiv \int_{-\infty}^{\infty} \delta f^2(\mathbf{x}, \mathbf{v}, t) d^3v = \sum_{\mathbf{m} > \mathbf{0}} [f_{\mathbf{m}}(\mathbf{x}, t)]^2, \quad (21)$$

where δf indicates the difference from the ambient Maxwellian and $f_{\mathbf{m}} \equiv f_{\mathbf{m}}(m_x, m_y, m_z)$ is the Hermite coefficient, from which the enstrophy spectrum $P(\mathbf{m}) = \langle f_{\mathbf{m}}(\mathbf{x}, t)^2 \rangle$ is defined. From this last quantity, reduced spectra (e.g. along perpendicular and/or parallel direction, as well as omnidirectional) can be evaluated. By taking advantage of highly accurate measurements from the Magnetospheric MultiScale mission (MMS), an enstrophy velocity-space cascade, revealed by evaluating the Hermite spectrum of the ion distribution function, has been observed in the Earth's magnetosheath (Servidio et al., 2017) and also in hybrid Vlasov-Maxwell simulations (Pezzi et al., 2018; Cerri et al., 2018). A Kolmogorov-like phenomenology has been also proposed to interpret the observed slopes of the Hermite spectrum. Here we want to further stress that the presence of this phase-space cascade is spatially intermittent and it is more developed close to current sheets (Fig. 12). This indicates that magnetic reconnection triggers non-thermal features in the distribution of particles, as also pointed out from *in-situ* observations and PIC simulations (Drake et al., 2006; Shay et al., 2007; Hesse et al., 1999; Pritchett, 2013; Shay et al., 2014; Drake et al., 2014; Shay et al., 2016; Pritchett, 2016; Lapenta et al., 2017; Hesse et al., 2017).

Thanks to the unprecedented-resolution observations MMS (Burch et al., 2016b; Fuselier et al., 2016; Torbert et al., 2016, 2018), electron scale reconnection has become finally accessible and have shown a complex picture where a nested set of diffusion regions, whose size range from ion to electron scales (Hesse et al., 2016). Fully-kinetic models need to be adopted to characterize the process at such small scales. Figure 13 show the occurrence of several secondary islands, which are unstable for tearing instability. The size of these reconnection sites is comparable with electron scales.

At small scales, the dissipation of turbulent energy is thought to occur. Although it is well accepted that turbulence efficiently transfers energy from large to smaller scales (Verma et al., 1995; Vasquez et al., 2007; Sorriso-Valvo et al., 2007; Marino et al., 2008; Hadid et al., 2018; Andrés et al., 2019), it is not clear which physical mechanisms –among a variety of proposed ones– are controlling the dissipation process (Vaivads et al., 2016; Matthaeus et al., 2020). Actually, several different definitions of the *word* dissipation have been recently proposed. One approach analyzes the dissipation associated with a peculiar phenomenon, either a kind of fluctuations (e.g. KAW and whistler) (Chandran et al., 2010; Salem et al., 2012; Gary et al., 2016; Vech et al., 2017; Sorriso-Valvo et al., 2018, 2019) or magnetic reconnection (Drake et al., 2010; Servidio et al., 2011a; Osman et al., 2011, 2012b,a; Wu et al., 2013; Shay et al., 2018).

Within the reconnection community, there has been a particular emphasis on examining the electromagnetic work on particles, i.e. $\mathbf{j} \cdot \mathbf{E}$ (\mathbf{j} the electric

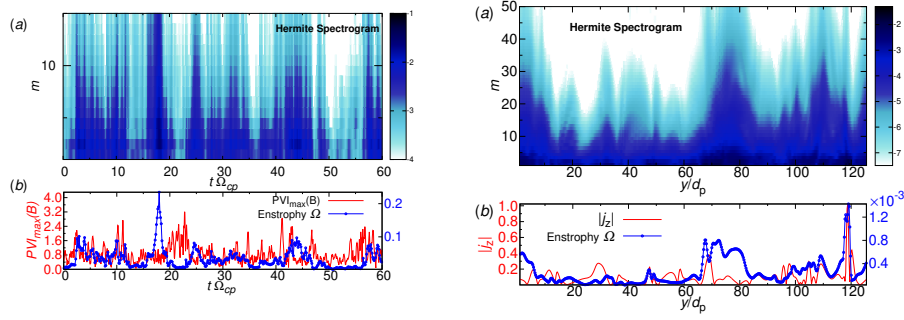


Fig. 12: (Color online) Magnetospheric Multi-Scale (MMS) in-situ observations (left columns) and Eulerian Hybrid Vlasov-Maxwell simulation (right columns) results, showing that the Hermite velocity-space cascade is intermittent and it is more developed close to intense current sheets. Left: Hermite spectrogram (top) and profile of the maximum PVI index for the magnetic field (i.e. magnetic field gradient, current density) bottom) as a function of time, from the MMS observations. Right: Hermite spectrogram (top) and profile of the current density j_z , together with the plasma enstrophy Ω (bottom), as a function of the spatial position in an one dimensional cut of the simulation (Adapted from Pezzi et al. (2018)). The Hermite spectrogram displays the evolution of the Hermite spectrum as a function of time and/or space.

current density, \mathbf{E} the electric field) as a dissipation proxy (Sundkvist et al., 2007; Zenitani et al., 2011; Wan et al., 2015). This has been instrumental in identifying a large number of active reconnection sites in MMS data (Burch and Phan, 2016a; Fuselier et al., 2017; Wilder et al., 2018). However it has also been demonstrated in MMS analysis (Chasapis et al., 2018) that some current sheets that are found to be reconnecting, with measures such as $\mathbf{j} \cdot \mathbf{E}$ indicating conversion of magnetic energy into particle energy, are actually *cooling* locally. This is not a paradox, since fundamental Vlasov-Maxwell theory shows that electromagnetic work exchanges energy with microscopic *flows*, while the actual conversion into internal energy of each species α is accomplished by $\Pi_{ij}^\alpha \nabla_i u_j^\alpha$ the contraction of the pressure tensor with fluid velocity gradients of each species Yang et al. (2017a,b). Further decomposed into a compressive part (pressure-dilatation) and an incompressible part (pressure-strain, or “Pi-D”) these quantities have recently been studied as direct channels of dissipation into heat (Yang et al., 2017a,b; Chasapis et al., 2018; Pezzi et al., 2019b; Matthaeus et al., 2020). It is important to note that within a collisional closure the pressure strain interaction is approximated by a viscosity (Braginskii, 1965) and becomes irreversible; however in the Vlasov-Maxwell case, lacking collisions, these terms are sign-indefinite, just as are the electromagnetic work and the turbulence scale-to-scale transfer (Matthaeus et al., 2020). Recently the statistical distribution of the Pi-D interaction has been examined in MMS data (Bandyopadhyay et al., 2020a), and found to be

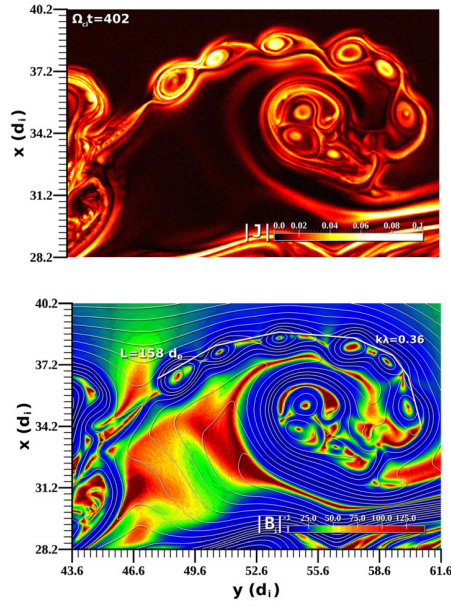


Fig. 13: (Color online) 2D fully-kinetic PIC simulation results ($m_i/m_e = 100$), showing the generation of secondary tearing islands at electron scales in a small sub-portion of the simulation box. Top: Contour plot of J showing the formation of chains of tearing islands. Bottom: Contour plot of the in-plane magnetic field B , highlighting the fact that tearing modes are formed in regions where the in-plane magnetic field is weak. Contours of vector potential a are also displayed. (reproduced from Karimabadi et al. (2013)).

consistent, in detail, with statistics from kinetic plasma simulation. It is encouraging that these highly fluctuating quantities in turbulent plasma give rise to statistical distributions that have reproducible properties.

The *field-particle correlator* has been furthermore proposed to point out features of particular phenomena associated with dissipation, e.g. Landau damping (Klein and Howes, 2016; Chen et al., 2019a; Klein et al., 2020). Although in general their role is thought of being weak (Speiser, 1965; Kasper et al., 2008; Maruca et al., 2011; Chhiber et al., 2016), collisional effects have been very recently also adopted to describe the ultimate dissipation, that produces an irreversible entropy growth (TenBarge et al., 2013; Pezzi et al., 2015; Navarro et al., 2016; Pezzi et al., 2016; Pezzi, 2017; Pezzi et al., 2019a; Vafin et al., 2019).

We conclude this section by highlighting that the support that numerical simulations can provide for interpreting and understanding *in-situ* observations is far from being exhausted. Indeed, magnetic reconnection is a multiscale phenomenon which goes “hand-in-hand” with turbulence evolution (Matthaeus and Velli, 2011). Several issues need to be additionally addressed to clarify

this puzzling picture. As introduced above, several simulations are performed in a reduced two-dimensional geometry, while the full three-dimensional case is much more complex and needs to be understood in detail. Another caveat concerns the unrealistic ion-to-electron mass ratio and the reduced box-size, that respectively affect the separation of different dynamical scales (i.e. the possibility to couple large and small scales) and the feasibility to achieve realistic Reynolds number. In this perspective, very recently, it has been proposed to couple different models, such as kinetic and global MHD (Daldorff et al., 2014; Drake et al., 2019). Finally, based on the MHD treatment, magnetic reconnection is associated with the introduction of irreversibility in the system. However, in a weakly-collisional plasma, the transition to an irreversible dynamics is a long-standing challenge (Navarro et al., 2016; Pezzi et al., 2016, 2019a). For a discussion of the relationship between collisional and collisionless cases, see (Matthaeus et al., 2020).

5 Theory of particle acceleration in dynamical flux ropes/magnetic islands.

Charged particle dynamics depends on the stochastic motion of magnetic field lines, whose random displacement affects the diffusion of particles both across and along the mean magnetic field (Jokipii and Parker, 1969). In fact, particles gyrate along the magnetic field but, if the field is turbulent, they spread in the perpendicular direction, “jumping” from one field line to another (Jokipii, 1966; Chandran et al., 2010; Ruffolo et al., 2012). The turbulent nature of the fields that scatter particles, makes the analytical treatment rather difficult. Because of this, we still lack an exact and universal theory to describe diffusion (Bieber and Matthaeus, 1997; Hussein and Shalchi, 2016; Dundovic et al., 2020).

Currently, among all diffusion theories, the nonlinear guiding centre (NLGC) (Matthaeus et al., 2003a) and its variations Ruffolo et al. (2012); Shalchi (2009) give a rather accurate prediction of the diffusion coefficient for systems with a three-dimensional (3D) geometry. However, a fully 3D numerical description of plasma turbulence requires huge computational efforts that can be streamlined by reducing the dimensionality of the problem. If a strong guiding magnetic field is present, turbulence becomes anisotropic and both 2D and 2.5D models become good approximations (Dobrowolny et al., 1980b,a; Shebalin et al., 1983; Matthaeus and Lamkin, 1986; Oughton et al., 1994; Dmitruk et al., 2004a). Due to this anisotropy, structures and phenomena related to turbulence, such as current sheets and reconnecting magnetic islands (Matthaeus and Lamkin, 1986; Greco et al., 2009; Servidio et al., 2011a), magnetic field topology changes and energy conversion (Parker, 1957; Matthaeus et al., 1984; Ambrosiano et al., 1988; Servidio et al., 2009, 2015), mainly occur due to dynamics in the plane perpendicular to the main field (Bruno and Carbone, 2016). In Pecora et al. (2018), a 2D version of 3D NLGC has been developed and tested with the 2.5D hybrid-PIC (Particle In Cell with kinetic ions and fluid electrons) simulation campaign described in (Servidio et al., 2016). As

turbulence develops, large-scale structures interact and smaller vortices and sharp current sheets appear, as shown in Figure 9. In particular, these magnetic structures represent magnetic islands (sections of three-dimensional flux tubes), and intense current sheets are associated to regions of strong magnetic gradients, in between reconnecting magnetic islands (Matthaeus and Montgomery, 1980; Servidio et al., 2015). Particles' trajectories show that they can be either trapped in magnetic vortices (Ambrosiano et al., 1988; Ruffolo et al., 2003; Dmitruk et al., 2004b; Tooprakai et al., 2007; Seripienlert et al., 2010; Tooprakai et al., 2016), or scattered by magnetic discontinuities such as current sheets (Rappazzo et al., 2017).

While at short times particles can be trapped in topological structures, typically a stochastic transport regime is achieved after rather long time intervals and can be statistically described within the theory of diffusion, based for example, on the relation

$$\langle \Delta s^2 \rangle = 2D\tau$$

where $\Delta \mathbf{s} = \mathbf{x}(t_0 + \tau) - \mathbf{x}(t_0)$ is the displacement of a particle, with \mathbf{x} being its position vector, D the diffusion coefficient, and the average operation $\langle \dots \rangle$ is taken over all the particles (Chandrasekhar, 1943; Batchelor, 1976; Wang et al., 2012). The diffusive description can be applied after initial transients, the simplest of which is referred to as the ballistic regime (Servidio et al., 2016). When applicable, particles must also escape from topological trapping in small flux tubes Tooprakai et al. (2007) prior to achieving diffusive transport. Generally speaking, transient regimes will last until particles sample uncorrelated correlated magnetic fields. As long as particles motion is followed for times shorter than the particle Lagrangian magnetic field correlation time, their motion cannot be found to be stochastic. This correlation time can be thought as the time one particle needs to move from one large scale magnetic vortex (island) to another. Low energy particles have longer correlation times as they cannot easily escape from vortices. Generally, the shape of trajectories suggests whether a particle has experienced trapping or scattering events, or both. Indeed, some particles have closed orbits that are a manifestation of trapping phenomena, while others show sharp turnovers that suddenly bend their trajectory when they experience strong local discontinuities (Drake et al., 2010; Haynes et al., 2014).

When charged particles move in a turbulent plasma, local properties and modifications in the topology, such as island contractions and magnetic reconnection, are possible acceleration mechanisms as discussed in previous sections. Among these, one that can lead straight to particle acceleration is the electric field parallel to the local magnetic field (Sturrock, 1966; le Roux et al., 2001; Comisso and Sironi, 2018). Particles with acceleration values that exceed the variance of the distribution are found to be non-uniformly distributed in space. These particles tend to cluster where the parallel electric field is more intense, mostly on the flanks of magnetic islands. This supports the idea that accelerating particles are located close to regions where dynamical activity is

occurring, notably along boundaries of interacting flux tubes, and near the associated current sheets, suggesting an association with magnetic reconnection. An example of this acceleration mechanism taking place is shown in Figure 14.

Particles can also be accelerated by perpendicular electric fields including betatron and curvature drift mechanisms that were discussed at some length in Section 3. It should be noted that much of the elegant formal theory presented in those preceding sections was based on conservation of adiabatic invariants and correspondingly, on guiding center drift theory Rossi and Olbert (1970). While applicable in many situations, the basis of this set of approximations is not always defensible; in particular adiabatic conservation laws such as conservation of magnetic moment are very sensitive to the presence of resonant power in the spectrum (Dalena et al., 2012). In this regard a test particle study in a hierarchical reduced MHD model Dalena et al. (2014) found that in early stages of acceleration, parallel electric field is most important, but later, the most energetic particles are found in a so-called betatron distribution, with parallel streaming relatively suppressed. The affected particles are typically trapped for extended periods of time in the acceleration region. The interaction with the electric field is found to be in the perpendicular direction and resonant in the time domain as seen by the accelerated particles. The locus of this acceleration is near magnetic boundaries of flux tubes as they are compressed due to interaction with neighboring flux tubes. There is a suggestion that the mechanism is limited by eventual pitch angle isotropization. As far as we are aware a transport theory describing this mechanism has not yet been developed.

Coherent structures, such as current sheets, contribute to non-Gaussian statistics and therefore to intermittency which is a fundamental property of turbulence and can be associated with kinetic effects such as particle acceleration (Marsch and Tu, 1997; Sorriso-Valvo et al., 1999; Osman et al., 2012b; Greco et al., 2012; Servidio et al., 2015; Wan et al., 2015). A well-established proxy to locate regions in which such structures appear is the Partial Variance of Increments (PVI) technique (Greco et al., 2009). In turbulence simulations, it has been found that the regions of large parallel electric field occur in correspondence of magnetic discontinuities rather than in smooth regions, at the boundaries of the magnetic islands as previously shown in Figure 15 of Greco et al. (2009).

Along with the parallel electric field, another feature has emerged to be extremely relevant in the process of acceleration and energization of particles. For energization to be effective, there must be a sort of spatial resonance between particle and diffusive characteristic scales. In particular, the gyroradius has to be comparable with Taylor dissipation length, $\lambda_T = \sqrt{\langle \delta b_{\perp}^2 \rangle / \langle j_z^2 \rangle}$, (qualitatively, the in-plane length of the largest current sheet). In Pecora et al. (2019b) this resonance is achieved in low- β simulations and particles are more effectively energized with respect to those in large- β plasmas. Indeed, changing plasma β does not change turbulence scales such as correlation and Taylor lengths. but it modifies plasma's thermal energy and hence particles' gyroradii. These local spatial resonances, at low β , make the magnetic moment

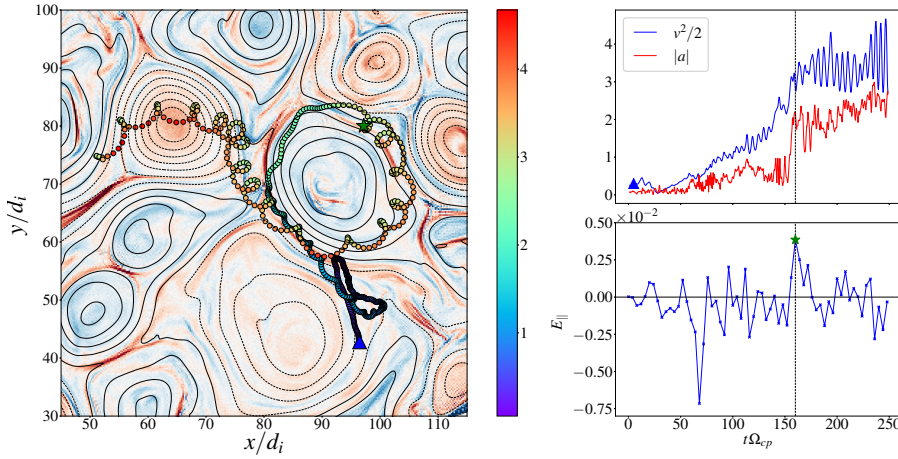


Fig. 14: Snapshot of turbulence simulation when one particle is subject to a peak of the parallel electric field, located at the flank of the magnetic island in which it is trapped (adapted from Pecora et al. (2018)). At the same time, the particle experiences an increase in acceleration and kinetic energy and is able to escape from the island (the trajectory starts at the blue triangle and the colour code represents particle’s kinetic energy).

no longer a constant of the motion, leading to acceleration and eventually to energization, reminiscent of the nonadiabatic betatron mechanism described above (Dalena et al., 2014).

. On the other hand, in larger- β plasma simulations, a consistent percentage of particles have a Larmor radius that is larger than the Taylor length, meaning that particles barely notice the current sheets during their gyrating motion and no resonance is possible, resulting in lower to none energization features.

Energization processes are ubiquitous in the whole universe and are not confined within the heliospheric description. High-energy particles, cosmic rays, black holes jets, all require a slightly different description that takes into account relativistic effects and strongly magnetized environments. As for non-relativistic plasmas, observations are tightly related to numerical simulations, especially when dealing with far unfathomable places. Magnetically dominated regions are a source of strong reconnection events and simulations show that acceleration of particles takes place as a two-stage process. First, the electric field acts as a primary source of acceleration in what can be considered an injection phase. Subsequently, many different processes, such as stochastic interaction with turbulent fluctuations, curvature drift and magnetic islands contraction, can take place and result in a Fermi-like acceleration (Guo et al., 2015, 2016b,a; Huang et al., 2017; Ball et al., 2018; Comisso and Sironi, 2019; Trotta et al., 2020).

There is a lot of observational evidence about the structured texture, previously depicted with simulations, of space plasmas at different spatial scales

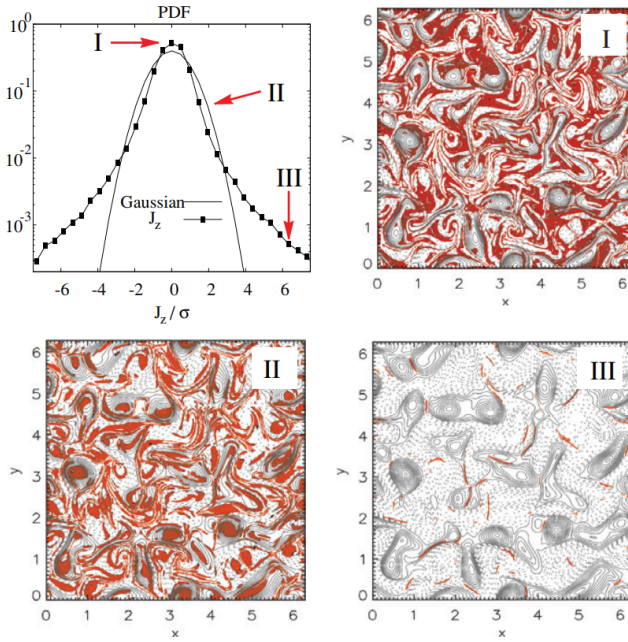


Fig. 15: PDF of the out-of-plane electric current density J_z from a 2D simulation, compared to a reference Gaussian (reproduced from Greco et al. (2009)). For each region I, II, and III, magnetic field lines (contours of constant magnetic potential $A_z > 0$ solid, $A_z < 0$ dashed) are shown; the coloured (red) regions are places where the selected band (I, II, or III) contributes.

(Schatten, 1971; Bruno et al., 2001; Borovsky, 2008; Khabarova and Zank, 2017; Malandraki et al., 2019; Verscharen et al., 2019). As discussed also in Part I of this review, cross-sections of 3D structures such as elongated plasmoids, flux ropes and blobs of different origins, are 2D magnetic islands. The presence of these structures, on-average aligned with the Parker spiral, was suggested by (Borovsky, 2008), following the spaghetti solar wind paradigm developed in 1970*th* (see Section 2.2 of Part I). There is no clue if such structures originate close to the Sun and then advected in the interplanetary space, or generate locally in the HCS and other SCSs filling the solar wind, due to magnetic reconnection and numerous instabilities (e.g., Khabarova et al. (2015, 2016); Khabarova and Zank (2017); Malandraki et al. (2019); Khabarova et al. (2020b)). Particularly relevant is the contribution given by the MMS mission (Curtis, 1999), whose measurements help unravelling the fine-scale structure of the near-Earth interplanetary space. Lots of effort have been dedicated into correlating spacecraft measurements to topological properties of the magnetic field and kinetic properties of plasma, showing also that reconnection sites can generate secondary structures such as reconnection-generated flux ropes within their exhausts (Lapenta et al., 2015; Burch et al., 2016a; Burch and

Phan, 2016b; Phan et al., 2016; Eastwood et al., 2016; Lapenta et al., 2018; Stawarz et al., 2018, 2019).

Of course, it is not possible to obtain a clear picture, like that provided by simulations, of the surroundings of a spacecraft, but there are powerful tools that can be used to get 2D and 3D information when specific conditions are met. A three-dimensional perspective of magnetic field lines can be recovered using the First Order Taylor Expansion (FOTE) method (Fu et al., 2015) that can be applied in the vicinity of a null point. This method requires multispacecraft measurements and the null point to be enclosed within the spacecrafts configuration volume but, despite the restricted regions of applicability, it can provide important information such as the identification of a 3D reconnection site where kinetic effects can be studied locally and linked to topological properties (Fu et al., 2016; Wang et al., 2019). On the other hand, the Grad-Shafranov (GS) reconstruction method (Hu and Sonnerup, 2002) is able to reveal the 2D magnetic field texture around one single spacecraft when it passes through an MHD stationary structure with cylindrical symmetry (e.g. a flux rope, whose 2D section in the plane perpendicular to the symmetry axis is a magnetic island). This technique has been also adopted to study the effect of magnetic clouds on galactic cosmic ray intensity (Benella et al., 2019). Very recently, Pecora et al. (2019a) enhanced the GS method by synergising it with the PVI technique providing additional observational evidence of the complex structure of the solar wind. In fact, the large-scale texture of the solar wind, reconstructed with the GS method at about $10^5 - 10^6$ km, shows flux tubes that are filamentary or “spaghetti-like”. The additional information provided by the PVI technique reveals where strong small-scale gradients of the magnetic fields are located. These regions are found at the boundaries of flux ropes/plasmoids where, possibly, reconnection, heating and particle acceleration are taking place. A few examples are shown in Figure 16. These structured flux tubes, hence, provide conduits for energetic particle transport and possible trapping and acceleration (see Tessein et al. (2013); Khabarova et al. (2016); Pecora et al. (2018) and Section 3).

The possibility to visualise 2D and 3D maps of the magnetic field and locate reconnection sites is extremely valuable when it comes to relating particle properties with the surrounding environment, as simulations already allow to do (Figure 14). Eventually, one may envision numerous applications in which the structures revealed by the combined GS/PVI method can be relevant to understand complex physics and turbulent interplanetary dynamics.

6 Summary and conclusions

In this review we have depicted the dynamics of magnetic and plasma structures, such as CSs, FRs/MIs and plasmoids/blobs, and their impact on the surrounding medium, especially related to particle energization. The complexity involved within such structures makes the adoption of the fully 3D approach essential since several important pieces of information are inevitably

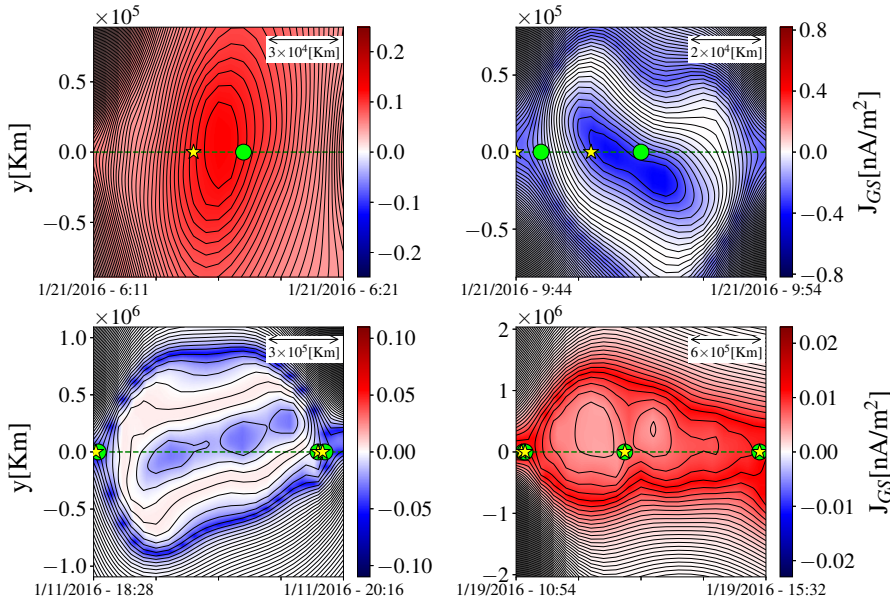


Fig. 16: Reconstructed flux ropes, adapted from Pecora et al. (2019a). The colour represents the out-of-plane current density, the black solid lines are the isocontour of the magnetic potential and the boundaries of a PVI event are indicated with a star (beginning) and a circle (end).

lost by adopting models with explicit symmetries (planar and/or spherical). Observations and numerical simulations in the last decades support these ideas (see, e.g., Lapenta et al. (2015); Lapenta et al. (2018); Adhikari et al. (2019); Khabarova et al. (2020b); Lazarian et al. (2020)). At the same time, the 2D approach can be employed in some cases. For instance, because of the spectral anisotropy, this is generally applicable for studying turbulence. Indeed, 2D/2.5D models of plasma turbulence are able to describe most of the features of both turbulence dissipation and magnetic reconnection, providing a valid tool for investigation of the related processes and understanding of particle heating and energization in astrophysical plasmas (e.g., Matthaeus et al. (2015)).

Modern theories and observational studies describe the HCS and similarly strong CSs as essentially non-planar complex plasma structures surrounded by a plasma sheet in which numerous small-scale reconnecting CSs separated by plasmoids occur (Khabarova et al., 2015; Malova et al., 2018; Adhikari et al., 2019; Mingalev et al., 2019). CSs are unstable in natural plasmas. Owing to the constantly changing environment, CSs are subject to different instabilities, including the tearing instability (Zelenyi et al., 1998, 2004; Tenerani et al., 2015a). These instabilities may impact CSs simultaneously with various fluctuations, destabilizing, triggering nonlinear processes at CSs and even

destroying them. Therefore, strong quasi-stable CSs, such as the HCS and CSs at leading edges of ICMEs and CIRs/SIRs, represent a well-known source of turbulence and intermittency. On the other hand, numerous thin and unstable CSs are generated in turbulent and intermittent regions (e.g. Servidio et al. (2009); Matthaeus et al. (2015)). This dualism reflects an intrinsic tie between instabilities, wave processes, magnetic reconnection, turbulence, and intermittency in space plasmas.

Summarizing the results of studies of particle acceleration associated with magnetic reconnection, we would like to stress out the fact that, besides the obvious role of the reconnection-induced electric field, charged particles can be energized by the first- and second- order Fermi mechanisms and the so-called anti-reconnection electric field operating during contraction and merging of FRs/plasmoids/MIs (Zank et al., 2014; le Roux et al., 2015, 2016; Xia and Zharkova, 2018, 2020; le Roux et al., 2019). Numerical simulations of processes occurring in turbulent plasmas successfully describe energization of charged particles by several acceleration mechanisms acting simultaneously. An analysis of observations confirms that theoretical predictions and results of numerical simulations discussed above correspond to reality and show that the ubiquitous occurrence of magnetic reconnection in the heliosphere makes this phenomenon essential for local particle acceleration (Khabarova et al., 2015, 2016, 2020b). Comprehensive studies of the formation, evolution and dynamics of CSs, FRs/plasmoids, MIs in the heliosphere are necessary for better understanding of the transport of energetic particles in the heliosphere, including galactic cosmic rays (Engelbrecht, 2019b).

CSs, FRs/MIs, and plasmoids/blobs of various origins and scales exist in the turbulent solar wind. Therefore, we provide an analysis of the main properties of solar wind turbulence, from large (MHD) to smaller (kinetic) scales for convenience of the readers interested in numerical simulations. Here, we particularly focus on the most recent advances in kinetic numerical simulations (e.g., Servidio et al. (2015)). Owing to the weak collisionality, plasma turbulence naturally evolves in the fully 6D phase-space and excites a variety of genuinely kinetic effects in the particle VDF (Valentini et al., 2016; Servidio et al., 2017; Pezzi et al., 2018), ranging from beams along the background magnetic field to a highly-structured velocity-space, as recently found via the Hermite decomposition of the particle VDF.

To conclude, one may offer numerous applications in which the structures revealed by the combined GS/PVI method can be relevant in understanding the complex physics and turbulent dynamics of both the interplanetary magnetic field and the solar wind plasma. It should be emphasized that most of contemporaneous theoretical works describing solar-wind properties have been made in a frame of 2D modeling and reconstructions. Very often, the available methods do not allow complete understanding the real shape of 3D plasma structures, as discussed in Part I of this review. Talking about 2D modeling, one should take into account a certain degree of uncertainty in the interpretation of the results, which is similar to problems of the interpretation of observations. In particular, the shapes and corresponding dynamics of

magneto-plasma structures in the solar wind may only be suggested since one considers a cross-section of real 3D structures which may be both FRs and/or finite shaped plasmoids/blobs. That is why we talk about 2D magnetic islands above. We admit that the lack of 3D models due to an obvious complexity of their building as well as the insufficiency of multi-spacecraft data to restore 3D structures are disadvantages of the modern theoretical and observational approaches. Meanwhile, we can conclude that employing contemporary 2D models and corresponding simplified methods widely used in space science allows general understanding of the numerous complex processes if one initially considers various possible 3D topologies occurring in the real space plasmas. The transition from the 2D to 3D models to describe complex 3D processes and non-planar structures in the solar wind is the next step of the development of heliospheric physics.

Acknowledgements This work is supported by the International Space Science Institute (ISSI) in the framework of International Team 405 entitled “Current Sheets, Turbulence, Structures and Particle Acceleration in the Heliosphere.”. O.P. thanks Dr. D. Trotta and Dr. F. Catapano for friendly and precious conversations on some of the topics discussed in this review.

Funding R.K., H.M. and O.K. are partially supported by Russian Foundation for Basic Research (RFBR) grant 19-02-00957. H.M. acknowledges the partial support of Volkswagen Foundation grant Az90 312. J. A. le Roux acknowledges support from NASA Grants NNX15AI65G, 80NSSC19K027, NSF-DOE grant PHY-1707247, and NSF-EPSCoR RII-Track-1 Cooperative Agreement OIA-1655280. S.S. acknowledges the European Union’s Horizon 2020 research and innovation programme under Grant Agreement No. 776262 (AIDA, www.aida-space.eu).

Conflicts of interest/Competing interests The authors declare no conflict of interests.

Availability of data and material (data transparency) All data and material used are from public open-access data depositories and archives (see Acknowledgements for details).

Code availability Not applicable

References

- Adhikari L, Zank GP, Hunana P, Shiota D, Bruno R, Hu Q, Telloni D (2017) II. transport of nearly incompressible magnetohydrodynamic turbulence from 1 to 75 au. *The Astrophysical Journal*841:85, DOI 10.3847/1538-4357/aa6f5d
- Adhikari L, Khabarova O, Zank GP, Zhao LL (2019) The Role of Magnetic Reconnection-associated Processes in Local Particle Acceleration in the Solar Wind. *The Astrophysical Journal*873(1):72, DOI 10.3847/1538-4357/ab05c6
- Alexandrova O, Carbone V, Veltri P, Sorriso-Valvo L (2008) Small scale energy cascade of the solar wind turbulence. *The Astrophysical Journal*674:1153–1157, DOI 10.1086/524056

- Amano T, Katou T, Kitamura N, Oka M, Matsumoto Y, Hoshino M, Saito Y, Yokota S, Giles BL, Paterson WR, Russell CT, Le Contel O, Ergun RE, Lindqvist PA, Turner DL, Fennell JF, Blake JB (2020) Observational Evidence for Stochastic Shock Drift Acceleration of Electrons at the Earth's Bow Shock. *Physical Review Letters*124(6):065101, DOI 10.1103/PhysRevLett.124.065101, 2002.06787
- Ambrosiano J, Matthaeus WH, Goldstein ML, Plante D (1988) Test particle acceleration in turbulent reconnecting magnetic fields. *Journal of Geophysical Research* 93:14383–14400, DOI 10.1029/JA093iA12p14383
- Andrés N, Sahraoui F, Galtier S, Hadid LZ, Ferrand R, Huang SY (2019) Energy Cascade Rate Measured in a Collisionless Space Plasma with MMS Data and Compressible Hall Magnetohydrodynamic Turbulence Theory. *Physical Review Letters*123(24):245101, DOI 10.1103/PhysRevLett.123.245101, 1911.09749
- Antiochos SK, DeVore CR (1999) The role of magnetic reconnection in solar activity. Washington DC American Geophysical Union Geophysical Monograph Series 199:113–120, astro-ph/9809161
- Apatenkov SV, Sergeev VA, Kubyshkina MV, Nakamura R, Baumjohann W, Runov A, Alexeev I, Fazakerley A, Frey H, Muhlbacher S, Daly PW, Sauvaud JA, Ganushkina N, Pulkkinen T, Reeves GD, Khotyaintsev Y (2007) Multi-spacecraft observation of plasma dipolarization/injection in the inner magnetosphere. *Annales Geophysicae* 25(3):801–814, URL <https://hal.archives-ouvertes.fr/hal-00330123>
- Artemyev AV, Petrukovich AA, Zelenyi L, Nakamura R, Malova H, Popov VY (2009a) Thin embedded current sheets: Cluster observations of ion kinetic structure and analytical models. *Annales Geophysicae* 27(10):4075–4087, DOI 10.5194/angeo-27-4075-2009
- Artemyev AV, Zelenyi LM, Malova HV, Zimbardo G, Delcourt D (2009b) Acceleration and transport of ions in turbulent current sheets: formation of non-maxwellian energy distribution. *Nonlinear Processes in Geophysics* 16(6):631–639, DOI 10.5194/npg-16-631-2009, URL <https://www.nonlin-processes-geophys.net/16/631/2009/>
- Ashour-Abdalla M, Berchem JP, Buechner J, Zelenyi LM (1993) Shaping of the magnetotail from the mantle: Global and local structuring. *Journal of Geophysical Research*98(A4):5651–5676, DOI 10.1029/92JA01662
- Aunai N, Hesse M, Kuznetsova M (2013) Electron nongyrotopropy in the context of collisionless magnetic reconnection. *Physics of Plasmas* 20(9):092903, DOI 10.1063/1.4820953, URL <https://doi.org/10.1063/1.4820953>, <https://doi.org/10.1063/1.4820953>
- Ball D, Sironi L, Özel F (2018) Electron and Proton Acceleration in Transrelativistic Magnetic Reconnection: Dependence on Plasma Beta and Magnetization. *The Astrophysical Journal* 862(1):80, DOI 10.3847/1538-4357/aac820
- Bandyopadhyay R, Matthaeus WH, Parashar TN, Yang Y, Chasapis A, Giles BL, Gershman DJ, Pollock CJ, Russell CT, Strangeway RJ, Torbert RB, Moore TE, Burch JL (2020a) Statistics of Kinetic Dissipation

- in the Earth's Magnetosheath: MMS Observations. *Physical Review Letters*124(25):255101, DOI 10.1103/PhysRevLett.124.255101, 2005.09232
- Bandyopadhyay R, Qudsi RA, Matthaeus WH, Parashar TN, Maruca BA, Gary SP, Roytershteyn V, Chasapis A, Giles BL, Gershman DJ, Pollock CJ, Russell CT, Strangeway RJ, Torbert RB, Moore TE, Burch JL (2020b) Interplay of Turbulence and Proton-Microinstability Growth in Space Plasmas. arXiv e-prints arXiv:2006.10316, 2006.10316
- Batchelor G (1976) Brownian diffusion of particles with hydrodynamic interaction. *Journal of Fluid Mechanics* 74(1):1–29
- Battarbee M, Dalla S, Marsh MS (2017) Solar energetic particle transport near a heliospheric current sheet. *The Astrophysical Journal* 836(1):138, DOI 10.3847/1538-4357/836/1/138, URL <https://doi.org/10.3847/2F1538-4357/2F836/2F1/2F138>
- Battarbee M, Dalla S, Marsh MS (2018) Modeling Solar Energetic Particle Transport near a Wavy Heliospheric Current Sheet. *The Astrophysical Journal*854(1):23, DOI 10.3847/1538-4357/aaa3fa, 1712.03729
- Baumjohann W, Matsuoka A, Glassmeier KH, Russell CT, Nagai T, Hoshino M, Nakagawa T, Balogh A, Slavin JA, Nakamura R, Magnes W (2006) The magnetosphere of Mercury and its solar wind environment: Open issues and scientific questions. *Advances in Space Research* 38(4):604–609, DOI 10.1016/j.asr.2005.05.117
- Behannon KW, Neubauer FM, Barnstorf H (1981) Fine-scale characteristics of interplanetary sector boundaries. *Journal of Geophysical Research*86(A5):3273–3287, DOI 10.1029/JA086iA05p03273
- Beinroth HJ, Neubauer FM (1981) Properties of whistler mode waves between 0.3 and 1.0 au from helios observations. *Journal of Geophysical Research: Space Physics* 86(A9):7755–7760, DOI 10.1029/JA086iA09p07755, URL <https://agupubs.onlinelibrary.wiley.com/doi/abs/10.1029/JA086iA09p07755>, <https://agupubs.onlinelibrary.wiley.com/doi/pdf/10.1029/JA086iA09p07755>
- Bell AR (1978a) The acceleration of cosmic rays in shock fronts - I. *Monthly Notices of the Royal Astronomical Society*182:147–156, DOI 10.1093/mnras/182.2.147
- Bell AR (1978b) The acceleration of cosmic rays in shock fronts - II. *Monthly Notices of the Royal Astronomical Society*182:443–455, DOI 10.1093/mnras/182.3.443
- Benella S, Grimani C, Laurenza M, Consolini G (2019) Grad-Shafranov reconstruction of a magnetic cloud: Effects of the magnetic-field topology on the galactic cosmic-ray intensity. *Nuovo Cimento C Geophysics Space Physics C* 42(1):44, DOI 10.1393/ncc/i2019-19044-7
- Bieber JW, Matthaeus WH (1997) Perpendicular Diffusion and Drift at Intermediate Cosmic-Ray Energies. *The Astrophysical Journal*485(2):655–659, DOI 10.1086/304464
- Bieber JW, Matthaeus WH, Smith CW, Wanner W, Kallenrode M, Wibberenz G (1994) Proton and Electron Mean Free Paths: The Palmer consensus revisited. *The Astrophysical Journal*420:294–306, DOI 10.1086/173559

- Bieber JW, Wanner W, Matthaeus WH (1996) Dominant two-dimensional solar wind turbulence with implications for cosmic ray transport. *Journal of Geophysical Research* 101:2511–2522, DOI 10.1029/95JA02588
- Birn J, Drake J, Shay M, Rogers B, Denton R, Hesse M, Kuznetsova M, Ma Z, Bhattacharjee A, Otto A, et al. (2001) Geospace environmental modeling (gem) magnetic reconnection challenge. *Journal of Geophysical Research: Space Physics* 106(A3):3715–3719
- Blandford RD, Ostriker JP (1978) Particle acceleration by astrophysical shocks. *The Astrophysical Journal Letters* 221:L29–L32, DOI 10.1086/182658
- Borgogno D, Grasso D, Porcelli F, Califano F, Pegoraro F, Farina D (2005) Aspects of three-dimensional magnetic reconnection. *Physics of Plasmas* 12(3):032309, DOI 10.1063/1.1857912
- Borovsky JE (2008) Flux tube texture of the solar wind: Strands of the magnetic carpet at 1 AU? *Journal of Geophysical Research (Space Physics)* 113(A8):A08110, DOI 10.1029/2007JA012684
- Braginskii S (1965) Transport processes in a plasma. *Reviews of plasma physics* 1
- Breuillard H, Matteini L, Argall MR, Sahraoui F, Andriopoulou M, Contel OL, Retinò A, Mirioni L, Huang SY, Gershman DJ, Ergun RE, Wilder FD, Goodrich KA, Ahmadi N, Yordanova E, Vaivads A, Turner DL, Khotyaintsev YV, Graham DB, Lindqvist PA, Chasapis A, Burch JL, Torbert RB, Russell CT, Magnes W, Strangeway RJ, Plaschke F, Moore TE, Giles BL, Paterson WR, Pollock CJ, Lavraud B, Fuselier SA, Cohen IJ (2018) "new insights into the nature of turbulence in the earth's magnetosheath using magnetospheric MultiScale mission data". *The Astrophysical Journal* 859(2):127, DOI 10.3847/1538-4357/aabae8, URL <https://doi.org/10.3847/2F1538-4357/2Faabae8>
- Brown MR, Cothran CD, Fung J (2006) Two fluid effects on three-dimensional reconnection in the Swarthmore Spheromak Experiment with comparisons to space data. *Physics of Plasmas* 13(5):056503, DOI 10.1063/1.2180729
- Bruno R, Carbone V (2016) *Turbulence in the solar wind*. Springer, DOI 10.1007/978-3-319-43440-7
- Bruno R, Carbone V, Veltri P, Pietropaolo E, Bavassano B (2001) Identifying intermittency events in the solar wind. *Planetary and Space Science* 49(12):1201–1210, DOI 10.1016/S0032-0633(01)00061-7
- Büchner J, Kuska JP (1999) Sausage mode instability of thin current sheets as a cause of magnetospheric substorms. *Annales Geophysicae* 17(5):604–612, DOI 10.1007/s00585-999-0604-5
- Buechner J, Zelenyi LM (1989) Regular and chaotic charged particle motion in magnetotail-like field reversals. 1. Basic theory of trapped motion. *Journal of Geophysical Research* 94(A9):11821–11842, DOI 10.1029/JA094iA09p11821
- Burch J, Phan T (2016a) Magnetic reconnection at the dayside magnetopause: Advances with mms. *Geophysical Research Letters* 43(16):8327–8338
- Burch J, Torbert R, Phan T, Chen LJ, Moore T, Ergun R, Eastwood J, Gershman D, Cassak P, Argall M, et al. (2016a) Electron-scale measurements

- of magnetic reconnection in space. *Science* 352(6290):aaf2939
- Burch JL, Phan TD (2016b) Magnetic reconnection at the dayside magnetopause: Advances with mms. *Geophysical Research Letters* 43(16):8327–8338, DOI 10.1002/2016GL069787
- Burch JL, Moore TE, Torbert RB, Giles BL (2016b) Magnetospheric Multiscale Overview and Science Objectives. *Space Sci Rev* 199:5–21, DOI 10.1007/s11214-015-0164-9
- Burger RA (2012) Modeling Drift along the Heliospheric Wavy Neutral Sheet. *The Astrophysical Journal* 760(1):60, DOI 10.1088/0004-637X/760/1/60
- Burger RA, Visser DJ (2010) Reduction of Drift Effects due to Solar Wind Turbulence. *The Astrophysical Journal* 725(1):1366–1372, DOI 10.1088/0004-637X/725/1/1366
- Burger RA, Moraal H, Webb GM (1985) Drift theory of charged particles in electric and magnetic fields. *Astrophysics and Space Science* 116(1):107–129, DOI 10.1007/BF00649278
- Burger RA, Krüger TPJ, Hitge M, Engelbrecht NE (2008) A Fisk-Parker Hybrid Heliospheric Magnetic Field with a Solar-Cycle Dependence. *The Astrophysical Journal* 674(1):511–519, DOI 10.1086/525039
- Burgess D (1987) Shock drift acceleration at low energies. *Journal of Geophysical Research* 92(A2):1119–1130, DOI 10.1029/JA092iA02p01119
- Caballero-Lopez RA, Engelbrecht NE, Richardson JD (2019) Correlation of Long-term Cosmic-Ray Modulation with Solar Activity Parameters. *The Astrophysical Journal* 883(1):73, DOI 10.3847/1538-4357/ab3c57
- Califano F, Cerri SS, Faganello M, Laveder D, Sisti M, Kunz MW (2020) Electron-only reconnection in plasma turbulence. *Frontiers in Physics* 8:317, DOI 10.3389/fphy.2020.00317
- Carbone V, Veltri P (1990) A shell model for anisotropic magnetohydrodynamic turbulence. *Geophysical & Astrophysical Fluid Dynamics* 52(1-3):153–181
- Cassak PA, Shay MA, Drake JF (2005) Catastrophe model for fast magnetic reconnection onset. *Phys Rev Lett* 95:235002, DOI 10.1103/PhysRevLett.95.235002, URL <https://link.aps.org/doi/10.1103/PhysRevLett.95.235002>
- Cassak PA, Drake JF, Shay MA, Eckhardt B (2007) Onset of fast magnetic reconnection. *Phys Rev Lett* 98:215001, DOI 10.1103/PhysRevLett.98.215001, URL <https://link.aps.org/doi/10.1103/PhysRevLett.98.215001>
- Catapano F, Artemyev AV, Zimbardo G, Vasko IY (2015) Current sheets with inhomogeneous plasma temperature: Effects of polarization electric field and 2D solutions. *Physics of Plasmas* 22(9):092905, DOI 10.1063/1.4931736
- Catapano F, Zimbardo G, Perri S, Greco A, Artemyev AV (2016) Proton and heavy ion acceleration by stochastic fluctuations in the Earth’s magnetotail. *Annales Geophysicae* 34(10):917–926, DOI 10.5194/angeo-34-917-2016
- Catapano F, Zimbardo G, Perri S, Greco A, Delcourt D, Retinò A, Cohen IJ (2017) Charge Proportional and Weakly Mass-Dependent Acceleration of Different Ion Species in the Earth’s Magnetotail. *Geophysical Research Letters* 44(20):10,108–10,115, DOI 10.1002/2017GL075092, 1709.09926

- Cerri SS, Califano F (2017) Reconnection and small-scale fields in 2D-3V hybrid-kinetic driven turbulence simulations. *New Journal of Physics* 19(2):025007, DOI 10.1088/1367-2630/aa5c4a
- Cerri SS, Servidio S, Califano F (2017) Kinetic cascade in solar-wind turbulence: 3d3v hybrid-kinetic simulations with electron inertia. *The Astrophysical Journal* 846(2):L18, DOI 10.3847/2041-8213/aa87b0
- Cerri SS, Kunz MW, Califano F (2018) Dual phase-space cascades in 3d hybrid-vlasov-maxwell turbulence. *The Astrophysical Journal* 856(1):L13, DOI 10.3847/2041-8213/aab557, URL <https://doi.org/10.3847/2F2041-8213%2Faab557>
- Chandran BDG, Li B, Rogers BN, Quataert E, Germaschewski K (2010) Perpendicular Ion Heating by Low-frequency Alfvén-wave Turbulence in the Solar Wind. *The Astrophysical Journal* 720:503–515, DOI 10.1088/0004-637X/720/1/503, 1001.2069
- Chandrasekhar S (1943) Stochastic problems in physics and astronomy. *Reviews of modern physics* 15(1):1
- Chasapis A, Matthaeus WH, Parashar TN, Wan M, Haggerty CC, Pollock CJ, Giles BL, Paterson WR, Dorelli J, Gershman DJ, Torbert RB, Russell CT, Lindqvist PA, Khotyaintsev Y, Moore TE, Ergun RE, Burch JL (2018) "in situ observation of intermittent dissipation at kinetic scales in the earth's magnetosheath". *The Astrophysical Journal* 856(1):L19, DOI 10.3847/2041-8213/aaadf8, URL <https://doi.org/10.3847/2F2041-8213%2Faaadf8>
- Chasapis A, Yang Y, Matthaeus WH, Parashar TN, Haggerty CC, Burch JL, Moore TE, Pollock CJ, Dorelli J, Gershman DJ, Torbert RB, Russell CT (2018) Energy Conversion and Collisionless Plasma Dissipation Channels in the Turbulent Magnetosheath Observed by the Magnetospheric Multiscale Mission. *Astrophys J* 862:32, DOI 10.3847/1538-4357/aac775
- Chasapis A, Yang Y, Matthaeus WH, Parashar TN, Haggerty CC, Burch JL, Moore TE, Pollock CJ, Dorelli J, Gershman DJ, Torbert RB, Russell CT (2018) Energy conversion and collisionless plasma dissipation channels in the turbulent magnetosheath observed by the magnetospheric multiscale mission. *The Astrophysical Journal* 862(1):32, DOI 10.3847/1538-4357/aac775, URL <https://doi.org/10.3847/2F1538-4357%2Faac775>
- Chen CHK, Boldyrev S, Xia Q, Perez JC (2013) Nature of subproton scale turbulence in the solar wind. *Phys Rev Lett* 110:225002, DOI 10.1103/PhysRevLett.110.225002, URL <https://link.aps.org/doi/10.1103/PhysRevLett.110.225002>
- Chen CHK, Klein KG, Howes GG (2019a) Evidence for electron Landau damping in space plasma turbulence. *Nature Communications* 10:740, DOI 10.1038/s41467-019-08435-3, 1902.05785
- Chen LJ, Wang S, Hesse M, Ergun RE, Moore T, Giles B, Bessho N, Russell C, Burch J, Torbert RB, Genestreti KJ, Paterson W, Pollock C, Lavraud B, Le Contel O, Strangeway R, Khotyaintsev YV, Lindqvist PA (2019b) Electron Diffusion Regions in Magnetotail Reconnection Under Varying Guide Fields. *Geophysical Research Letters* 46(12):6230–6238, DOI

- 10.1029/2019GL082393
- Chen Y, Hu Q, le Roux JA (2019c) Analysis of small-scale magnetic flux ropes covering the whole ulysses mission. *The Astrophysical Journal*881(1):58, DOI 10.3847/1538-4357/ab2ccf, 1905.00986
- Chhiber R, Usmanov A, Matthaeus W, Goldstein M (2016) SOLAR WIND COLLISIONAL AGE FROM a GLOBAL MAGNETOHYDRODYNAMICS SIMULATION. *The Astrophysical Journal* 821(1):34, DOI 10.3847/0004-637x/821/1/34, URL <https://doi.org/10.3847%2F0004-637x%2F821%2F1%2F34>
- Chhiber R, Usmanov AV, Matthaeus WH, Parashar TN, Goldstein ML (2019) Contextual Predictions for Parker Solar Probe. II. Turbulence Properties and Taylor Hypothesis. *The Astrophysical Journal Supplement*242(1):12, DOI 10.3847/1538-4365/ab16d7, 1902.03340
- Christon SP, Williams DJ, Mitchell DG, Frank LA, Huang CY (1989) Spectral characteristics of plasma sheet ion and electron populations during undisturbed geomagnetic conditions. *Journal of Geophysical Research*94(A10):13409–13424, DOI 10.1029/JA094iA10p13409
- Collier MR (1999) Evolution of kappa distributions under velocity space diffusion: A model for the observed relationship between their spectral parameters. *Journal of Geophysical Research*104(A12):28559–28564, DOI 10.1029/1999JA900355
- Comisso L, Sironi L (2018) Particle acceleration in relativistic plasma turbulence. *Physical review letters* 121(25):255101
- Comisso L, Sironi L (2019) The Interplay of Magnetically Dominated Turbulence and Magnetic Reconnection in Producing Nonthermal Particles. *The Astrophysical Journal* 886(2):122, DOI 10.3847/1538-4357/ab4c33
- Coppi B, Laval G, Pellat R (1966) Dynamics of the geomagnetic tail. *Phys Rev Lett* 16:1207–1210, DOI 10.1103/PhysRevLett.16.1207, URL <https://link.aps.org/doi/10.1103/PhysRevLett.16.1207>
- Coroniti FV (1980) On the tearing mode in quasi-neutral sheets. *Journal of Geophysical Research*85(A12):6719–6728, DOI 10.1029/JA085iA12p06719
- Cowley SWH, Shull J P (1983) Current sheet acceleration of ions in the geomagnetic tail and the properties of ion bursts observed at the lunar distance. *Planetary and Space Science*31(2):235–245, DOI 10.1016/0032-0633(83)90058-2
- Crooker NU, Siscoe GL, Shodhan S, Webb DF, Gosling JT, Smith EJ (1993) Multiple heliospheric current sheets and coronal streamer belt dynamics. *Journal of Geophysical Research*98(A6):9371–9382, DOI 10.1029/93JA00636
- Crooker NU, Kahler SW, Larson DE, Lin RP (2004) Large-scale magnetic field inversions at sector boundaries. *Journal of Geophysical Research (Space Physics)* 109(A3):A03108, DOI 10.1029/2003JA010278
- Curtis S (1999) The magnetospheric multiscale mission. Resolving Fundamental Processes in Space Plasmas, NASA Goddard Space Flight Center
- Dahlburg RB, Karpen JT (1995) A triple current sheet model for adjoining coronal helmet streamers. *Journal of Geophysical Research*100(A12):23489–

- 23498, DOI 10.1029/95JA02496
- Dahlin JT, Drake JF, Swisdak M (2016) Parallel electric fields are inefficient drivers of energetic electrons in magnetic reconnection. *Physics of Plasmas* 23:120704
- Dahlin JT, Drake JF, Swisdak M (2017) The role of three-dimensional transport in driving enhanced electron acceleration during magnetic reconnection. *Physics of Plasmas* 24:092110
- Daldorff LKS, Tóth G, Gombosi TI, Lapenta G, Amaya J, Markidis S, Brackbill JU (2014) Two-way coupling of a global Hall magnetohydrodynamics model with a local implicit particle-in-cell model. *Journal of Computational Physics* 268:236–254, DOI 10.1016/j.jcp.2014.03.009
- Dalena S, Rappazzo AF, Dmitruk P, Greco A, Matthaeus WH (2014) Test-particle Acceleration in a Hierarchical Three-dimensional Turbulence Model. *Astrophys J* 783:143, DOI 10.1088/0004-637X/783/2/143, 1402.3745
- Dalena S, Greco A, Rappazzo AF, Mace RL, Matthaeus WH (2012) Magnetic moment nonconservation in magnetohydrodynamic turbulence models. *Phys Rev E* 86(1, Part 2), DOI {10.1103/PhysRevE.86.016402}
- Dalla S, Marsh MS, Kelly J, Laitinen T (2013) Solar energetic particle drifts in the Parker spiral. *Journal of Geophysical Research (Space Physics)* 118(10):5979–5985, DOI 10.1002/jgra.50589, 1307.2165
- Daughton W (1999) The unstable eigenmodes of a neutral sheet. *Physics of Plasmas* 6(4):1329–1343, DOI 10.1063/1.873374
- Daughton W, Roytershteyn V, Karimabadi H, Yin L, Albright BJ, Bergen B, Bowers KJ (2011) Role of electron physics in the development of turbulent magnetic reconnection in collisionless plasmas. *Nature Physics* 7:539–542, DOI 10.1038/nphys1965
- Delcourt DC (2002) Particle acceleration by inductive electric fields in the inner magnetosphere. *Journal of Atmospheric and Solar-Terrestrial Physics* 64(5-6):551–559, DOI 10.1016/S1364-6826(02)00012-3
- Delcourt DC, Sauvaud JA (1994) Plasma sheet ion energization during dipolarization events. *Journal of Geophysical Research* 99(A1):97–108, DOI 10.1029/93JA01895
- Delcourt DC, Seki K, Terada N, Miyoshi Y (2005) Electron dynamics during substorm dipolarization in Mercury's magnetosphere. *Annales Geophysicae* 23(10):3389–3398, DOI 10.5194/angeo-23-3389-2005
- Delzanno G (2015) Multi-dimensional, fully-implicit, spectral method for the vlasov–maxwell equations with exact conservation laws in discrete form. *Journal of Computational Physics* 301:338 – 356, DOI <https://doi.org/10.1016/j.jcp.2015.07.028>, URL <http://www.sciencedirect.com/science/article/pii/S0021999115004738>
- Dmitruk P, Matthaeus WH (2006) Structure of the electromagnetic field in three-dimensional Hall magnetohydrodynamic turbulence. *Physics of Plasmas* 13(4):042307, DOI 10.1063/1.2192757
- Dmitruk P, Matthaeus WH, Seenu N (2004a) Test Particle Energization by Current Sheets and Nonuniform Fields in Magnetohydrodynamic Turbulence. *The Astrophysical Journal* 617:667–679, DOI 10.1086/425301

- Dmitruk P, Matthaeus WH, Seenu N (2004b) Test Particle Energization by Current Sheets and Nonuniform Fields in Magnetohydrodynamic Turbulence. *The Astrophysical Journal* 617:667–679, DOI 10.1086/425301
- Dobrowolny M, Mangeney A, Veltri P (1980a) Fully Developed Anisotropic Hydromagnetic Turbulence in Interplanetary Space. *Physical Review Letters* 45(2):144–147, DOI 10.1103/PhysRevLett.45.144
- Dobrowolny M, Mangeney A, Veltri P (1980b) Properties of magnetohydrodynamic turbulence in the solar wind. *Astronomy and Astrophysics* 83(1-2):26–32
- Donato S, Servidio S, Dmitruk P, Carbone V, Shay MA, Cassak PA, Matthaeus WH (2012) Reconnection events in two-dimensional hall magnetohydrodynamic turbulence. *Physics of Plasmas* 19(9):092307, DOI 10.1063/1.4754151, URL <https://doi.org/10.1063/1.4754151>, <https://doi.org/10.1063/1.4754151>
- Drake J, Swisdak M, Schoeffler K, Rogers B, Kobayashi S (2006) Formation of secondary islands during magnetic reconnection. *Geophysical research letters* 33(13)
- Drake JF, Gerber J, Kleva RG (1994) Turbulence and transport in the magnetopause current layer. *Journal of Geophysical Research* 99(A6):11211–11224, DOI 10.1029/93JA03253
- Drake JF, Swisdak M, Che H, Shay MA (2006) Electron acceleration from contracting magnetic islands during reconnection. *Nature* 443(7111):553–556, DOI 10.1038/nature05116
- Drake JF, Opher M, Swisdak M, Chamoun JN (2010) A Magnetic Reconnection Mechanism for the Generation of Anomalous Cosmic Rays. *The Astrophysical Journal* 709:963–974, DOI 10.1088/0004-637X/709/2/963, 0911.3098
- Drake JF, Swisdak M, Fermo R (2013) The Power-law Spectra of Energetic Particles during Multi-island Magnetic Reconnection. *The Astrophysical Journal* 763:L5, DOI 10.1088/2041-8205/763/1/L5, 1210.4830
- Drake JF, Swisdak M, Cassak PA, Phan TD (2014) On the 3-D structure and dissipation of reconnection-driven flow bursts. *Geophysical Research Letters* 41(11):3710–3716, DOI 10.1002/2014GL060249, 1401.7056
- Drake JF, Arnold H, Swisdak M, Dahlin JT (2019) A computational model for exploring particle acceleration during reconnection in macroscale systems. *Physics of Plasmas* 26(1):012901, DOI 10.1063/1.5058140, 1809.04568
- Du S, Guo F, Zank GP, Li X, Stanier A (2018) Plasma Energization in Colliding Magnetic Flux Ropes. *The Astrophysical Journal* 867:16
- Dundovic A, Pezzi O, Blasi P, Evoli C, Matthaeus WH (2020) Novel aspects of cosmic ray diffusion in synthetic magnetic turbulence. *arXiv e-prints arXiv:2007.09142*, 2007.09142
- Eastwood JP, Phan TD, Cassak PA, Gershman DJ, Haggerty C, Malakit K, Shay MA, Mistry R, Øieroset M, Russell CT, Slavin JA, Argall MR, Avakov LA, Burch JL, Chen LJ, Dorelli JC, Ergun RE, Giles BL, Khotyaintsev Y, Lavraud B, Lindqvist PA, Moore TE, Nakamura R, Paterson W, Pollock C, Strangeway RJ, Torbert RB, Wang S (2016) Ion-scale secondary flux ropes

- generated by magnetopause reconnection as resolved by mms. *Geophysical Research Letters* 43(10):4716–4724, DOI 10.1002/2016GL068747
- Effenberger F, Litvinenko YE (2014) The Diffusion Approximation versus the Telegraph Equation for Modeling Solar Energetic Particle Transport with Adiabatic Focusing. I. Isotropic Pitch-angle Scattering. *The Astrophysical Journal* 783:15
- Engelbrecht NE (2019a) On the Pitch-angle-dependent Perpendicular Diffusion Coefficients of Solar Energetic Protons in the Inner Heliosphere. *The Astrophysical Journal* 880(1):60, DOI 10.3847/1538-4357/ab2871
- Engelbrecht NE (2019b) The Implications of Simple Estimates of the 2D Outerscale Based on Measurements of Magnetic Islands for the Modulation of Galactic Cosmic-Ray Electrons. *The Astrophysical Journal* 872(2):124, DOI 10.3847/1538-4357/aafe7f
- Engelbrecht NE, Burger RA (2013) An ab initio model for cosmic-ray modulation. *The Astrophysical Journal* 772:46, DOI 10.1088/0004-637X/772/1/46
- Engelbrecht NE, Burger RA (2015) Sensitivity of Cosmic-Ray Proton Spectra to the Low-wavenumber Behavior of the 2D Turbulence Power Spectrum. *The Astrophysical Journal* 814(2):152, DOI 10.1088/0004-637X/814/2/152
- Engelbrecht NE, Strauss RD, le Roux JA, Burger RA (2017) Toward a Greater Understanding of the Reduction of Drift Coefficients in the Presence of Turbulence. *The Astrophysical Journal* 841(2):107, DOI 10.3847/1538-4357/aa7058
- Engelbrecht NE, Mohlolo ST, Ferreira SES (2019) An Improved Treatment of Neutral Sheet Drift in the Inner Heliosphere. *The Astrophysical Journal Letters* 884(2):L54, DOI 10.3847/2041-8213/ab4ad6
- Ergun RE, Ahmadi N, Kromyda L, Schwartz SJ, Chasapis A, Hoilijoki S, Wilder FD, Cassak PA, Stawarz JE, Goodrich KA, Turner DL, Pucci F, Pouquet A, Matthaeus WH, Drake JF, Hesse M, Shay MA, Torbert RB, Burch JL (2020a) Particle Acceleration in Strong Turbulence in the Earth’s Magnetotail. *The Astrophysical Journal* 898(2):153, DOI 10.3847/1538-4357/ab9ab5
- Ergun RE, Ahmadi N, Kromyda L, Schwartz SJ, Chasapis A, Hoilijoki S, Wilder FD, Stawarz JE, Goodrich KA, Turner DL, Cohen IJ, Bingham ST, Holmes JC, Nakamura R, Pucci F, Torbert RB, Burch JL, Lindqvist PA, Strangeway RJ, Le Contel O, Giles BL (2020b) Observations of Particle Acceleration in Magnetic Reconnection-driven Turbulence. *The Astrophysical Journal* 898(2):154, DOI 10.3847/1538-4357/ab9ab6
- Fermi E (1949) On the Origin of the Cosmic Radiation. *Physical Review* 75(8):1169–1174, DOI 10.1103/PhysRev.75.1169
- Fermi E (1954) Galactic Magnetic Fields and the Origin of Cosmic Radiation. *The Astrophysical Journal* 119:1, DOI 10.1086/145789
- Ferreira SES, Potgieter MS, Heber B, Fichtner H (2003) Charge-sign dependent modulation in the heliosphere over a 22-year cycle. *Annales Geophysicae* 21(6):1359–1366, DOI 10.5194/angeo-21-1359-2003
- Forman MA, Jokipii JR, Owens AJ (1974) Cosmic-ray streaming perpendicular to the mean magnetic field. *The Astrophysical Journal* 192:535–540

- Franci L, Verdini A, Matteini L, Landi S, Hellinger P (2015) Solar Wind Turbulence from MHD to Sub-ion Scales: High-resolution Hybrid Simulations. *The Astrophys J Lett* 804:L39, DOI 10.1088/2041-8205/804/2/L39, 1503.05457
- Franci L, Cerri SS, Califano F, Landi S, Papini E, Verdini A, Matteini L, Jenko F, Hellinger P (2017) Magnetic Reconnection as a Driver for a Sub-ion-scale Cascade in Plasma Turbulence. *The Astrophysical Journal Letters* 850(1):L16, DOI 10.3847/2041-8213/aa93fb, 1707.06548
- Franci L, Landi S, Verdini A, Matteini L, Hellinger P (2018) Solar wind turbulent cascade from MHD to sub-ion scales: Large-size 3d hybrid particle-in-cell simulations. *The Astrophysical Journal* 853(1):26, DOI 10.3847/1538-4357/aaa3e8, URL <https://doi.org/10.3847/1538-4357/2Faa3e8>
- Franci L, Stawarz JE, Papini E, Hellinger P, Nakamura T, Burgess D, Landi S, Verdini A, Matteini L, Ergun R, Le Contel O, Lindqvist PA (2020) Modeling MMS Observations at the Earth's Magnetopause with Hybrid Simulations of Alfvénic Turbulence. *The Astrophysical Journal* 898(2):175, DOI 10.3847/1538-4357/ab9a47
- Fu HS, Vaivads A, Khotyaintsev YV, Olshevsky V, André M, Cao JB, Huang SY, Retinò A, Lapenta G (2015) How to find magnetic nulls and reconstruct field topology with MMS data? *Journal of Geophysical Research (Space Physics)* 120:3758–3782, DOI 10.1002/2015JA021082
- Fu HS, Cao JB, Vaivads A, Khotyaintsev YV, André M, Dunlop M, Liu WL, Lu HY, Huang SY, Ma YD, Eriksson E (2016) Identifying magnetic reconnection events using the FOTE method. *Journal of Geophysical Research: Space Physics* 121(2):1263–1272, DOI 10.1002/2015JA021701
- Fuselier S, Vines S, Burch J, Petrinec S, Trattner K, Cassak P, Chen LJ, Ergun R, Eriksson S, Giles B, et al. (2017) Large-scale characteristics of reconnection diffusion regions and associated magnetopause crossings observed by mms. *Journal of Geophysical Research: Space Physics* 122(5):5466–5486
- Fuselier SA, Lewis WS, Schiff C, Ergun R, Burch JL, Petrinec SM, Trattner KJ (2016) Magnetospheric multiscale science mission profile and operations. *Space Science Reviews* 199(1):77–103, DOI 10.1007/s11214-014-0087-x
- G M Webb HM M J Martinic (1981) Scatter free propagation and drifts of cosmic-rays in the heliosphere. In: *International Cosmic Ray Conference, International Cosmic Ray Conference*, vol 10, p 109
- Galeev AA, Zelenyi LM (1976) Tearing instability in plasma configurations. *Zhurnal Eksperimentalnoi i Teoreticheskoi Fiziki* 70:2133–2151
- Garrel C, Vlahos L, Isliker H, Pisokas T (2018) Diffusive shock acceleration and turbulent reconnection. *Monthly Notices of the Royal Astronomical Society* 478(3):2976–2986, DOI 10.1093/mnras/sty1260, URL <https://doi.org/10.1093/mnras/sty1260>, <https://academic.oup.com/mnras/article-pdf/478/3/2976/25062453/sty1260.pdf>
- Gary SP, Yin L, Winske D, Ofman L, Goldstein BE, Neugebauer M (2003) Consequences of proton and alpha anisotropies in the solar wind: Hybrid simulations. *Journal of Geophysical Research (Space Physics)* 108(A2):1068,

- DOI 10.1029/2002JA009654
- Gary SP, Saito S, Narita Y (2010) Whistler Turbulence Wavevector Anisotropies: Particle-in-cell Simulations. *The Astrophysical Journal*716(2):1332–1335, DOI 10.1088/0004-637X/716/2/1332
- Gary SP, Hughes RS, Wang J (2016) Whistler Turbulence Heating of Electrons and Ions: Three-dimensional Particle-in-cell Simulations. *The Astrophysical Journal*816(2):102, DOI 10.3847/0004-637X/816/2/102
- Gekelman W, Tang SW, DeHaas T, Vincena S, Pribyl P, Sydora R (2019) Spiky electric and magnetic field structures in flux rope experiments. *Proceedings of the National Academy of Science* 116(37):18239–18244, DOI 10.1073/pnas.1721343115
- Ghizzo A, Sarrat M, Del Sarto D (2017) Vlasov models for kinetic Weibel-type instabilities. *Journal of Plasma Physics* 83(1):705830101, DOI 10.1017/S0022377816001215
- Ghosh S, Matthaeus W, Roberts D, Goldstein M (1998) The evolution of slab fluctuations in the presence of pressure-balanced magnetic structures and velocity shears. *Journal of Geophysical Research: Space Physics* (1978–2012) 103(A10):23691–23704
- Giacalone J (1992) Shock drift acceleration of energetic protons at a planetary bow shock. *Journal of Geophysical Research*97(A6):8307–8318, DOI 10.1029/92JA00313
- Gieseler J, Heber B, Herbst K (2017) An Empirical Modification of the Force Field Approach to Describe the Modulation of Galactic Cosmic Rays Close to Earth in a Broad Range of Rigidities. *Journal of Geophysical Research*122(11):10,964–10,979, DOI 10.1002/2017JA024763, 1710.10834
- Glassmeier KH, Mager PN, Klimushkin DY (2003) Concerning ULF pulsations in Mercury’s magnetosphere. *Geophysical Research Letters*30(18):1928, DOI 10.1029/2003GL017175
- Goldstein ML, Roberts DA (1999) Magnetohydrodynamic turbulence in the solar wind. *Phys Plasmas* 6:4154, DOI 10.1063/1.873680
- Gomez T, Politano H, Pouquet A (2000) Exact relationship for third-order structure functions in helical flows. *Physical Review E* 61(5):5321
- González CA, Parashar TN, Gomez D, Matthaeus WH, Dmitruk P (2019) Turbulent electromagnetic fields at sub-proton scales: Two-fluid and full-kinetic plasma simulations. *Physics of Plasmas* 26(1):012306, DOI 10.1063/1.5054110, 1809.00985
- Gosling JT (2007) Observations of Magnetic Reconnection in the Turbulent High-Speed Solar Wind. *The Astrophysical Journal Letters*671(1):L73–L76, DOI 10.1086/524842
- Grad H (1949) On the kinetic theory of rarefied gases. *Communications on Pure and Applied Mathematics*2:331
- Gray PC, Matthaeus WH (1992) MHD turbulence, reconnection, and test-particle acceleration. In: Zank GP, Gaisser TK (eds) *Particle Acceleration in Cosmic Plasmas*, American Institute of Physics Conference Series, vol 264, pp 261–266, DOI 10.1063/1.42738

- Greco A, Matthaeus WH, Servidio S, Chuychai P, Dmitruk P (2009) Statistical Analysis of Discontinuities in Solar Wind ACE Data and Comparison with Intermittent MHD Turbulence. *The Astrophysical Journal* 691:L111–L114, DOI 10.1088/0004-637X/691/2/L111
- Greco A, Valentini F, Servidio S, Matthaeus W (2012) Inhomogeneous kinetic effects related to intermittent magnetic discontinuities. *Physical Review E* 86(6):066405
- Grigorenko EE, Malova HV, Artemyev AV, Mingalev OV, Kronberg EA, Koleva R, Daly PW, Cao JB, Sauvaud JA, Owen CJ, Zelenyi LM (2013) Current sheet structure and kinetic properties of plasma flows during a near-Earth magnetic reconnection under the presence of a guide field. *Journal of Geophysical Research (Space Physics)* 118(6):3265–3287, DOI 10.1002/jgra.50310
- Grošelj D, Cerri SS, Navarro AB, Willmott C, Told D, Loureiro NF, Califano F, Jenko F (2017) Fully kinetic versus reduced-kinetic modeling of collisionless plasma turbulence. *The Astrophysical Journal* 847(1):28, DOI 10.3847/1538-4357/aa894d, URL <https://doi.org/10.3847/1538-4357/aa894d>
- Guo F, Liu YH, Daughton W, Li H (2015) Particle Acceleration and Plasma Dynamics During Magnetic Reconnection in the Magnetically Dominated Regime. *Astrophysical Journal* 806(2):167, DOI 10.1088/0004-637X/806/2/167
- Guo F, Li H, Daughton W, Li X, Liu YH (2016a) Particle acceleration during magnetic reconnection in a low-beta pair plasma. *Physics of Plasmas* 23(5), DOI 10.1063/1.4948284
- Guo F, Li X, Li H, Daughton W, Zhang B, Lloyd-Ronning N, Liu YH, Zhang H, Deng W (2016b) Efficient Production of High-Energy Nonthermal Particles During Magnetic Reconnection in a Magnetically Dominated Ion–Electron Plasma. *The Astrophysical Journal* 818(1):L9, DOI 10.3847/2041-8205/818/1/19
- Hadid LZ, Sahraoui F, Galtier S, Huang SY (2018) Compressible Magnetohydrodynamic Turbulence in the Earth’s Magnetosheath: Estimation of the Energy Cascade Rate Using in situ Spacecraft Data. *Physical Review Letters* 120(5):055102, DOI 10.1103/PhysRevLett.120.055102, 1710.04691
- Haggerty CC, Parashar TN, Matthaeus WH, Shay MA, Yang Y, Wan M, Wu P, Servidio S (2017) Exploring the statistics of magnetic reconnection x-points in kinetic particle-in-cell turbulence. *Physics of Plasmas* 24(10):102308, DOI 10.1063/1.5001722, URL <https://doi.org/10.1063/1.5001722>, <https://doi.org/10.1063/1.5001722>
- Harris EG (1962) On a plasma sheath separating regions of oppositely directed magnetic field. *Il Nuovo Cimento (1955-1965)* 23(1):115–121
- Haynes CT, Burgess D, Camporeale E (2014) Reconnection and Electron Temperature Anisotropy in Sub-proton Scale Plasma Turbulence. *The Astrophysical Journal* 783:38, DOI 10.1088/0004-637X/783/1/38, 1304.1444
- Heber B, Sanderson TR, Zhang M (1999) Corotating interaction regions. *Advances in Space Research* 23(3):567–579, DOI 10.1016/S0273-1177(99)

80013-1

- Hellinger P, Velli M, Trávníček P, Gary SP, Goldstein BE, Liewer PC (2005) Alfvén wave heating of heavy ions in the expanding solar wind: Hybrid simulations. *Journal of Geophysical Research (Space Physics)* 110(A12):A12109, DOI 10.1029/2005JA011244
- Hellinger P, Trávníček P, Kasper JC, Lazarus AJ (2006) Solar wind proton temperature anisotropy: Linear theory and WIND/SWE observations. *Geophys Res Lett* 33:L09101, DOI 10.1029/2006GL025925
- Hellinger P, Matteini L, Landi S, Franci L, Verdini A, Papini E (2019) Turbulence versus Fire-hose Instabilities: 3D Hybrid Expanding Box Simulations. *The Astrophysical Journal* 883(2):178, DOI 10.3847/1538-4357/ab3e01, 1908.07760
- Hesse M, Schindler K, Birn J, Kuznetsova M (1999) The diffusion region in collisionless magnetic reconnection. *Physics of Plasmas* 6(5):1781–1795, DOI 10.1063/1.873436
- Hesse M, Aunai N, Birn J, Cassak P, Denton RE, Drake JF, Gombosi T, Hoshino M, Matthaeus W, Sibeck D, Zenitani S (2016) Theory and modeling for the magnetospheric multiscale mission. *Space Science Reviews* 199(1):577–630, DOI 10.1007/s11214-014-0078-y, URL <https://doi.org/10.1007/s11214-014-0078-y>
- Hesse M, Chen LJ, Liu YH, Bessho N, Burch JL (2017) Population mixing in asymmetric magnetic reconnection with a guide field. *Phys Rev Lett* 118:145101, DOI 10.1103/PhysRevLett.118.145101, URL <https://link.aps.org/doi/10.1103/PhysRevLett.118.145101>
- Higginson AK, Lynch BJ (2018) Structured slow solar wind variability: Streamer-blob flux ropes and torsional alfvén waves. *The Astrophysical Journal* 859(1):6, DOI 10.3847/1538-4357/aabc08, URL <https://doi.org/10.3847/1538-4357/aabc08>
- Hoeksema JT, Wilcox JM, Scherrer PH (1983) The structure of the heliospheric current sheet: 1978–1982. *Journal of Geophysical Research: Space Physics* 88(A12):9910–9918, DOI 10.1029/JA088iA12p09910, URL <https://agupubs.onlinelibrary.wiley.com/doi/abs/10.1029/JA088iA12p09910>, <https://agupubs.onlinelibrary.wiley.com/doi/pdf/10.1029/JA088iA12p09910>
- Hoshino M (2005) Electron surfing acceleration in magnetic reconnection. *J Geophys Res* 110:A10215, DOI 10.1029/2005JA011229
- Howes G, Dorland W, Cowley S, Hammett G, Quataert E, Schekochihin A, Tatsuno T (2008a) Kinetic simulations of magnetized turbulence in astrophysical plasmas. *Physical Review Letters* 100(6):065004
- Howes GG (2015) The inherently three-dimensional nature of magnetized plasma turbulence. *Journal of Plasma Physics* 81(2):325810203, DOI 10.1017/S0022377814001056, 1306.4589
- Howes GG, Cowley SC, Dorland W, Hammett GW, Quataert E, Schekochihin AA (2008b) A model of turbulence in magnetized plasmas: Implications for the dissipation range in the solar wind. *Journal of Geophysical Research: Space Physics* (1978–2012) 113(A05103)

- Hu Q, Sonnerup BU (2002) Reconstruction of magnetic clouds in the solar wind: Orientations and configurations. *Journal of Geophysical Research: Space Physics* 107(A7):SSH-10
- Huang C, Lu Q, Wang R, Guo F, Wu M, Lu S, Wang S (2017) Development of Turbulent Magnetic Reconnection in a Magnetic Island. *The Astrophysical Journal* 835(2):245, DOI 10.3847/1538-4357/835/2/245
- Hussein M, Shalchi A (2016) Simulations of energetic particles interacting with dynamical magnetic turbulence. *The Astrophysical Journal* 817(2):136
- Isenberg PA (1997) A hemispherical model of anisotropic interstellar pickup ions. *Journal of Geophysical Research* 102:4719, DOI 10.1029/96JA03671
- J Birn KS M Hesse (1989) Filamentary structure of a three-dimensional plasmoid. *Journal of Geophysical Research* 94:241
- Janvier M, Démoulin P, Dasso S (2014) Are There Different Populations of Flux Ropes in the Solar Wind? *Solar Physics* 289(7):2633–2652, DOI 10.1007/s11207-014-0486-x, 1401.6812
- Jiang K, Huang SY, Yuan ZG, Sahraoui F, Deng XH, Yu XD, He LH, Deng D, Wei YY, Xu SB (2019) The Role of Upper Hybrid Waves in the Magnetotail Reconnection Electron Diffusion Region. *The Astrophysical Journal Letters* 881(2):L28, DOI 10.3847/2041-8213/ab36b9
- Johnson JR, Cheng CZ (2001) Stochastic ion heating at the magnetopause due to kinetic Alfvén waves. *Geophysical Research Letters* 28(23):4421–4424, DOI 10.1029/2001GL013509
- Jokipii J (1966) Cosmic-ray propagation. i. charged particles in a random magnetic field. *The Astrophysical Journal* 146:480
- Jokipii J, Parker E (1969) Stochastic aspects of magnetic lines of force with application to cosmic-ray propagation. *The Astrophysical Journal* 155:777
- Jokipii JR, Kopriva DA (1979) Effects of particle drift on the transport of cosmic rays. III. Numerical models of galactic cosmic-ray modulation. *The Astrophysical Journal* 234:384–392, DOI 10.1086/157506
- Jokipii JR, Thomas B (1981) Effects of drift on the transport of cosmic rays. IV - Modulation by a wavy interplanetary current sheet. *The Astrophysical Journal* 243:1115–1122, DOI 10.1086/158675
- Jokipii JR, Levy EH, Hubbard WB (1977) Effects of particle drift on cosmic-ray transport. I. General properties, application to solar modulation. *The Astrophysical Journal* 213:861–868, DOI 10.1086/155218
- Juno J, Hakim A, TenBarge J, Shi E, Dorland W (2018) Discontinuous galerkin algorithms for fully kinetic plasmas. *Journal of Computational Physics* 353:110 – 147, DOI <https://doi.org/10.1016/j.jcp.2017.10.009>, URL <http://www.sciencedirect.com/science/article/pii/S0021999117307477>
- Karimabadi H, Pritchett PL, Daughton W, Krauss-Varban D (2003) Ion-ion kink instability in the magnetotail: 2. Three-dimensional full particle and hybrid simulations and comparison with observations. *Journal of Geophysical Research (Space Physics)* 108(A11):1401, DOI 10.1029/2003JA010109
- Karimabadi H, Roytershteyn V, Wan M, Matthaeus WH, Daughton W, Wu P, Shay M, Loring B, Borovsky J, Leonardis E, Chapman SC, Nakamura TKM (2013) Coherent structures, intermittent turbulence, and dissipa-

- tion in high-temperature plasmas. *Physics of Plasmas* 20(1):012303, DOI 10.1063/1.4773205
- Kasper J, Lazarus A, Gary S (2008) Hot solar-wind helium: Direct evidence for local heating by alfvén-cyclotron dissipation. *Physical review letters* 101(26):261103
- Katou T, Amano T (2019) Theory of stochastic shock drift acceleration for electrons in the shock transition region. *The Astrophysical Journal* 874(2):119, DOI 10.3847/1538-4357/ab0d8a, URL <https://doi.org/10.3847/2F1538-4357%2Fab0d8a>
- Khabarova OV, Zank GP (2017) Energetic particles of keV–MeV energies observed near reconnecting current sheets at 1 au. *The Astrophysical Journal* 843(1):4, DOI 10.3847/1538-4357/aa7686
- Khabarova OV, Zank GP, Li G, le Roux JA, Webb GM, Dosch A, Malandraki OE (2015) Small-scale Magnetic Islands in the Solar Wind and Their Role in Particle Acceleration. I. Dynamics of Magnetic Islands Near the Heliospheric Current Sheet. *The Astrophysical Journal* 808(2):181, DOI 10.1088/0004-637X/808/2/181, 1504.06616
- Khabarova OV, Zank GP, Li G, Malandraki OE, le Roux JA, Webb GM (2016) Small-scale magnetic islands in the solar wind and their role in particle acceleration. ii. particle energization inside magnetically confined cavities. *The Astrophysical Journal* 827(2):122
- Khabarova OV, Malandraki O, Malova H, Kislov R, Greco A, Bruno R, Pezzi O, Servidio S, Li G, Matthaeus WH, le Roux J, Engelbrecht N, Pecora F, Zelenyi L, Obridko V, Kuznetsov V (2020a) Current sheets, plasmoids and flux ropes in the heliosphere. part i. general and observational aspects: 2-d or not 2-d? *Space Science Reviews* (submit)
- Khabarova OV, Zharkova V, Xia Q, Malandraki OE (2020b) Counterstreaming Strahls and Heat Flux Dropouts as Possible Signatures of Local Particle Acceleration in the Solar Wind. *The Astrophysical Journal Letters* 894(1):L12, DOI 10.3847/2041-8213/ab8cb8
- Klein KG, Howes GG (2016) Measuring Collisionless Damping in Heliospheric Plasmas using Field-Particle Correlations. *The Astrophysical Journal Letters* 826(2):L30, DOI 10.3847/2041-8205/826/2/L30, 1607.01738
- Klein KG, Howes GG, TenBarge JM, Valentini F (2020) Diagnosing collisionless energy transfer using field-particle correlations: Alfvén-ion cyclotron turbulence. *Journal of Plasma Physics* 86(4):905860402, DOI 10.1017/S0022377820000689, 2006.02563
- Knorr G (1977) Two-dimensional turbulence of electrostatic Vlasov plasmas. *Plasma Physics* 19:529–538, DOI 10.1088/0032-1028/19/6/004
- Kobak T, Ostrowski M (2000) Energetic particle acceleration in a three-dimensional magnetic field reconnection model: the role of magnetohydrodynamic turbulence. *Monthly Notices of the Royal Astronomical Society* 317(4):973–978, DOI 10.1046/j.1365-8711.2000.03722.x, astro-ph/0006045
- Kota J (1977) Energy Loss in the Solar System and Modulation of Cosmic Radiation. In: *International Cosmic Ray Conference, International Cosmic*

- Ray Conference, vol 11, p 186
- Kota J, Jokipii JR (1983) Effects of drift on the transport of cosmic rays. VI - A three-dimensional model including diffusion. *The Astrophysical Journal* 265:573–581, DOI 10.1086/160701
- Kowal G, Lazarian A, Vishniac ET, Otmianowska-Mazur K (2009) Numerical Tests of Fast Reconnection in Weakly Stochastic Magnetic Fields. *The Astrophysical Journal* 700(1):63–85, DOI 10.1088/0004-637X/700/1/63, 0903.2052
- Kowal G, de Gouveia Dal Pino EM, Lazarian A (2011) Magnetohydrodynamic Simulations of Reconnection and Particle Acceleration: Three-dimensional Effects. *The Astrophysical Journal* 735(2):102, DOI 10.1088/0004-637X/735/2/102, 1103.2984
- Kowal G, de Gouveia Dal Pino EM, Lazarian A (2012) Particle Acceleration in Turbulence and Weakly Stochastic Reconnection. *Physical Review Letters* 108(24):241102, DOI 10.1103/PhysRevLett.108.241102, 1202.5256
- Kuznetsova MM, Zelenyi LM (1991) Magnetic reconnection in collisionless field reversals: the universality of the ion tearing mode. *Geophysical Research Letters* 18(10):1825–1828, DOI 10.1029/91GL02245
- Lapenta G (2008) Self-feeding turbulent magnetic reconnection on macroscopic scales. *Physical review letters* 100(23):235001
- Lapenta G, Brackbill JU (1997) A kinetic theory for the drift-kink instability. *Journal of Geophysical Research* 102(A12):27099–27108, DOI 10.1029/97JA02140
- Lapenta G, Markidis S, Goldman MV, Newman DL (2015) Secondary reconnection sites in reconnection-generated flux ropes and reconnection fronts. *Nature Physics* 11(8):690–695
- Lapenta G, Ashour-Abdalla M, Walker RJ, El Alaoui M (2016) A multi-scale study of ion heating in Earth's magnetotail. *Geophysical Research Letters* 43(2):515–524, DOI 10.1002/2015GL066689
- Lapenta G, Berchem J, Zhou M, Walker RJ, El-Alaoui M, Goldstein ML, Paterson WR, Giles BL, Pollock CJ, Russell CT, Strangeway RJ, Ergun RE, Khotyaintsev YV, Torbert RB, Burch JL (2017) On the origin of the crescent-shaped distributions observed by MMS at the magnetopause. *Journal of Geophysical Research (Space Physics)* 122(2):2024–2039, DOI 10.1002/2016JA023290, 1702.03550
- Lapenta G, Pucci F, Olshevsky V, Servidio S, Sorriso-Valvo L, Newman DL, Goldman MV (2018) Nonlinear waves and instabilities leading to secondary reconnection in reconnection outflows. *Journal of Plasma Physics* 84(1):715840103, DOI 10.1017/S002237781800003X, 1808.08612
- Lapenta G, Pucci F, Goldman M, Newman D (2020) Local regimes of turbulence in 3d magnetic reconnection. *The Astrophysical Journal* 888(2):104
- Lazarian A, Vishniac ET (1999) Reconnection in a weakly stochastic field. *The Astrophysical Journal* 517(2):700
- Lazarian A, Eyink G, Vishniac E, Kowal G (2015) Turbulent reconnection and its implications. *Philosophical Transactions of the Royal Society of London Series A* 373:20140144–20140144, DOI 10.1098/rsta.2014.0144, 1502.01396

- Lazarian A, Eyink GL, Jafari A, Kowal G, Li H, Xu S, Vishniac ET (2020) 3D turbulent reconnection: Theory, tests, and astrophysical implications. *Physics of Plasmas* 27(1):012305, DOI 10.1063/1.5110603, 2001.00868
- Le Contel O, Retinò A, Breuillard H, Mirioni L, Robert P, Chasapis A, Lavraud B, Chust T, Rezeau L, Wilder FD, Graham DB, Argall MR, Gershman DJ, Lindqvist PA, Khotyaintsev YV, Marklund G, Ergun RE, Goodrich KA, Burch JL, Torbert RB, Needell J, Chutter M, Rau D, Dors I, Russell CT, Magnes W, Strangeway RJ, Bromund KR, Leinweber HK, Plaschke F, Fischer D, Anderson BJ, Le G, Moore TE, Pollock CJ, Giles BL, Dorelli JC, Avakov L, Saito Y (2016) Whistler mode waves and hall fields detected by mms during a dayside magnetopause crossing. *Geophysical Research Letters* 43(12):5943–5952, DOI 10.1002/2016GL068968, URL <https://agupubs.onlinelibrary.wiley.com/doi/abs/10.1002/2016GL068968>, <https://agupubs.onlinelibrary.wiley.com/doi/pdf/10.1002/2016GL068968>
- le Roux JA, Zank GP, Webb GM, Khabarova O (2015) A Kinetic Transport Theory for Particle Acceleration and Transport in Regions of Multiple Contracting and Reconnecting Inertial-scale Flux Ropes. *The Astrophysical Journal* 801:112, DOI 10.1088/0004-637X/801/2/112
- le Roux JA, Zank GP, Webb GM, Khabarova OV (2016) Combining Diffusive Shock Acceleration with Acceleration by Contracting and Reconnecting Small-scale Flux Ropes at Heliospheric Shocks. *The Astrophysical Journal* 827:47
- le Roux JA, Zank GP, Khabarova OV (2018) Self-consistent Energetic Particle Acceleration by Contracting and Reconnecting Small-scale Flux Ropes: The Governing Equations. *The Astrophysical Journal* 864:158
- le Roux JA, Webb GM, Khabarova OV, Zhao LL, Adhikari L (2019) Modeling Energetic Particle Acceleration and Transport in a Solar Wind Region with Contracting and Reconnecting Small-scale Flux Ropes at Earth Orbit. *The Astrophysical Journal* 887(1):77, DOI 10.3847/1538-4357/ab521f
- Leamon RJ, Matthaeus WH, Smith CW, Wong HK (1998) Contribution of cyclotron-resonant damping to kinetic dissipation of interplanetary turbulence. *The Astrophysical Journal* 507:L181
- Leonardis E, Chapman SC, Daughton W, Roytershteyn V, Karimabadi H (2013) Identification of Intermittent Multifractal Turbulence in Fully Kinetic Simulations of Magnetic Reconnection. *Physical Review Letters* 110(20):205002, DOI 10.1103/PhysRevLett.110.205002, 1302.1749
- Leroy MM, Mangeney A (1984) A theory of energization of solar wind electrons by the Earth's bow shock. *Annales Geophysicae* 2:449–456
- Li TC, Howes GG, Klein KG, TenBarge JM (2016) Energy Dissipation and Landau Damping in Two- and Three-dimensional Plasma Turbulence. *The Astrophysical Journal Letters* 832(2):L24, DOI 10.3847/2041-8205/832/2/L24, 1510.02842
- Li X, Guo F, Li H, Li G (2015) Nonthermally Dominated Electron Acceleration during Magnetic Reconnection in a Low- β Plasma. *The Astrophysical Journal Letters* 811:L24

- Li X, Guo F, Li H, Li G (2017) Particle Acceleration during Magnetic Reconnection in a Low-beta Plasma. *The Astrophysical Journal*843(1):21, DOI 10.3847/1538-4357/aa745e
- Li X, Guo F, Birn J (2018) The Roles of Fluid Compression and Shear in Electron Energization during Magnetic Reconnection. *The Astrophysical Journal*855:80
- Li X, Guo F, Li H (2019) Particle Acceleration in Kinetic Simulations of Non-relativistic Magnetic Reconnection with Different Ion-Electron Mass Ratios. *The Astrophysical Journal*879(1):5, DOI 10.3847/1538-4357/ab223b, 1905.08797
- Liang H, Cassak PA, Servidio S, Shay MA, Drake JF, Swisdak M, Argall MR, Dorelli JC, Scime EE, Matthaeus WH, Roytershteyn V, Delzanno GL (2019) Decomposition of plasma kinetic entropy into position and velocity space and the use of kinetic entropy in particle-in-cell simulations. *Physics of Plasmas* 26(8):082903, DOI 10.1063/1.5098888, 1902.02733
- Liang H, Hasan Barbhuiya M, Cassak PA, Pezzi O, Servidio S, Valentini F, Zank GP (2020) Kinetic Entropy-Based Measures of Distribution Function Non-Maxwellianity: Theory and Simulations. arXiv e-prints arXiv:2008.06669, 2008.06669
- Liu YCM, Huang J, Wang C, Klecker B, Galvin AB, Simunac KDC, Popecki MA, Kistler L, Farrugia C, Lee MA, Kucharek H, Opitz A, Luhmann JG, Jian L (2014) A statistical analysis of heliospheric plasma sheets, heliospheric current sheets, and sector boundaries observed in situ by STEREO. *Journal of Geophysical Research (Space Physics)* 119(11):8721–8732, DOI 10.1002/2014JA019956
- Loureiro N, Uzdensky D, Schekochihin A, Cowley S, Yousef T (2009) Turbulent magnetic reconnection in two dimensions. *Monthly Notices of the Royal Astronomical Society: Letters* 399(1):L146–L150
- Lu Q, Huang C, Xie J, Wang R, Wu M, Vaivads A, Wang S (2010) Features of separatrix regions in magnetic reconnection: Comparison of 2-d particle-in-cell simulations and cluster observations. *Journal of Geophysical Research: Space Physics* 115(A11), DOI 10.1029/2010JA015713, URL <https://agupubs.onlinelibrary.wiley.com/doi/abs/10.1029/2010JA015713>, <https://agupubs.onlinelibrary.wiley.com/doi/pdf/10.1029/2010JA015713>
- Lu S, Angelopoulos V, Artemyev AV, Pritchett PL, Liu J, Runov A, Tenerani A, Shi C, Velli M (2019) Turbulence and Particle Acceleration in Collisionless Magnetic Reconnection: Effects of Temperature Inhomogeneity across Pre-reconnection Current Sheet. *The Astrophysical Journal*878(2):109, DOI 10.3847/1538-4357/ab1f6b
- Lu S, Artemyev AV, Angelopoulos V, Pritchett PL, Runov A (2019) Effects of cross-sheet density and temperature inhomogeneities on magnetotail reconnection. *Geophysical Research Letters* 46(1):28–36, DOI 10.1029/2018GL081420, URL <https://agupubs.onlinelibrary.wiley.com/doi/abs/10.1029/2018GL081420>, <https://agupubs.onlinelibrary.wiley.com/doi/pdf/10.1029/2018GL081420>

- Lui ATY (1996) Current disruption in the Earth's magnetosphere: Observations and models. *Journal of Geophysical Research*101(A6):13067–13088, DOI 10.1029/96JA00079
- Lutsenko VN, Kirpichev IP, Grechko TV, Delcourt D (2005) Source positions of energetic particles responsible for the fine dispersion structures: numerical simulation results. *Planetary and Space Science*53(1-3):275–281, DOI 10.1016/j.pss.2004.09.053
- Lyons LR, Speiser TW (1982) Evidence for current sheet acceleration in the geomagnetic tail. *Journal of Geophysical Research*87(A4):2276–2286, DOI 10.1029/JA087iA04p02276
- Lyutikov M (2003) Explosive reconnection in magnetars. *Monthly Notices of the Royal Astronomical Society* 346(2):540–554, DOI 10.1046/j.1365-2966.2003.07110.x, URL <https://dx.doi.org/10.1046/j.1365-2966.2003.07110.x>, <http://oup.prod.sis.lan/mnras/article-pdf/346/2/540/4293592/346-2-540.pdf>
- M L Cartwright MBM (2010) Heliospheric evolution of solar wind small-scale magnetic flux ropes. *Journal of Geophysical Research*115:A08102
- Ma ZW, Bhattacharjee A (2001) Hall magnetohydrodynamic reconnection: The Geospace Environment Modeling challenge. *J Geophys Res* 106:3773–3782, DOI 10.1029/1999JA001004
- Malandraki O, Khabarova O, Bruno R, Zank GP, Li G, Jackson B, Bisi MM, Greco A, Pezzi O, Matthaeus W, Chasapis Giannakopoulos A, Servidio S, Malova H, Kislov R, Effenberger F, le Roux J, Chen Y, Hu Q, Engelbrecht NE (2019) Current Sheets, Magnetic Islands, and Associated Particle Acceleration in the Solar Wind as Observed by Ulysses near the Ecliptic Plane. *The Astrophysical Journal*881(2):116, DOI 10.3847/1538-4357/ab289a
- Malara F, Velli M (1996) Parametric instability of a large-amplitude non-monochromatic Alfvén wave. *Physics of Plasmas* 3(12):4427–4433, DOI 10.1063/1.872043
- Malara F, Veltri P, Carbone V (1992) Competition among nonlinear effects in tearing instability saturation. *Physics of Fluids B: Plasma Physics (1989-1993)* 4(10):3070–3086
- Malara F, Nigro G, Valentini F, Sorriso-Valvo L (2019) Electron Heating by Kinetic Alfvén Waves in Coronal Loop Turbulence. *The Astrophysical Journal*871(1):66, DOI 10.3847/1538-4357/aaf168
- Malkov MA, Sagdeev RZ (2015) Cosmic Ray Transport with Magnetic Focusing and the "Telegraph" Model. *The Astrophysical Journal*808:157
- Malova H, Popov VY, Grigorenko E, Petrukovich A, Delcourt D, Sharma A, Khabarova O, Zelenyi L (2017) Evidence for quasi-adiabatic motion of charged particles in strong current sheets in the solar wind. *The Astrophysical Journal* 834(1):34, DOI 10.3847/1538-4357/834/1/34
- Malova H, Popov VY, Khabarova OV, Grigorenko EE, Petrukovich AA, Zelenyi LM (2018) Structure of Current Sheets with Quasi-Adiabatic Dynamics of Particles in the Solar Wind. *Cosmic Research* 56(6):462–470, DOI 10.1134/S0010952518060060

- Maneva YG, Poedts S (2018) Generation and evolution of anisotropic turbulence and related energy transfer in drifting proton-alpha plasmas. *Astronomy and Astrophysics*613:A10, DOI 10.1051/0004-6361/201731204
- Maneva YG, Viñas AF, Ofman L (2013) Turbulent heating and acceleration of He^{++} ions by spectra of Alfvén-cyclotron waves in the expanding solar wind: 1.5-D hybrid simulations. *Journal of Geophysical Research (Space Physics)* 118:2842–2853, DOI 10.1002/jgra.50363
- Maneva YG, Araneda JA, Marsch E (2014) Regulation of Ion Drifts and Anisotropies by Parametrically Unstable Finite-amplitude Alfvén-cyclotron Waves in the Fast Solar Wind. *The Astrophysical Journal*783(2):139, DOI 10.1088/0004-637X/783/2/139
- Maneva YG, Ofman L, Viñas A (2015) Relative drifts and temperature anisotropies of protons and α particles in the expanding solar wind: 2.5D hybrid simulations. *Astronomy and Astrophysics*578:A85, DOI 10.1051/0004-6361/201424401, 1410.3358
- Mangeney A, Califano F, Cavazzoni C, Travnicek P (2002) A numerical scheme for the integration of the vlasov–maxwell system of equations. *Journal of Computational Physics* 179(2):495–538
- Marino R, Sorriso-Valvo L, Carbone V, Noullez A, Bruno R, Bavassano B (2008) Heating the Solar Wind by a Magnetohydrodynamic Turbulent Energy Cascade. *The Astrophysical Journal Letters*677(1):L71, DOI 10.1086/587957
- Marsch E (2006) Kinetic physics of the solar corona and solar wind. *Living Reviews in Solar Physics* 3(1):1, DOI 10.12942/lrsp-2006-1, URL <https://doi.org/10.12942/lrsp-2006-1>
- Marsch E, Tu CY (1997) Intermittency, non-gaussian statistics and fractal scaling of mhd fluctuations in the solar wind. *Nonlinear processes in Geophysics* 4(2):101–124
- Marsh MS, Dalla S, Kelly J, Laitinen T (2013) Drift-induced Perpendicular Transport of Solar Energetic Particles. *The Astrophysical Journal*774(1):4, DOI 10.1088/0004-637X/774/1/4, 1307.1585
- Maruca BA, Kasper JC, Bale SD (2011) What are the relative roles of heating and cooling in generating solar wind temperature anisotropies? *Phys Rev Lett* 107:201101, DOI 10.1103/PhysRevLett.107.201101, URL <https://link.aps.org/doi/10.1103/PhysRevLett.107.201101>
- Matteini L, Hellinger P, Goldstein BE, Landi S, Velli M, Neugebauer M (2013) Signatures of kinetic instabilities in the solar wind. *Journal of Geophysical Research (Space Physics)* 118:2771–2782, DOI 10.1002/jgra.50320
- Matthaeus W, Qin G, Bieber J, Zank G (2003a) Nonlinear collisionless perpendicular diffusion of charged particles. *The Astrophysical Journal Letters* 590(1):L53
- Matthaeus WH, Lamkin SL (1985) Rapid magnetic reconnection caused by finite amplitude fluctuations. *Physics of Fluids* 28:303
- Matthaeus WH, Lamkin SL (1986) Turbulent magnetic reconnection. *Physics of Fluids (1958-1988)* 29(8):2513–2534

- Matthaeus WH, Montgomery D (1980) Selective decay hypothesis at high mechanical and magnetic Reynolds numbers. *Annals of the New York Academy of Sciences* 357(1):203–222
- Matthaeus WH, Velli M (2011) Who needs turbulence? *Space science reviews* 160(1-4):145–168
- Matthaeus WH, Ambrosiano JJ, Goldstein ML (1984) Particle-acceleration by turbulent magnetohydrodynamic reconnection. *Physical Review Letters* 53:1449–1452, DOI 10.1103/PhysRevLett.53.1449
- Matthaeus WH, Goldstein ML, Roberts DA (1990a) Evidence for the presence of quasi-two-dimensional nearly incompressible fluctuations in the solar wind. *J Geophys Res* 95(20):673–20
- Matthaeus WH, Goldstein ML, Roberts DA (1990b) Evidence for the presence of quasi-two-dimensional nearly incompressible fluctuations in the solar wind. *Journal of Geophysical Research* 95:20 673–20 683, DOI 10.1029/JA095iA12p20673
- Matthaeus WH, Qin G, Bieber JW, Zank GP (2003b) Nonlinear collisionless perpendicular diffusion of charged particles. *The Astrophysical Journal Letters* 590:L53–L56
- Matthaeus WH, Bieber JW, Ruffolo D, Chuychai P, Minnie J (2007) Spectral properties and length scales of two-dimensional magnetic field models. *The Astrophysical Journal* 667:956–962, DOI 10.1086/520924
- Matthaeus WH, Wan M, Servidio S, Greco A, Osman KT, Oughton S, Dmitruk P (2015) Intermittency, nonlinear dynamics and dissipation in the solar wind and astrophysical plasmas. *Philosophical Transactions of the Royal Society of London Series A* 373(2041):20140154–20140154, DOI 10.1098/rsta.2014.0154
- Matthaeus WH, Yang Y, Wan M, Parashar TN, Bandyopadhyay R, Chasapis Ar, Pezzi O, Valentini F (2020) Pathways to Dissipation in Weakly Collisional Plasmas. *The Astrophysical Journal* 891(1):101, DOI 10.3847/1538-4357/ab6d6a
- McComas DJ, Phillips JL, Hundhausen AJ, Burkepile JT (1991) Observations of disconnection of open magnetic structures. *Geophysical Research Letters* 18(1):73–76, DOI 10.1029/90GL02480
- Metzler R, Klafter J (2000) The random walk’s guide to anomalous diffusion: a fractional dynamics approach. *Physics Reports* 339(1):1–77, DOI 10.1016/S0370-1573(00)00070-3
- Metzler R, Klafter J (2004) TOPICAL REVIEW: The restaurant at the end of the random walk: recent developments in the description of anomalous transport by fractional dynamics. *Journal of Physics A Mathematical General* 37(31):R161–R208, DOI 10.1088/0305-4470/37/31/R01
- Milovanov AV, Zelenyi LM (1994) Development of fractal structure in the solar wind and distribution of magnetic field in the photosphere. Washington DC American Geophysical Union Geophysical Monograph Series 84:43–52, DOI 10.1029/GM084p0043
- Milovanov AV, Zelenyi LM (2001) “strange” fermi processes and power-law nonthermal tails from a self-consistent fractional kinetic equation. *Phys Rev*

- E 64:052101, DOI 10.1103/PhysRevE.64.052101, URL <https://link.aps.org/doi/10.1103/PhysRevE.64.052101>
- Milovanov AV, Zelenyi LM, Veltri P, Zimbardo G, Taktakishvili AL (2001) Geometric description of the magnetic field and plasma coupling in the near-Earth stretched tail prior to a substorm. *Journal of Atmospheric and Solar-Terrestrial Physics* 63(7):705–721, DOI 10.1016/S1364-6826(00)00186-3
- Mingalev OV, Khabarova OV, Malova KV, Mingalev IV, Kislov RA, Mel'nik MN, Setsko PV, Zelenyi LM, Zank GP (2019) Modeling of Proton Acceleration in a Magnetic Island Inside the Ripple of the Heliospheric Current Sheet. *Solar System Research* 53(1):30–55, DOI 10.1134/S0038094619010064
- Minnie J, Bieber JW, Matthaeus WH, Burger RA (2007) Suppression of Particle Drifts by Turbulence. *The Astrophysical Journal* 670(2):1149–1158, DOI 10.1086/522026
- Moloto KD, Engelbrecht NE, Burger RA (2018) A Simplified Ab Initio Cosmic-ray Modulation Model with Simulated Time Dependence and Predictive Capability. *The Astrophysical Journal* 859(2):107, DOI 10.3847/1538-4357/aac174
- Navarro ABn, Teaca B, Told D, Grosej D, Crandall P, Jenko F (2016) Structure of plasma heating in gyrokinetic alfvénic turbulence. *Phys Rev Lett* 117:245101, DOI 10.1103/PhysRevLett.117.245101, URL <https://link.aps.org/doi/10.1103/PhysRevLett.117.245101>
- Ofman L, Viñas AF (2007) Two-dimensional hybrid model of wave and beam heating of multi-ion solar wind plasma. *Journal of Geophysical Research (Space Physics)* 112(A6):A06104, DOI 10.1029/2006JA012187
- Ofman L, Viñas AF, Moya PS (2011) Hybrid models of solar wind plasma heating. *Annales Geophysicae* 29(6):1071–1079, DOI 10.5194/angeo-29-1071-2011
- Øieroset M, Phan TD, Fujimoto M, Lin RP, Lepping RP (2001) In situ detection of collisionless reconnection in the Earth's magnetotail. *Nature* 412(6845):414–417, DOI 10.1038/35086520
- Oka M, Phan TD, Krucker S, Fujimoto M, Shinohara I (2010) Electron Acceleration by Multi-Island Coalescence. *The Astrophysical Journal* 714:915–926, DOI 10.1088/0004-637X/714/1/915, 1004.1154
- Osman KT, Matthaeus WH, Greco A, Servidio S (2011) Evidence for Inhomogeneous Heating in the Solar Wind. *Astrophys J Lett* 727:L11, DOI 10.1088/2041-8205/727/1/L11
- Osman KT, Matthaeus WH, Hnat B, Chapman SC (2012a) Kinetic Signatures and Intermittent Turbulence in the Solar Wind Plasma. *Physical Review Letters* 108(26):261103, DOI 10.1103/PhysRevLett.108.261103, 1203.6596
- Osman KT, Matthaeus WH, Wan M, Rappazzo AF (2012b) Intermittency and local heating in the solar wind. *Physical Review Letters* 108(26):261102, DOI 10.1103/PhysRevLett.108.261102
- Oughton S, Matthaeus WH (2020) Critical Balance and the Physics of Magnetohydrodynamic Turbulence. *The Astrophysical Journal* 897(1):37, DOI 10.3847/1538-4357/ab8f2a, 2006.04677

- Oughton S, Priest ER, Matthaeus WH (1994) The influence of a mean magnetic field on three-dimensional magnetohydrodynamic turbulence. *Journal of Fluid Mechanics* 280:95–117
- Oughton S, Matthaeus WH, Smith CW, Breech B, Isenberg PA (2011) Transport of solar wind fluctuations: A two-component model. *Journal of Geophysical Research* 116:A08105, DOI 10.1029/2010JA016365
- Oughton S, Matthaeus WH, Dmitruk P (2017) Reduced MHD in Astrophysical Applications: Two-dimensional or Three-dimensional? *The Astrophysical Journal* 839(1):2, DOI 10.3847/1538-4357/aa67e2
- Palmer ID (1982) Transport coefficients of low-energy cosmic rays in interplanetary space. *Reviews of Geophysics and Space Physics* 20:335–351, DOI 10.1029/RG020i002p00335
- Panov EV, Büchner J, Fränz M, Korth A, Savin SP, Rème H, Fornacon KH (2008) High-latitude Earth's magnetopause outside the cusp: Cluster observations. *Journal of Geophysical Research (Space Physics)* 113(A1):A01220, DOI 10.1029/2006JA012123
- Papini E, Franci L, Landi S, Verdini A, Matteini L, Hellinger P (2019) Can Hall Magnetohydrodynamics Explain Plasma Turbulence at Sub-ion Scales? *The Astrophysical Journal* 870(1):52, DOI 10.3847/1538-4357/aaf003, 1810.02210
- Parashar TN, Matthaeus WH (2016) PROPINQUITY OF CURRENT AND VORTEX STRUCTURES: EFFECTS ON COLLISIONLESS PLASMA HEATING. *The Astrophysical Journal* 832(1):57, DOI 10.3847/0004-637x/832/1/57, URL <https://doi.org/10.3847/2F0004-637x%2F832%2F1%2F57>
- Parashar TN, Shay MA, Cassak PA, Matthaeus WH (2009) Kinetic dissipation and anisotropic heating in a turbulent collisionless plasma. *Physics of Plasmas* 16(3):032310, DOI 10.1063/1.3094062, URL <https://doi.org/10.1063/1.3094062>, <https://doi.org/10.1063/1.3094062>
- Parashar TN, Matthaeus WH, Shay MA (2018) Dependence of Kinetic Plasma Turbulence on Plasma β . *The Astrophysical Journal* 864(1):L21, DOI 10.3847/2041-8213/aadb8b, 1807.11371
- Parker EN (1957) Sweet's Mechanism for Merging Magnetic Fields in Conducting Fluids. *Journal of Geophysical Research* 62:509–520, DOI 10.1029/JZ062i004p00509
- Parkhomenko EI, Malova HV, Grigorenko EE, Popov VY, Petrukovich AA, Delcourt DC, Kronberg EA, Daly PW, Zelenyi LM (2019) Acceleration of plasma in current sheet during substorm dipolarizations in the Earth's magnetotail: Comparison of different mechanisms. *Physics of Plasmas* 26(4):042901, DOI 10.1063/1.5082715
- Pecora F, Servidio S, Greco A, Matthaeus WH, Burgess D, Haynes CT, Carboni V, Veltri P (2018) Ion diffusion and acceleration in plasma turbulence. *Journal of Plasma Physics* 84(6):725840601
- Pecora F, Greco A, Hu Q, Servidio S, Chasapis AG, Matthaeus WH (2019a) Single-spacecraft identification of flux tubes and current sheets in the solar wind. *The Astrophysical Journal* 881(1):L11, DOI 10.3847/2041-8213/

- ab32d9, URL <https://doi.org/10.3847/2F2041-8213%2Fab32d9>
- Pecora F, Pucci F, Lapenta G, Burgess D, Servidio S (2019b) Statistical analysis of ions in two-dimensional plasma turbulence. *Solar Physics* 294(9):114, DOI 10.1007/s11207-019-1507-6, URL <https://doi.org/10.1007/s11207-019-1507-6>
- Pei C, Bieber JW, Burger RA, Clem J (2012) Three-dimensional Wavy Heliospheric Current Sheet Drifts. *The Astrophysical Journal* 744(2):170, DOI 10.1088/0004-637X/744/2/170
- Pellat R, Coroniti FV, Pritchett PL (1991) Does ion tearing exist? *Geophysical Research Letters* 18(2):143–146, DOI 10.1029/91GL00123
- Perri S, Zimbardo G (2007) Evidence of Superdiffusive Transport of Electrons Accelerated at Interplanetary Shocks. *The Astrophysical Journal Letters* 671(2):L177–L180, DOI 10.1086/525523
- Perri S, Zimbardo G (2012) Superdiffusive Shock Acceleration. *The Astrophysical Journal* 750(2):87, DOI 10.1088/0004-637X/750/2/87
- Perri S, Perrone D, Yordanova E, Sorriso-Valvo L, Paterson WR, Gershman DJ, Giles BL, Pollock CJ, Dorelli JC, Avannov LA, Lavraud B, Saito Y, Nakamura R, Fischer D, Baumjohann W, Plaschke F, Narita Y, Magnes W, Russell CT, Strangeway RJ, Contel OL, Khotyaintsev Y, Valentini F (2020) On the deviation from Maxwellian of the ion velocity distribution functions in the turbulent magnetosheath. *Journal of Plasma Physics* 86(1):905860108, DOI 10.1017/S0022377820000021, 1905.09466
- Perrone D, Valentini F, Veltri P (2011) The role of alpha particles in the evolution of the solar-wind turbulence toward short spatial scales. *The Astrophysical Journal* 741(1):43, URL <http://stacks.iop.org/0004-637X/741/i=1/a=43>
- Perrone D, Valentini F, Servidio S, Dalena S, Veltri P (2013) Vlasov simulations of multi-ion plasma turbulence in the solar wind. *The Astrophysical Journal* 762(2):99, URL <http://stacks.iop.org/0004-637X/762/i=2/a=99>
- Perrone D, Bourouaine S, Valentini F, Marsch E, Veltri P (2014a) Generation of temperature anisotropy for alpha particle velocity distributions in solar wind at 0.3 AU: Vlasov simulations and Helios observations. *Journal of Geophysical Research (Space Physics)* 119(4):2400–2410, DOI 10.1002/2013JA019564
- Perrone D, Valentini F, Servidio S, Dalena S, Veltri P (2014b) Analysis of intermittent heating in a multi-component turbulent plasma. *European Physical Journal D* 68(7):209, DOI 10.1140/epjd/e2014-50152-1
- Perrone D, Passot T, Laveder D, Valentini F, Sulem PL, Zouganelis I, Veltri P, Servidio S (2018) Fluid simulations of plasma turbulence at ion scales: Comparison with vlasov-maxwell simulations. *Physics of Plasmas* 25(5):052302, DOI 10.1063/1.5026656, URL <https://doi.org/10.1063/1.5026656>, <https://doi.org/10.1063/1.5026656>
- Pezzi O (2017) Solar wind collisional heating. *Journal of Plasma Physics* 83(3):555830301, DOI 10.1017/S0022377817000368

- Pezzi O, Valentini F, Veltri P (2015) Collisional relaxation: Landau versus dougherty operator. *Journal of Plasma Physics* 81(1):305810107, DOI 10.1017/S0022377814000877
- Pezzi O, Camporeale E, Valentini F (2016) Collisional effects on the numerical recurrence in vlasov-poisson simulations. *Physics of Plasmas* 23(2):022103, DOI 10.1063/1.4940963, URL <https://doi.org/10.1063/1.4940963>, <https://doi.org/10.1063/1.4940963>
- Pezzi O, Valentini F, Veltri P (2016) Collisional Relaxation of Fine Velocity Structures in Plasmas. *Physical Review Letters* 116(14):145001, DOI 10.1103/PhysRevLett.116.145001
- Pezzi O, Malara F, Servidio S, Valentini F, Parashar TN, Matthaeus WH, Veltri P (2017a) Turbulence generation during the head-on collision of alfvénic wave packets. *Phys Rev E* 96:023201, DOI 10.1103/PhysRevE.96.023201, URL <https://link.aps.org/doi/10.1103/PhysRevE.96.023201>
- Pezzi O, Parashar TN, Servidio S, Valentini F, Vásconez CL, Yang Y, Malara F, Matthaeus WH, Veltri P (2017b) Colliding alfvénic wave packets in magnetohydrodynamics, hall and kineticsimulations. *Journal of Plasma Physics* 83(1):705830108, DOI 10.1017/S0022377817000113
- Pezzi O, Parashar TN, Servidio S, Valentini F, Vásconez CL, Yang Y, Malara F, Matthaeus WH, Veltri P (2017c) Revisiting a classic: The parker-moffatt problem. *The Astrophysical Journal* 834(2):166, URL <http://stacks.iop.org/0004-637X/834/i=2/a=166>
- Pezzi O, Servidio S, Perrone D, Valentini F, Sorriso-Valvo L, Greco A, Matthaeus WH, Veltri P (2018) Velocity-space cascade in magnetized plasmas: Numerical simulations. *Physics of Plasmas* 25(6):060704, DOI 10.1063/1.5027685, URL <https://doi.org/10.1063/1.5027685>, <https://doi.org/10.1063/1.5027685>
- Pezzi O, Cozzani G, Califano F, Valentini F, Guarrasi M, Camporeale E, Brunetti G, Retinò A, Veltri P (2019) Vida: a vlasov-darwin solver for plasma physics at electron scales. *Journal of Plasma Physics* 85(5):905850506, DOI 10.1017/S0022377819000631
- Pezzi O, Perrone D, Servidio S, Valentini F, Sorriso-Valvo L, Veltri P (2019a) Proton-proton collisions in the turbulent solar wind: Hybrid Boltzmann-Maxwell simulations. arXiv e-prints arXiv:1903.03398, 1903.03398
- Pezzi O, Yang Y, Valentini F, Servidio S, Chasapis A, Matthaeus WH, Veltri P (2019b) Energy conversion in turbulent weakly collisional plasmas: Eulerian hybrid Vlasov-Maxwell simulations. *Physics of Plasmas* 26(7):072301, DOI 10.1063/1.5100125, 1904.07715
- Pezzi O, et al. (2020) Dissipation measures in weakly-collisional plasmas. *J Plasma Phys* (subm)
- Phan TD, Eastwood JP, Cassak PA, Øieroset M, Gosling JT, Gershman DJ, Mozer FS, Shay MA, Fujimoto M, Daughton W, Drake JF, Burch JL, Torbert RB, Ergun RE, Chen LJ, Wang S, Pollock C, Dorelli JC, Lavraud B, Giles BL, Moore TE, Saito Y, Avannov LA, Paterson W, Strangeway RJ, Russell CT, Khotyaintsev Y, Lindqvist PA, Oka M, Wilder FD (2016) Mms observations of electron-scale filamentary currents in the reconnection ex-

- haust and near the x line. *Geophysical Research Letters* 43(12):6060–6069, DOI 10.1002/2016GL069212
- Phan TD, Eastwood JP, Shay M, Drake J, Sonnerup BÖ, Fujimoto M, Cassak P, Øieroset M, Burch J, Torbert R, et al. (2018) Electron magnetic reconnection without ion coupling in earth’s turbulent magnetosheath. *Nature* 557(7704):202
- Potgieter MS (2013) Solar Modulation of Cosmic Rays. *Living Reviews in Solar Physics* 10(1):3, DOI 10.12942/lrsp-2013-3, 1306.4421
- Priest ER, Pontin DI (2009) Three-dimensional null point reconnection regimes. *Physics of Plasmas* 16(12):122101, DOI 10.1063/1.3257901
- Primavera L, Malara F, Servidio S, Nigro G, Veltri P (2019) Parametric Instability in Two-dimensional Alfvénic Turbulence. *The Astrophysical Journal* 880(2):156, DOI 10.3847/1538-4357/ab29f5
- Pritchett P (2008) Collisionless magnetic reconnection in an asymmetric current sheet. *Journal of Geophysical Research: Space Physics* 113(A06210)
- Pritchett PL (2013) The influence of intense electric fields on three-dimensional asymmetric magnetic reconnection. *Physics of Plasmas* 20(6):061204, DOI 10.1063/1.4811123
- Pritchett PL (2016) Three-dimensional structure and kinetic features of reconnection exhaust jets. *Journal of Geophysical Research (Space Physics)* 121(1):214–226, DOI 10.1002/2015JA022053
- Pritchett PL, Coroniti FV, Decyk VK (1996) Three-dimensional stability of thin quasi-neutral current sheets. *Journal of Geophysical Research* 101(A12):27413–27430, DOI 10.1029/96JA02665
- Pucci F, Vásconez CL, Pezzi O, Servidio S, Valentini F, Matthaeus WH, Malara F (2016) From Alfvén waves to kinetic Alfvén waves in an inhomogeneous equilibrium structure. *Journal of Geophysical Research (Space Physics)* 121(2):1024–1045, DOI 10.1002/2015JA022216
- Pucci F, Servidio S, Sorriso-Valvo L, Olshevsky V, Matthaeus WH, Malara F, Goldman MV, Newman DL, Lapenta G (2017) Properties of turbulence in the reconnection exhaust: Numerical simulations compared with observations. *The Astrophysical Journal* 841(1):60, DOI 10.3847/1538-4357/aa704f, URL <https://doi.org/10.3847/2F1538-4357/2Faa704f>
- Pucci F, Velli M, Tenerani A (2017) Fast Magnetic Reconnection: “Ideal” Tearing and the Hall Effect. *The Astrophysical Journal* 845(1):25, DOI 10.3847/1538-4357/aa7b82, 1704.08793
- Pucci F, Matthaeus WH, Chasapis A, Servidio S, Sorriso-Valvo L, Olshevsky V, Newman DL, Goldman MV, Lapenta G (2018) Generation of turbulence in colliding reconnection jets. *The Astrophysical Journal* 867(1):10, DOI 10.3847/1538-4357/aadd0a, URL <https://doi.org/10.3847/2F1538-4357/2Faadd0a>
- Pucci F, Velli M, Tenerani A, Del Sarto D (2018) Onset of fast “ideal” tearing in thin current sheets: Dependence on the equilibrium current profile. *Physics of Plasmas* 25(3):032113, DOI 10.1063/1.5022988, 1801.08412
- Qudsi RA, Bandyopadhyay R, Maruca BA, Parashar TN, Matthaeus WH, Chasapis Ar, Gary SP, Giles BL, Gershman DJ, Pollock CJ, Strange-

- way RJ, Torbert RB, Moore TE, Burch JL (2020) Intermittency and Ion Temperature-Anisotropy Instabilities: Simulation and Magnetosheath Observation. *The Astrophysical Journal* 895(2):83, DOI 10.3847/1538-4357/ab89ad, 2004.06164
- Rappazzo A, Matthaeus W, Ruffolo D, Velli M, Servidio S (2017) Coronal heating topology: The interplay of current sheets and magnetic field lines. *The Astrophysical Journal* 844(1):87
- Rappazzo AF, Velli M, Einaudi G, Dahlburg RB (2007) Coronal Heating, Weak MHD Turbulence, and Scaling Laws. *The Astrophysical Journal Letters* 657(1):L47–L51, DOI 10.1086/512975, astro-ph/0701872
- Rappazzo AF, Velli M, Einaudi G (2010) Shear Photospheric Forcing and the Origin of Turbulence in Coronal Loops. *The Astrophysical Journal* 722(1):65–78, DOI 10.1088/0004-637X/722/1/65, 1003.3872
- Rappazzo AF, Matthaeus WH, Ruffolo D, Velli M, Servidio S (2017) Coronal Heating Topology: The Interplay of Current Sheets and Magnetic Field Lines. *Astrophys J* 844(1):87, DOI 10.3847/1538-4357/aa79f2, 1706.08983
- Retinò A, Sundkvist D, Vaivads A, Mozer F, André M, Owen CJ (2007) In situ evidence of magnetic reconnection in turbulent plasma. *Nature Physics* 3:236–238, DOI 10.1038/nphys574
- Réville V, Velli M, Rouillard AP, Lavraud B, Tenerani A, Shi C, Strugarek A (2020) Tearing Instability and Periodic Density Perturbations in the Slow Solar Wind. *The Astrophysical Journal Letters* 895(1):L20, DOI 10.3847/2041-8213/ab911d, 2005.02679
- Rossi BB, Olbert S (1970) *Introduction to the Physics of Space*. McGraw-Hill
- le Roux JA, Matthaeus WH, Zank GP (2001) Pickup ion acceleration by turbulent electric fields in the slow solar wind. *Geophysical Research Letters* 28(20):3831–3834, DOI 10.1029/2001GL013400, <https://agupubs.onlinelibrary.wiley.com/doi/pdf/10.1029/2001GL013400>
- Roytershteyn V, Boldyrev S, Delzanno GL, Chen CHK, Grošelj D, Loureiro NF (2019) Numerical Study of Inertial Kinetic-Alfvén Turbulence. *The Astrophysical Journal* 870(2):103, DOI 10.3847/1538-4357/aaf288
- Ruffenach A, Lavraud B, Owens MJ, Sauvaud JA, Savani NP, Rouillard AP, Démoulin P, Foullon C, Opitz A, Fedorov A, Jacquy CJ, Génot V, Louarn P, Luhmann JG, Russell CT, Farrugia CJ, Galvin AB (2012) Multispacecraft observation of magnetic cloud erosion by magnetic reconnection during propagation. *Journal of Geophysical Research (Space Physics)* 117(A9):A09101, DOI 10.1029/2012JA017624
- Ruffolo D, Matthaeus WH, Chuychai P (2003) Trapping of Solar Energetic Particles by the Small-Scale Topology of Solar Wind Turbulence. *Astrophys J Lett* 597:L169–L172, DOI 10.1086/379847
- Ruffolo D, Pianpanit T, Matthaeus WH, Chuychai P (2012) Random Ballistic Interpretation of Nonlinear Guiding Center Theory. *The Astrophysical Journal Letters* 747:L34, DOI 10.1088/2041-8205/747/2/L34
- Runov A, Sergeev VA, Baumjohann W, Nakamura R, Apatenkov S, Asano Y, Volwerk M, Vörös Z, Zhang TL, Petrukovich A, Balogh A, Sauvaud JA, Klecker B, Rème H (2005) Electric current and magnetic field geometry in

- flapping magnetotail current sheets. *Annales Geophysicae* 23(4):1391–1403, DOI 10.5194/angeo-23-1391-2005
- Runov A, Sergeev VA, Nakamura R, Baumjohann W, Apatenkov S, Asano Y, Takada T, Volwerk M, Vörös Z, Zhang TL, Sauvaud JA, Rème H, Balogh A (2006) Local structure of the magnetotail current sheet: 2001 cluster observations. *Annales Geophysicae* 24(1):247–262, DOI 10.5194/angeo-24-247-2006, URL <https://www.ann-geophys.net/24/247/2006/>
- Sahraoui F, Goldstein ML, Robert P, Khotyaintsev YV (2009) Evidence of a Cascade and Dissipation of Solar-Wind Turbulence at the Electron Gyroscale. *Physical Review Letters* 102(23):231102, DOI 10.1103/PhysRevLett.102.231102
- Salem CS, Howes GG, Sundkvist D, Bale SD, Chaston CC, Chen CHK, Mozer FS (2012) Identification of Kinetic Alfvén Wave Turbulence in the Solar Wind. *The Astrophysical Journal Letters* 745(1):L9, DOI 10.1088/2041-8205/745/1/L9
- Sanchez-Diaz E, Rouillard AP, Lavraud B, Kilpua E, Davies JA (2019) In situ measurements of the variable slow solar wind near sector boundaries. *The Astrophysical Journal* 882(1):51, DOI 10.3847/1538-4357/ab341c, URL <https://doi.org/10.3847/1538-4357/ab341c>
- Sarris ET, Krimigis SM, Bostrom CO, Iijima T, Armstrong TP (1976) Location of the source of magnetospheric energetic particle bursts by multispacecraft observations. *Geophysical Research Letters* 3(8):437–440, DOI 10.1029/GL003i008p00437
- Schatten KH (1971) Large-scale properties of the interplanetary magnetic field. *Reviews of Geophysics and Space Physics* 9:773–812, DOI 10.1029/RG009i003p00773
- Schekochihin AA, Cowley SC, Dorland W, Hammett GW, Howes GG, Quataert E, Tatsuno T (2009) Astrophysical Gyrokinetics: Kinetic and Fluid Turbulent Cascades in Magnetized Weakly Collisional Plasmas. *The Astrophysical Journal Supplement* 182(1):310–377, DOI 10.1088/0067-0049/182/1/310, 0704.0044
- Schekochihin AA, Parker JT, Highcock EG, Dellar PJ, Dorland W, Hammett GW (2016) Phase mixing versus nonlinear advection in drift-kinetic plasma turbulence. *Journal of Plasma Physics* 82(2):905820212, DOI 10.1017/S0022377816000374, 1508.05988
- Schindler K (1979) Theories of Tail Structures (Article published in the special issues: Proceedings of the Symposium on Solar Terrestrial Physics held in Innsbruck, May– June 1978. (pp. 137–538)). *Space Science Reviews* 23(3):365–374, DOI 10.1007/BF00172245
- Schindler K, Hesse M, Birn J (1988) General magnetic reconnection, parallel electric fields, and helicity. *J Geophys Res* 93:5547–5557, DOI 10.1029/JA093iA06p05547
- Schmitz H, Grauer R (2006a) Darwin–vlasov simulations of magnetised plasmas. *Journal of Computational Physics* 214(2):738–756
- Scudder JD, Daughton W (2008) “Illuminating” electron diffusion regions of collisionless magnetic reconnection using electron agyrotropy. *J Geophys*

- Res 113:A06222, DOI 10.1029/2008JA013035
- Seripienlert A, Ruffolo D, Matthaeus WH, Chuychai P (2010) Dropouts in Solar Energetic Particles: Associated with Local Trapping Boundaries or Current Sheets? *The Astrophysical Journal* 711:980–989, DOI 10.1088/0004-637X/711/2/980
- Servidio S, Carbone V, Primavera L, Veltri P, Stasiewicz K (2007) Compressible turbulence in Hall Magnetohydrodynamics. *Planetary and Space Science* 55(15):2239–2243, DOI 10.1016/j.pss.2007.05.023
- Servidio S, Matthaeus WH, Shay MA, Cassak PA, Dmitruk P (2009) Magnetic Reconnection in Two-Dimensional Magnetohydrodynamic Turbulence. *Physical Review Letters* 102(11):115003, DOI 10.1103/PhysRevLett.102.115003
- Servidio S, Matthaeus WH, Shay MA, Dmitruk P, Cassak PA, Wan M (2010) Statistics of magnetic reconnection in two-dimensional magnetohydrodynamic turbulence. *Physics of Plasmas* 17(3):032315, DOI 10.1063/1.3368798, URL <https://doi.org/10.1063/1.3368798>, <https://doi.org/10.1063/1.3368798>
- Servidio S, Dmitruk P, Greco A, Wan M, Donato S, Cassak P, Shay M, Carbone V, Matthaeus W (2011a) Magnetic reconnection as an element of turbulence. *Nonlinear Processes in Geophysics* 18(5):675–695
- Servidio S, Greco A, Matthaeus WH, Osman KT, Dmitruk P (2011b) Statistical association of discontinuities and reconnection in magnetohydrodynamic turbulence. *Journal of Geophysical Research: Space Physics* 116(A9), DOI 10.1029/2011JA016569
- Servidio S, Valentini F, Califano F, Veltri P (2012) Local Kinetic Effects in Two-Dimensional Plasma Turbulence. *Physical Review Letters* 108(4):045001, DOI 10.1103/PhysRevLett.108.045001
- Servidio S, Osman KT, Valentini F, Perrone D, Califano F, Chapman S, Matthaeus WH, Veltri P (2014) Proton Kinetic Effects in Vlasov and Solar Wind Turbulence. *The Astrophysical Journal Letters* 781(2):L27, DOI 10.1088/2041-8205/781/2/L27, 1306.6455
- Servidio S, Valentini F, Perrone D, Greco A, Califano F, Matthaeus WH, Veltri P (2015) A kinetic model of plasma turbulence. *Journal of Plasma Physics* 81(1):325810107, DOI 10.1017/S0022377814000841
- Servidio S, Haynes CT, Matthaeus WH, Burgess D, Carbone V, Veltri P (2016) Explosive particle dispersion in plasma turbulence. *Phys Rev Lett* 117:095101, DOI 10.1103/PhysRevLett.117.095101, URL <https://link.aps.org/doi/10.1103/PhysRevLett.117.095101>
- Servidio S, Chasapis A, Matthaeus WH, Perrone D, Valentini F, Parashar TN, Veltri P, Gershman D, Russell CT, Giles B, Fuselier SA, Phan TD, Burch J (2017) Magnetospheric multiscale observation of plasma velocity-space cascade: Hermite representation and theory. *Phys Rev Lett* 119:205101, DOI 10.1103/PhysRevLett.119.205101, URL <https://link.aps.org/doi/10.1103/PhysRevLett.119.205101>
- Shalchi A (2009) *Nonlinear Cosmic Ray Diffusion Theories*, Astrophysics and Space Science Library, vol 362. Springer, Berlin, DOI 10.1007/

- 978-3-642-00309-7
- Shalchi A (2010) A Unified Particle Diffusion Theory for Cross-field Scattering: Subdiffusion, Recovery of Diffusion, and Diffusion in Three-dimensional Turbulence. *The Astrophysical Journal Letters* 720(2):L127–L130, DOI 10.1088/2041-8205/720/2/L127
- Shalchi A, Li G, Zank GP (2010) Analytic forms of the perpendicular cosmic ray diffusion coefficient for an arbitrary turbulence spectrum and applications on transport of Galactic protons and acceleration at interplanetary shocks. *Astrophys Space Sci* 325(1):99–111, DOI 10.1007/s10509-009-0168-6
- Shay MA, Drake JF, Swisdak M (2007) Two-Scale Structure of the Electron Dissipation Region during Collisionless Magnetic Reconnection. *Physical Review Letters* 99(15):155002, DOI 10.1103/PhysRevLett.99.155002, 0704.0818
- Shay MA, Haggerty CC, Phan TD, Drake JF, Cassak PA, Wu P, Oieroset M, Swisdak M, Malakit K (2014) Electron heating during magnetic reconnection: A simulation scaling study. *Physics of Plasmas* 21(12):122902, DOI 10.1063/1.4904203, 1410.1206
- Shay MA, Phan TD, Haggerty CC, Fujimoto M, Drake JF, Malakit K, Cassak PA, Swisdak M (2016) Kinetic signatures of the region surrounding the X line in asymmetric (magnetopause) reconnection. *Geophysical Research Letters* 43(9):4145–4154, DOI 10.1002/2016GL069034, 1602.00779
- Shay MA, Haggerty CC, Matthaeus WH, Parashar TN, Wan M, Wu P (2018) Turbulent heating due to magnetic reconnection. *Physics of Plasmas* 25(1):012304, DOI 10.1063/1.4993423
- Shebalin JV, Matthaeus WH, Montgomery D (1983) Anisotropy in MHD turbulence due to a mean magnetic field. *Journal of Plasma Physics* 29:525–547, DOI 10.1017/S0022377800000933
- Shuster JR, Gershman DJ, Chen LJ, Wang S, Bessho N, Dorelli JC, da Silva DE, Giles BL, Paterson WR, Denton RE, Schwartz SJ, Norgren C, Wilder FD, Cassak PA, Swisdak M, Uritsky V, Schiff C, Rager AC, Smith S, Avakov LA, Viñas AF (2019) MMS Measurements of the Vlasov Equation: Probing the Electron Pressure Divergence Within Thin Current Sheets. *Geophysical Research Letters* 46(14):7862–7872, DOI 10.1029/2019GL083549
- Silin I, Büchner J, Zelenyi L (2002) Instabilities of collisionless current sheets: Theory and simulations. *Physics of Plasmas*, v9, 1104-1112 (2002) 9:1104–1112, DOI 10.1063/1.1459056
- Sioulas N, Isliker H, Vlahos L (2020) Stochastic Turbulent Acceleration in a Fractal Environment. *The Astrophysical Journal Letters* 895(1):L14, DOI 10.3847/2041-8213/ab9092, 2005.02668
- Sitnov MI, Malova HV, Lui ATY (1997) Quasi-neutral sheet tearing instability induced by electron preferential acceleration from stochasticity. *Journal of Geophysical Research* 102(A1):163–174, DOI 10.1029/96JA01872
- Sitnov MI, Sharma AS, Guzdar PN, Yoon PH (2002) Reconnection onset in the tail of Earth’s magnetosphere. *Journal of Geophysical Research (Space Physics)* 107(A9):1256, DOI 10.1029/2001JA009148

- Sitnov MI, Lui ATY, Guzdar PN, Yoon PH (2004) Current-driven instabilities in forced current sheets. *Journal of Geophysical Research (Space Physics)* 109(A3):A03205, DOI 10.1029/2003JA010123
- Skoutnev V, Hakim A, Juno J, TenBarge JM (2019) Temperature-dependent Saturation of Weibel-type Instabilities in Counter-streaming Plasmas. *The Astrophysical Journal Letters* 872(2):L28, DOI 10.3847/2041-8213/ab0556, 1902.08672
- Slavin JA (2004) Mercury's magnetosphere. *Advances in Space Research* 33(11):1859–1874, DOI 10.1016/j.asr.2003.02.019
- Slavin JA, Acuña MH, Anderson BJ, Baker DN, Benna M, Gloeckler G, Gold RE, Ho GC, Killen RM, Korth H, Krimigis SM, McNutt RL, Nittler LR, Raines JM, Schriver D, Solomon SC, Starr RD, Trávníček P, Zurbuchen TH (2008) Mercury's Magnetosphere After MESSENGER's First Flyby. *Science* 321(5885):85, DOI 10.1126/science.1159040
- Smith CW, Matthaeus WH, Zank GP, Ness NF, Oughton S, Richardson JD (2001) Heating of the low-latitude solar wind by dissipation of turbulent magnetic fluctuations. *Journal of Geophysical Research: Space Physics* 106(A5):8253–8272
- Smith CW, Isenberg PA, Matthaeus WH, Richardson JD (2006) Turbulent Heating of the Solar Wind by Newborn Interstellar Pickup Protons. *The Astrophysical Journal* 638(1):508–517, DOI 10.1086/498671
- Smith D, Ghosh S, Dmitruk P, Matthaeus WH (2004) Hall and turbulence effects on magnetic reconnection. *Geophysical Research Letters* 31(2), DOI 10.1029/2003GL018689, URL <https://agupubs.onlinelibrary.wiley.com/doi/abs/10.1029/2003GL018689>, <https://agupubs.onlinelibrary.wiley.com/doi/pdf/10.1029/2003GL018689>
- Somov BV (2013) The Solar Corona: Why It Is Interesting for Us. *Astronomicheskij Tsirkulyar* 1596:1–6
- Song HQ, Chen Y, Liu K, Feng SW, Xia LD (2009) Quasi-Periodic Releases of Streamer Blobs and Velocity Variability of the Slow Solar Wind near the Sun. *Solar Physics* 258(1):129–140, DOI 10.1007/s11207-009-9411-0, 0907.0819
- Sonnerup BUÖ (1979) Magnetic field reconnection. In: *Solar system plasma physics*. Volume 3. (A79-53667 24-46), vol 3, Amsterdam, North-Holland Publishing Co., pp 45–108
- Sorriso-Valvo L, Carbone V, Veltri P, Consolini G, Bruno R (1999) Intermittency in the solar wind turbulence through probability distribution functions of fluctuations. *Geophysical Research Letters* 26(13):1801–1804, DOI 10.1029/1999GL900270, physics/9903043
- Sorriso-Valvo L, Marino R, Carbone V, Noullez A, Lepreti F, Veltri P, Bruno R, Bavassano B, Pietropaolo E (2007) Observation of Inertial Energy Cascade in Interplanetary Space Plasma. *Physical Review Letters* 99(11):115001, DOI 10.1103/PhysRevLett.99.115001, astro-ph/0702264
- Sorriso-Valvo L, Perrone D, Pezzi O, Valentini F, Servidio S, Zouganelis I, Veltri P (2018) Local energy transfer rate and kinetic processes: the fate of turbulent energy in two-dimensional hybrid vlasov-maxwell nu-

- merical simulations. *Journal of Plasma Physics* 84(2):725840201, DOI 10.1017/S0022377818000302
- Sorriso-Valvo L, Catapano F, Retinò A, Le Contel O, Perrone D, Roberts OW, Coburn JT, Panebianco V, Valentini F, Perri S, Greco A, Malara F, Carbone V, Veltri P, Pezzi O, Fraternali F, Di Mare F, Marino R, Giles B, Moore TE, Russell CT, Torbert RB, Burch JL, Khotyaintsev YV (2019) Turbulence-driven ion beams in the magnetospheric kelvin-helmholtz instability. *Phys Rev Lett* 122:035102, DOI 10.1103/PhysRevLett.122.035102, URL <https://link.aps.org/doi/10.1103/PhysRevLett.122.035102>
- Speiser TW (1965) Particle Trajectories in Model Current Sheets, 1, Analytical Solutions. *Journal of Geophysical Research*70(17):4219–4226, DOI 10.1029/JZ070i017p04219
- Stawarz JE, Eastwood JP, Genestreti KJ, Nakamura R, Ergun RE, Burgess D, Burch JL, Fuselier SA, Gershman DJ, Giles BL, Le Contel O, Lindqvist PA, Russell CT, Torbert RB (2018) Intense electric fields and electron-scale substructure within magnetotail flux ropes as revealed by the magnetospheric multiscale mission. *Geophysical Research Letters* 45(17):8783–8792, DOI 10.1029/2018GL079095
- Stawarz JE, Eastwood JP, Phan TD, Gingell IL, Shay MA, Burch JL, Ergun RE, Giles BL, Gershman DJ, Contel OL, Lindqvist PA, Russell CT, Strange-way RJ, Torbert RB, Argall MR, Fischer D, Magnes W, Franci L (2019) Properties of the turbulence associated with electron-only magnetic reconnection in earth's magnetosheath. *The Astrophysical Journal* 877(2):L37, DOI 10.3847/2041-8213/ab21c8
- Strauss RD, Potgieter MS, Büsching I, Kopp A (2012) Modelling heliospheric current sheet drift in stochastic cosmic ray transport models. *Astrophysics and Space Science*339(2):223–236, DOI 10.1007/s10509-012-1003-z
- Sturrock PA (1966) Stochastic acceleration. *Phys Rev* 141:186–191, DOI 10.1103/PhysRev.141.186, URL <https://link.aps.org/doi/10.1103/PhysRev.141.186>
- Sundkvist D, Retinò A, Vaivads A, Bale SD (2007) Dissipation in turbulent plasma due to reconnection in thin current sheets. *Phys Rev Lett* 99:025004, DOI 10.1103/PhysRevLett.99.025004, URL <https://link.aps.org/doi/10.1103/PhysRevLett.99.025004>
- Syrovatskii SI (1971) Formation of Current Sheets in a Plasma with a Frozen-in Strong Magnetic Field. *Soviet Journal of Experimental and Theoretical Physics* 33:933
- Tatsuno T, Dorland W, Schekochihin AA, Plunk GG, Barnes M, Cowley SC, Howes GG (2009) Nonlinear Phase Mixing and Phase-Space Cascade of Entropy in Gyrokinetic Plasma Turbulence. *Physical Review Letters* 103(1):015003, DOI 10.1103/PhysRevLett.103.015003, 0811.2538
- Tautz RC, Shalchi A (2012) Drift Coefficients of Charged Particles in Turbulent Magnetic Fields. *The Astrophysical Journal*744(2):125, DOI 10.1088/0004-637X/744/2/125
- TenBarge JM, Howes GG (2013) Current Sheets and Collisionless Damping in Kinetic Plasma Turbulence. *The Astrophys J Lett* 771:L27, DOI 10.1088/

- 2041-8205/771/2/L27, 1304.2958
- TenBarge JM, Howes GG, Dorland W (2013) Collisionless Damping at Electron Scales in Solar Wind Turbulence. *The Astrophysical Journal* 774(2):139, DOI 10.1088/0004-637X/774/2/139
- Tenerani A, Rappazzo AF, Velli M, Pucci F (2015a) The tearing mode instability of thin current sheets: the transition to fast reconnection in the presence of viscosity. *The Astrophysical Journal* 801(2):145
- Tenerani A, Velli M, Rappazzo AF, Pucci F (2015b) Magnetic reconnection: Recursive current sheet collapse triggered by “ideal” tearing. *The Astrophysical Journal Letters* 813(2):L32
- Tessein JA, Matthaeus WH, Wan M, Osman KT, Ruffolo D, Giacalone J (2013) Association of Suprathermal Particles with Coherent Structures and Shocks. *The Astrophysical Journal* 776:L8, DOI 10.1088/2041-8205/776/1/L8
- Thampi SV, Krishnaprasad C, Shreedevi PR, Pant TK, Bhardwaj A (2019) Acceleration of Energetic Ions in Corotating Interaction Region near 1.5 au: Evidence from MAVEN. *The Astrophysical Journal Letters* 880(1):L3, DOI 10.3847/2041-8213/ab2b43, 1908.00816
- Tooprakai P, Chuychai P, Minnie J, Ruffolo D, Bieber JW, Matthaeus WH (2007) Temporary topological trapping and escape of charged particles in a flux tube as a cause of delay in time asymptotic transport. *Geophys Res Lett* 34:17105, DOI 10.1029/2007GL030672
- Tooprakai P, Seripienlert A, Ruffolo D, Chuychai P, Matthaeus WH (2016) Simulations of Lateral Transport and Dropout Structure of Energetic Particles from Impulsive Solar Flares. *Astrophys J* 831:195, DOI 10.3847/0004-637X/831/2/195
- Torbert RB, Burch JL, Giles BL, Gershman D, Pollock CJ, Dorelli J, Avanov L, Argall MR, Shuster J, Strangeway RJ, Russell CT, Ergun RE, Wilder FD, Goodrich K, Faith HA, Farrugia CJ, Lindqvist PA, Phan T, Khotyaintsev Y, Moore TE, Marklund G, Daughton W, Magnes W, Kletzing CA, Bounds S (2016) Estimates of terms in ohm’s law during an encounter with an electron diffusion region. *Geophysical Research Letters* 43(12):5918–5925, DOI 10.1002/2016GL069553, URL <https://agupubs.onlinelibrary.wiley.com/doi/abs/10.1002/2016GL069553>, <https://agupubs.onlinelibrary.wiley.com/doi/pdf/10.1002/2016GL069553>
- Torbert RB, Burch JL, Phan TD, Hesse M, Argall MR, Shuster J, Ergun RE, Alm L, Nakamura R, Genestreti KJ, Gershman DJ, Paterson WR, Turner DL, Cohen I, Giles BL, Pollock CJ, Wang S, Chen LJ, Stawarz JE, Eastwood JP, Hwang KJ, Farrugia C, Dors I, Vaith H, Mouikis C, Ardakani A, Mauk BH, Fuselier SA, Russell CT, Strangeway RJ, Moore TE, Drake JF, Shay MA, Khotyaintsev YV, Lindqvist PA, Baumjohann W, Wilder FD, Ahmadi N, Dorelli JC, Avanov LA, Oka M, Baker DN, Fennell JF, Blake JB, Jaynes AN, Le Contel O, Petrinec SM, Lavraud B, Saito Y (2018) Electron-scale dynamics of the diffusion region during symmetric magnetic reconnection in space. *Science* 362(6421):1391–1395, DOI 10.1126/science.aat2998, URL <https://science.sciencemag.org/content/>

- 362/6421/1391, <https://science.sciencemag.org/content/362/6421/1391.full.pdf>
- Tronci C, Camporeale E (2015) Neutral vlasov kinetic theory of magnetized plasmas. *Physics of Plasmas* 22(2):020704, DOI 10.1063/1.4907665, URL <https://doi.org/10.1063/1.4907665>
- Trotta D, Franci L, Burgess D, Hellinger P (2020) Fast Acceleration of Transrelativistic Electrons in Astrophysical Turbulence. *The Astrophysical Journal* 894(2):136, DOI 10.3847/1538-4357/ab873c, URL <http://dx.doi.org/10.3847/1538-4357/ab873c>, 1910.11935
- Ukhorskiy AY, Sitnov MI, Merkin VG, Gkioulidou M, Mitchell DG (2017) Ion acceleration at dipolarization fronts in the inner magnetosphere. *Journal of Geophysical Research (Space Physics)* 122(3):3040–3054, DOI 10.1002/2016JA023304
- Umeda T, Wada Y (2016) Secondary instabilities in the collisionless Rayleigh-Taylor instability: Full kinetic simulation. *Physics of Plasmas* 23(11):112117, DOI 10.1063/1.4967859
- Umeda T, Wada Y (2017) Non-MHD effects in the nonlinear development of the MHD-scale Rayleigh-Taylor instability. *Physics of Plasmas* 24(7):072307, DOI 10.1063/1.4991409
- Umeda T, Togano K, Ogino T (2009) Two-dimensional full-electromagnetic Vlasov code with conservative scheme and its application to magnetic reconnection. *Computer Physics Communications* 180(3):365–374, DOI 10.1016/j.cpc.2008.11.001
- Umeda T, Miwa Ji, Matsumoto Y, Nakamura TKM, Togano K, Fukazawa K, Shinohara I (2010) Full electromagnetic Vlasov code simulation of the Kelvin-Helmholtz instability. *Physics of Plasmas* 17(5):052311, DOI 10.1063/1.3422547
- Uzdensky DA (2011) Magnetic reconnection in extreme astrophysical environments. *Space Science Reviews* 160(1):45–71, DOI 10.1007/s11214-011-9744-5, URL <https://doi.org/10.1007/s11214-011-9744-5>
- Vafin S, Riazantseva M, Pohl M (2019) Coulomb Collisions as a Candidate for Temperature Anisotropy Constraints in the Solar Wind. *The Astrophysical Journal Letters* 871(1):L11, DOI 10.3847/2041-8213/aafb11
- Vaivads A, Khotyaintsev Y, André M, Retinò A, Buchert SC, Rogers BN, Décréau P, Paschmann G, Phan TD (2004) Structure of the magnetic reconnection diffusion region from four-spacecraft observations. *Phys Rev Lett* 93:105001, DOI 10.1103/PhysRevLett.93.105001, URL <https://link.aps.org/doi/10.1103/PhysRevLett.93.105001>
- Vaivads A, Retinò A, Soucek J, Khotyaintsev YV, Valentini F, Escoubet CP, Alexandrova O, André M, Bale SD, Balikhin M, et al (2016) Turbulence heating observer – satellite mission proposal. *Journal of Plasma Physics* 82(5):905820501, DOI 10.1017/S0022377816000775
- Valentini F, Trávníček P, Califano F, Hellinger P, Mangeney A (2007) A hybrid-vlasov model based on the current advance method for the simulation of collisionless magnetized plasma. *Journal of Computational Physics*

- 225(1):753–770
- Valentini F, Veltri P, Califano F, Mangeney A (2008) Cross-Scale Effects in Solar-Wind Turbulence. *Physical Review Letters*101(2):025006, DOI 10.1103/PhysRevLett.101.025006
- Valentini F, Califano F, Perrone D, Pegoraro F, Veltri P (2011a) New Ion-Wave Path in the Energy Cascade. *Physical Review Letters*106(16):165002, DOI 10.1103/PhysRevLett.106.165002
- Valentini F, Perrone D, Veltri P (2011b) SHORT-WAVELENGTH ELECTROSTATIC FLUCTUATIONS IN THE SOLAR WIND. *The Astrophysical Journal* 739(1):54, DOI 10.1088/0004-637x/739/1/54, URL <https://doi.org/10.1088%2F0004-637x%2F739%2F1%2F54>
- Valentini F, Servidio S, Perrone D, Califano F, Matthaeus W, Veltri P (2014) Hybrid vlasov-maxwell simulations of two-dimensional turbulence in plasmas. *Physics of Plasmas* 21(8):082307
- Valentini F, Perrone D, Stabile S, Pezzi O, Servidio S, Marco RD, Marcucci F, Bruno R, Lavraud B, Keyser JD, Consolini G, Brienza D, Sorriso-Valvo L, Retinò A, Vaivads A, Salatti M, Veltri P (2016) Differential kinetic dynamics and heating of ions in the turbulent solar wind. *New Journal of Physics* 18(12):125001, URL <http://stacks.iop.org/1367-2630/18/i=12/a=125001>
- Valentini, F, Vásconez, C L, Pezzi, O, Servidio, S, Malara, F, Pucci, F (2017) Transition to kinetic turbulence at proton scales driven by large-amplitude kinetic alfvén fluctuations. "Astronomy and Astrophysics" 599:"A8", DOI "10.1051/0004-6361/201629240", URL "<https://doi.org/10.1051/0004-6361/201629240>"
- Vásconez CL, Pucci F, Valentini F, Servidio S, Matthaeus WH, Malara F (2015) Kinetic alfvén wave generation by large-scale phase mixing. *The Astrophysical Journal* 815(1):7, URL <http://stacks.iop.org/0004-637X/815/i=1/a=7>
- Vasko IY, Kuzichev IV, Artemyev AV, Bale SD, Bonnell JW, Mozer FS (2020) On quasi-parallel whistler waves in the solar wind. *Physics of Plasmas* 27(8):082902, DOI 10.1063/5.0003401, URL <https://doi.org/10.1063/5.0003401>, <https://doi.org/10.1063/5.0003401>
- Vasquez BJ, Smith CW, Hamilton K, MacBride BT, Leamon RJ (2007) Evaluation of the turbulent energy cascade rates from the upper inertial range in the solar wind at 1 AU. *Journal of Geophysical Research (Space Physics)* 112(A7):A07101, DOI 10.1029/2007JA012305
- Vasyliunas VM (1968) Low-energy electrons in the magnetosphere as observed by ogo-1 and ogo-3. In: *Physics of the Magnetosphere*, Springer, pp 622–640
- Vech D, Klein KG, Kasper JC (2017) Nature of Stochastic Ion Heating in the Solar Wind: Testing the Dependence on Plasma Beta and Turbulence Amplitude. *The Astrophysical Journal Letters*850(1):L11, DOI 10.3847/2041-8213/aa9887, 1711.01508
- Verma M, Roberts D, Goldstein M (1995) Turbulent heating and temperature evolution in the solar wind plasma. *Journal of Geophysical Research: Space Physics* 100(A10):19839–19850

- Verscharen D, Klein KG, Maruca BA (2019) The multi-scale nature of the solar wind. *Living Reviews in Solar Physics* 16(1):5
- Wan M, Matthaeus WH, Servidio S, Oughton S (2013) Generation of X-points and secondary islands in 2D magnetohydrodynamic turbulence. *Physics of Plasmas* 20:042307, DOI 10.1063/1.4802985
- Wan M, Rappazzo AF, Matthaeus WH, Servidio S, Oughton S (2014) Dissipation and reconnection in boundary-driven reduced magnetohydrodynamics. *Astrophys J* 797:63, DOI 10.1088/0004-637X/797/1/63
- Wan M, Matthaeus WH, Roytershteyn V, Karimabadi H, Parashar T, Wu P, Shay M (2015) Intermittent Dissipation and Heating in 3D Kinetic Plasma Turbulence. *Physical Review Letters* 114(17):175002, DOI 10.1103/PhysRevLett.114.175002
- Wan M, Matthaeus WH, Roytershteyn V, Parashar TN, Wu P, Karimabadi H (2016) Intermittency, coherent structures and dissipation in plasma turbulence. *Physics of Plasmas* 23(4):042307, DOI 10.1063/1.4945631
- Wang B, Kuo J, Bae SC, Granick S (2012) When brownian diffusion is not gaussian. *Nature materials* 11(6):481
- Wang S, Wang R, Lu Q, Fu H, Wang S (2020) Direct evidence of secondary reconnection inside filamentary currents of magnetic flux ropes during magnetic reconnection. *Nature Communications* 11(1):1–8
- Wang YM, Hess P (2018) Gradual streamer expansions and the relationship between blobs and inflows. *The Astrophysical Journal* 859(2):135, DOI 10.3847/1538-4357/aabfd5, URL <https://doi.org/10.3847/1538-4357/aabfd5>
- Wang YM, Sheeley J N R, Walters JH, Brueckner GE, Howard RA, Michels DJ, Lamy PL, Schwenn R, Simnett GM (1998) Origin of Streamer Material in the Outer Corona. *The Astrophysical Journal Letters* 498(2):L165–L168, DOI 10.1086/311321
- Wang YM, Sheeley NR, Socker DG, Howard RA, Rich NB (2000) The dynamical nature of coronal streamers. *Journal of Geophysical Research* 105(A11):25133–25142, DOI 10.1029/2000JA000149
- Wang Z, Fu HS, Liu CM, Liu YY, Cozzani G, Giles BL, Hwang KJ, Burch JL (2019) Electron Distribution Functions Around a Reconnection X-Line Resolved by the FOTE Method. *Geophysical Research Letters* 46(3):1195–1204, DOI 10.1029/2018GL081708
- Wilcox JM, Hoeksema JT, Scherrer PH (1980) Origin of the warped heliospheric current sheet. *Science* 209:603–605, DOI 10.1126/science.209.4456.603
- Wilder F, Ergun R, Burch J, Ahmadi N, Eriksson S, Phan T, Goodrich K, Shuster J, Rager A, Torbert R, et al. (2018) The role of the parallel electric field in electron-scale dissipation at reconnecting currents in the magnetosheath. *Journal of Geophysical Research: Space Physics* 123(8):6533–6547
- Wu P, Perri S, Osman K, Wan M, Matthaeus WH, Shay MA, Goldstein ML, Karimabadi H, Chapman S (2013) Intermittent Heating in Solar Wind and Kinetic Simulations. *The Astrophysical Journal Letters* 763(2):L30, DOI 10.1088/2041-8205/763/2/L30

- Xia Q, Zharkova V (2018) Particle acceleration in coalescent and squashed magnetic islands - i. test particle approach. *A&A* 620:A121, DOI 10.1051/0004-6361/201833599, URL <https://doi.org/10.1051/0004-6361/201833599>
- Xia Q, Zharkova V (2020) Particle acceleration in coalescent and squashed magnetic islands. II. Particle-in-cell approach. *Astronomy and Astrophysics* 635:A116, DOI 10.1051/0004-6361/201936420
- Xu F, Li G, Zhao L, Zhang Y, Khabarova O, Miao B, le Roux J (2015) Angular Distribution of Solar Wind Magnetic Field Vector at 1 AU. *The Astrophysical Journal* 801(1):58, DOI 10.1088/0004-637X/801/1/58
- Xu X, Wei F, Feng X (2011) Observations of reconnection exhausts associated with large-scale current sheets within a complex icme at 1 au. *Journal of Geophysical Research: Space Physics* 116(A5), DOI 10.1029/2010JA016159, URL <https://agupubs.onlinelibrary.wiley.com/doi/abs/10.1029/2010JA016159>, <https://agupubs.onlinelibrary.wiley.com/doi/pdf/10.1029/2010JA016159>
- Yang Y, Matthaeus WH, Parashar TN, Haggerty CC, Roytershteyn V, Daughton W, Wan M, Shi Y, Chen S (2017a) Energy transfer, pressure tensor, and heating of kinetic plasma. *Physics of Plasmas* 24(7):072306, DOI 10.1063/1.4990421, URL <https://doi.org/10.1063/1.4990421>, <https://doi.org/10.1063/1.4990421>
- Yang Y, Matthaeus WH, Parashar TN, Wu P, Wan M, Shi Y, Chen S, Roytershteyn V, Daughton W (2017b) Energy transfer channels and turbulence cascade in vlasov-maxwell turbulence. *Phys Rev E* 95:061201, DOI 10.1103/PhysRevE.95.061201, URL <https://link.aps.org/doi/10.1103/PhysRevE.95.061201>
- Yao ST, Shi QQ, Guo RL, Yao ZH, Fu HS, Degeling AW, Zong QG, Wang XG, Russell CT, Tian AM, Xiao YC, Zhang H, Wang SM, Hu HQ, Liu J, Liu H, Li B, Giles BL (2020) Kinetic-scale flux rope in the magnetosheath boundary layer. *The Astrophysical Journal* 897(2):137, DOI 10.3847/1538-4357/ab9620
- Yoon PH, Lui ATY (2001) On the drift-sausage mode in one-dimensional current sheet. *Journal of Geophysical Research* 106(A2):1939–1948, DOI 10.1029/2000JA000130
- Zank GP, Rice WKM, Wu CC (2000) Particle acceleration and coronal mass ejection driven shocks: A theoretical model. *Journal of Geophysical Research: Space Physics* 105(A11):25079–25095, DOI 10.1029/1999JA000455, URL <https://agupubs.onlinelibrary.wiley.com/doi/abs/10.1029/1999JA000455>, <https://agupubs.onlinelibrary.wiley.com/doi/pdf/10.1029/1999JA000455>
- Zank GP, le Roux JA, Webb GM, Dosch A, Khabarova O (2014) Particle Acceleration via Reconnection Processes in the Supersonic Solar Wind. *The Astrophysical Journal* 797:28, DOI 10.1088/0004-637X/797/1/28
- Zank GP, Hunana P, Mostafavi P, le Roux JA, Li G, Webb GM, Khabarova O, Cummings A, Stone E, Decker R (2015a) Diffusive Shock Acceleration and Reconnection Acceleration Processes. *The Astrophysical Journal* 814:137,

- DOI 10.1088/0004-637X/814/2/137
- Zank GP, Hunana P, Mostafavi P, le Roux JA, Li G, Webb GM, Khabarova OV (2015b) Particle acceleration by combined diffusive shock acceleration and downstream multiple magnetic island acceleration. In: *Journal of Physics: Conference Series*, IOP Publishing, vol 642, p 012031
- Zeiler A, Biskamp D, Drake JF, Rogers BN, Shay MA, Scholer M (2002) Three-dimensional particle simulations of collisionless magnetic reconnection. *Journal of Geophysical Research: Space Physics* 107(A9):SMP 6–1–SMP 6–9, DOI 10.1029/2001JA000287, URL <https://agupubs.onlinelibrary.wiley.com/doi/abs/10.1029/2001JA000287>, <https://agupubs.onlinelibrary.wiley.com/doi/pdf/10.1029/2001JA000287>
- Zelenyi L, Milovanov AV, Zimbardo G (1998) Multiscale magnetic structure of the distant tail: self-consistent fractal approach. *GEOPHYSICAL MONOGRAPH-AMERICAN GEOPHYSICAL UNION* 105:321–339
- Zelenyi L, Sitnov M, Malova H, Sharma A (2000) Thin and superthin ion current sheets. quasi-adiabatic and nonadiabatic models. *Nonlinear Processes in Geophysics* 7, DOI 10.5194/npg-7-127-2000
- Zelenyi L, Malova H, Popov VY, Delcourt D, Sharma A (2004) Nonlinear equilibrium structure of thin currents sheets: influence of electron pressure anisotropy. *Nonlinear Processes in Geophysics* 11:579–587, DOI 10.5194/npg-11-579-2004
- Zelenyi L, Artemiev A, Malova H, Popov V (2008) Marginal stability of thin current sheets in the earth’s magnetotail. *Journal of atmospheric and solar-terrestrial physics* 70(2-4):325–333, DOI 10.1016/j.jastp.2007.08.019
- Zelenyi L, Malova H, Artemyev A, Popov VY, Petrukovich A (2011) Thin current sheets in collisionless plasma: Equilibrium structure, plasma instabilities, and particle acceleration. *Plasma Physics Reports* 37(2):118–160, DOI 10.1134/S1063780X1102005X
- Zelenyi L, Malova H, Grigorenko E, Popov V, Delcourt D (2019) Current sheets in planetary magnetospheres. *Plasma Physics and Controlled Fusion* 61(5):054002, DOI 10.1088/1361-6587/aafbbf
- Zelenyi LM, Milovanov AV (2004) REVIEWS OF TOPICAL PROBLEMS: Fractal topology and strange kinetics: from percolation theory to problems in cosmic electrodynamics. *Physics Uspekhi* 47(8):R01, DOI 10.1070/PU2004v047n08ABEH001705
- Zelenyi LM, Lipatov AS, Lominadze DG, Taktakishvili AL (1984) The dynamics of the energetic proton bursts in the course of the magnetic field topology reconstruction in the earth’s magnetotail. *Planetary and Space Science* 32(3):313–324, DOI 10.1016/0032-0633(84)90167-3
- Zelenyi LM, Lominadze JG, Taktakishvili AL (1990) Generation of the energetic proton and electron bursts in planetary magnetotails. *Journal of Geophysical Research* 95(A4):3883–3891, DOI 10.1029/JA095iA04p03883
- Zelenyi LM, Malova H, Popov V (2003) Splitting of thin current sheets in the earth’s magnetosphere. *JETP Letters* 78:296–299, DOI 10.1134/1.1625728
- Zelenyi LM, Malova HV, Popov VY, Delcourt DC, Ganushkina NY, Sharma AS (2006) “Matreshka” model of multilayered current sheet. *Geophysical*

- Research Letters 33(5):L05105, DOI 10.1029/2005GL025117
- Zelenyi LM, Dolgonosov MS, Grigorenko EE, Sauvaud JA (2007) Universal properties of the nonadiabatic acceleration of ions in current sheets. *Soviet Journal of Experimental and Theoretical Physics Letters* 85(4):187–193, DOI 10.1134/S0021364007040017
- Zelenyi LM, Artemyev AV, Petrukovich AA, Nakamura R, Malova HV, Popov VY (2009a) Low frequency eigenmodes of thin anisotropic current sheets and Cluster observations. *Annales Geophysicae* 27(2):861–868, DOI 10.5194/angeo-27-861-2009
- Zelenyi LM, Kropotkin AP, Domrin VI, Artemyev AV, Malova HV, Popov VY (2009b) Tearing mode in thin current sheets of the Earth's magnetosphere: A scenario of transition to unstable state. *Cosmic Research* 47(5):352–360, DOI 10.1134/S0010952509050025
- Zelenyi LM, Petrukovich A, Artemyev AV, Malova KV, Nakamura R (2010) Metastability of current sheets. *Physics-Uspekhi* 53(9):933–941, DOI 10.3367/UFNr.0180.201009g.0973
- Zenitani S, Hesse M, Klimas A, Kuznetsova M (2011) New measure of the dissipation region in collisionless magnetic reconnection. *Physical review letters* 106(19):195003
- Zhao LL, Zank GP, Khabarova O, Du S, Chen Y, Adhikari L, Hu Q (2018) An unusual energetic particle flux enhancement associated with solar wind magnetic island dynamics. *The Astrophysical Journal Letters* 864(2):L34
- Zhao LL, Zank GP, Adhikari L, Hu Q, Kasper JC, Bale SD, Korreck KE, Case AW, Stevens M, Bonnell JW, Dudok de Wit T, Goetz K, Harvey PR, MacDowall RJ, Malaspina DM, Pulupa M, Larson DE, Livi R, Whittlesey P, Klein KG (2020) Identification of Magnetic Flux Ropes from Parker Solar Probe Observations during the First Encounter. *The Astrophysical Journal Supplement* 246(2):26, DOI 10.3847/1538-4365/ab4ff1, 1912.02349
- Zharkova VV, Khabarova OV (2012) Particle dynamics in the reconnecting heliospheric current sheet: Solar wind data versus three-dimensional particle-in-cell simulations. *The Astrophysical Journal* 752(1):35, DOI 10.1088/0004-637X/752/1/35
- Zharkova VV, Khabarova OV (2015) Additional acceleration of solar-wind particles in current sheets of the heliosphere. *Annales Geophysicae* 33(4):457–470, DOI 10.5194/angeo-33-457-2015
- Zhdankin V, Uzdensky DA, Perez JC, Boldyrev S (2013) Statistical analysis of current sheets in three-dimensional magnetohydrodynamic turbulence. *Astrophys J* 771:124, DOI 10.1088/0004-637X/771/2/124
- Zheng J, Hu Q (2018) Observational Evidence for Self-generation of Small-scale Magnetic Flux Ropes from Intermittent Solar Wind Turbulence. *The Astrophysical Journal Letters* 852:L23
- Zhou XZ, Angelopoulos V, Sergeev VA, Runov A (2010) Accelerated ions ahead of earthward propagating dipolarization fronts. *Journal of Geophysical Research (Space Physics)* 115(A8):A00I03, DOI 10.1029/2010JA015481
- Zhu Z, Winglee RM (1996) Tearing instability, flux ropes, and the kinetic current sheet kink instability in the Earth's magnetotail: A three-

- dimensional perspective from particle simulations. *Journal of Geophysical Research* 101(A3):4885–4898, DOI 10.1029/95JA03144
- Zimbardo G, Perri S (2013) From Lévy Walks to Superdiffusive Shock Acceleration. *The Astrophysical Journal* 778(1):35, DOI 10.1088/0004-637X/778/1/35
- Zimbardo G, Perri S (2017) Superdiffusive shock acceleration at galaxy cluster shocks. *Nature Astronomy* 1:0163, DOI 10.1038/s41550-017-0163
- Zimbardo G, Pommois P, Veltri P (2006) Superdiffusive and Subdiffusive Transport of Energetic Particles in Solar Wind Anisotropic Magnetic Turbulence. *The Astrophysical Journal Letters* 639(2):L91–L94, DOI 10.1086/502676
- Zimbardo G, Amato E, Bovet A, Effenberger F, Fasoli A, Fichtner H, Furno I, Gustafson K, Ricci P, Perri S (2015) Superdiffusive transport in laboratory and astrophysical plasmas. *Journal of Plasma Physics* 81(6):495810601, DOI 10.1017/S0022377815001117
- Zimbardo G, Perri S, Effenberger F, Fichtner H (2017) Fractional Parker equation for the transport of cosmic rays: steady-state solutions. *Astronomy and Astrophysics* 607:A7, DOI 10.1051/0004-6361/201731179